INFRARED PHOTODISSOCIATION OF VAN DER WAALS MOLECULES

Thesis by

Michael Paul Casassa

In Partial Fulfillment of the Requirements

for the Degree of Doctor of Philosophy

California Institute of Technology

Pasadena, California

1984

(Submitted November 18, 1983)

ACKNOWLEDGEMENTS

It is a pleasure to thank Ken Janda for his guidance during the past five years. The many successes described in this thesis are largely attributable to his help and encouragement. I would also like to thank Ahmed Zewail for his help in understanding line broadening mechanisms which are central to the interpretation of our experiments. I thank Jack Beauchamp for the loan of both his CO_2 laser, without which there would be no experiments, and his student, David Bomse. David provided the boost which got me and this project started, and together we relished the first ethylene dimer success. Since then I have enjoyed working closely with Francis Celii and Colin Western, both of whom helped to accomplish the work described in this thesis.

Many fellow graduate students have given up valuable time to help with various problems. Among them are Sam Batchelder, David Brinza, Sally Hair, Bill Lambert and Barry Swartz. Members of the technical staff who have been exceptionally helpful are Dee Barr, Tom Dunn and Bill Schuelke Sr. Bill Schuelke Jr. deserves credit for building our molecular beam apparatus. Thanks also go to Gwen Anastasi for typing this thesis.

Organizations who have helped support me and this research are Caltech, NSF, Shell Companies Foundation, Procter & Gamble, Atlantic Richfield Foundation, ACS and DOE.

Finally, my heartfelt thanks and love to my wife, Joanne, and to many close friends who have enriched my life.

ABSTRACT

Infrared photodissociation of van der Waals molecules is investigated using low power cw infrared lasers. Information gained concerns the dynamics of vibrational predissociation and the van der Waals interactions. Clusters formed in supersonic molecular beams are irradiated for approximately 0.5 msec and the fraction of clusters remaining intact is measured as a function of laser wavelength and power. Detailed homogeneous and inhomogeneous line shape models are presented and used to analyze the results. Effects such as fluence broadening and orientational inhomogeneity are described.

Van der Waals molecules studied include dimeric clusters of ethylene with rare gases, hydrogen halides and non-hydrogen bonding polyatomic molecules. Homogeneous widths of clusters excited near the ν_7 frequency of free ethylene correspond to lifetimes ranging from 0.44 psec for $(C_2H_4)_2$ to greater than 10 psec for $Ne \cdot C_2H_4$. These are attributed to vibrational predissociation constrained by conservation of angular momentum. Other conceivable broadening mechanisms are discussed.

Spectra obtained by exciting the ν_7 mode in different types of ethylene clusters are quite dissimilar. Lineshape analysis indicates that the ν_7 transition in $(C_2H_4)_2$ occurs as a hybrid band. The same transition in $C_2H_4 \cdot HF$ occurs as a perpendicular band. The rare gas-ethylene clusters are

less rigid than the others and excitation of hindered internal rotation of C_2H_4 accompanies the ν_7 absorption. All of the ethylene clusters exhibit blue shifts and intensity enhancement, as compared to ν_7 absorption by free ethylene, which are attributed largely to electrostatic interactions.

TABLE OF CONTENTS

Chapter 1

Introduction

The quintessential van der Waals molecule infrared photodissociation experiment was originally described by Klemperer in 1974.[1] He proposed that infrared active constituents of weakly bound clusters formed in molecular beams could be vibrationally excited using narrow band lasers. The quantum of vibration would, in general, be larger than the van der Waals bond energy. Subsequent intramolecular vibrational energy redistribution would lead to fragmentation of the complex which could be detected as beam loss by using a mass spectrometer.

The information gained from such experiments is important in two major areas of chemical physics. First, since the dynamics of the initially excited state are reflected in spectral linewidths, factors which control the rate and direction of vibrational energy flow in molecules can be discerned. Fast randomization of this energy is a postulate of statistical unimolecular reaction theories. On the other hand, the success of laser selective chemistry depends on the existence of metastable vibrational energy distributions. The second area is understanding the nature of weak interactions between molecules. In addition to dynamical information, photodissociation spectra contain, in principle, all of the types of information found in traditional spectroscopies. Structure, frequencies and intensities observed are all a consequence of the intramolecular potential.

Based on an empirical half-collision model, Klemperer estimated that HF···HF(ν=1) should dissociate within 50 psec.[1] At the same time, vibrational predissociation theories[2] were unable to account for the widths of diffuse bands in hydrogen-bonded liquids. Soon afterward, Child[3] and Ewing[4] calculated lifetimes on the order of seconds for some clusters. Theoretical work of Beswick and Jortner[5] was successful in accounting for the widths of levels of vibronically excited HeI_2 observed by Levy and coworkers, but (at the same time) their theory also predicted very long lifetimes for other clusters. Before 1979, two direct observations of infrared photodissociation of van der Waals molecules had been reported. The first was a study of N_2O clusters by Gough et al.[6] These spectra were evidently inhomogeneous, and uncertainty in the cluster size precluded analysis. The second experiment was performed by Gentry and coworkers[7] on ethylene dimer. They observed intense photodissociation over a range of nearly 200 cm^{-1}, suggesting an incredibly fast decay rate.

The incongruity of the results listed above were the motivation for the work presented in this thesis. The chapters, which are arranged roughly in chronological order, reflect an effort to vary the intramolecular potential to see how it influences the photodissociation spectrum. They are interspersed with sections on the lineshape analysis which became increasingly detailed as measurements became

more precise. Using very detailed lineshape analysis, we have discovered that it is possible to learn a great deal, even from spectra which appear as broad featureless blobs.

Chapter 2 contains our original ethylene cluster results, including ethylene dimer. Chapter 3 is a demonstration of the facility and isotopic selectivity of infrared photodissociation of weakly bound complexes. Chapter 4 describes the homogeneous lineshape analysis which reconciles the dimer width originally observed by Hoffbauer et al.[7] and the 12 cm^{-1} width observed in our laboratory. Chapter 4 also includes an application of a similar lineshape model to test the feasibility of a laser induced desorption experiment analogous to van der Waals molecule photodissociation. Chapter 5 contains our measurements on $C_2H_4 \cdot HF$ and $C_2H_4 \cdot HCl$ which exhibit significantly narrower widths than $(C_2H_4)_2$. The observed blue shifts and intensity enhancement of the cluster-bound C_2H_4 vibration, as compared to free C_2H_4, are interpreted using an electrostatic interaction model. Since the hydrogen-bound clusters' spectra are narrow, it is possible that inhomogeneous broadening affects the band profile. This possibility is addressed in Chapter 6 where an inhomogeneous lineshape model is presented. With this model, seemingly disparate measurements of the $(C_2H_4)_2$ width over a wide range of laser powers have been quantitatively reconciled. Spectra of $Ne \cdot C_2H_4$ and $Ar \cdot C_2H_4$ are reported in Chapter 7. These are rich in structure and $Ne \cdot C_2H_4$ has the narrowest lines yet observed

in ethylene cluster spectra. The structure is due to hindered internal rotation by the ethylene. Evidently the other clusters mentioned above are rigid when compared to $Ne \cdot C_2H_4$ and $Ar \cdot C_2H_4$. Comparison of results obtained for all of the ethylene clusters indicates that widths are due to vibrational predissociation constrained by angular momentum conservation. Chapter 8 discusses line broadening mechanisms and their importance in van der Waals molecule photodissociation spectra. These considerations are crucial to interpretation of our experiments since linewidths only give a decay rate, while the decay mechanism must be inferred. Chapter 9 summarizes highlights of the previous chapters.

REFERENCES

1. W. Klemperer, Ber. Bunsenges. Phys. Chem. 78, 128 (1974).
2. C. A. Coulson and G. N. Robertson, Proc. R. Soc. London A342, 289 (1975).
3. M. S. Child, Faraday Discuss. Chem. Soc. 62, 307 (1977).
4. G. Ewing, Chem. Phys. 29, 253 (1978).
5. J. A. Beswick and J. Jortner, J. Chem. Phys. 69, 512 (1978).
6. T. E. Gough, R. E. Miller and G. Scoles, J. Chem. Phys. 69, 1588 (1978).
7. M. A. Hoffbauer, W. R. Gentry and C. F. Giese, in Laser-Induced Processes in Molecules, edited by K. L. Kompa and S. D. Smith (Springer-Verlag, Berlin, Heidelberg, New York, 1979).

Chapter 2

Infrared Photodissociation Spectra of Clusters of C_2H_4 with C_2H_4, C_2F_4, Ar, Kr and Ne.

Infrared Photodissociation of van der Waals Molecules Containing Ethylene

Mike P. Casassa,[a] David S. Bomse,[b] and Kenneth C. Janda

Arthur Amos Noyes Laboratory of Chemical Physics,[c]

California Institute of Technology

Pasadena, California 91125

[a]National Science Foundation Predoctoral Fellow.

[b]Josephine de Karman Fellow and Monsanto Fellow.

[c]Contribution No. 6351.

Abstract

Vibrational predissociation lineshapes in the ν_7 region of the ethylene spectrum are measured for van der Waals molecules of ethylene bound to Ne, Ar, Kr, C_2H_4 and C_2F_4. The predissociative rate is very fast for this group of molecules. The range of vibrationally excited state lifetimes is 0.44 to 0.89×10^{-12} seconds for $(C_2H_4)_2$ and $C_2H_4 \cdot C_2F_4$. That the observed lineshapes are homogeneous is demonstrated by the fact that a low-power, narrow frequency bandwidth laser can dissociate a large fraction of the initial ensemble of ethylene clusters. The observed transition probability is proportional to the number of ethylene subunits for clusters containing three or fewer ethylene subunits. These observations are interpreted in terms of intramolecular energy flow directly from ethylene ν_7 to the weak van der Waals modes of motion.

I. INTRODUCTION

Van der Waals molecules present relatively simple systems for studying intramolecular vibrational energy flow. Klemperer[1] originally speculated that vibrationally excited $(HF)_2$ should dissociate within $5x10^{-11}$ sec based on an empirical half-collision V-T transfer model. Shortly thereafter, using Fermi's Golden Rule, Child[2] calculated lifetimes many orders of magnitude longer for Ar·HCl. Meanwhile, theoretical models[3] were unable to account for diffuse bands in infrared absorption spectra of gas phase hydrogen-bonded complexes.[4] These disparate themes have been reechoed for the most part in considerable subsequent experimental[5-18] and theoretical[19-30] work to understand energy transfer rates in weakly bound molecules.

In one such study Gentry et al.[17] found efficient dissociation of ethylene clusters with a pulsed CO_2 laser operating anywhere between 900 and 1100 cm^{-1}. This suggested the possibility of an exceedingly fast dissociation process. Subsequent experiments[31] with a low-power, cw CO_2 laser showed that the vibrational process is indeed fast, but at least an order of magnitude slower than suggested by the pulsed laser experiments.

In this paper we present a complete description of the cw CO_2 laser dissociation of ethylene dimer at 950 cm^{-1}. To provide additional insight we have also studied lineshapes for 950 cm^{-1} vibrational predissociation

of ethylene bound to Ne, Ar, Kr, C_2F_4 and larger ethylene clusters. Rates for this set of molecules are all in the range of $3x10^{12}$ sec^{-1} to 10^{12} sec^{-1} indicating that energy transfer out of the initially excited ν_7 mode of ethylene controls the order of magnitude of the rate. The qualitative variation of rate versus bonding partner is reasonable with regard to the theories of Beswick[19-23] and Ewing.[24-26] Unfortunately, this class of molecule is much too complicated to yield to a detailed application of theory.

II. EXPERIMENTAL

Van der Waals molecules were synthesized in supersonic expansions which were skimmed to form molecular beams. Molecular beam composition was determined by mass spectroscopy and controlled by varying the composition and pressure of the expanding gas mixture. Nearly complete cooling of internal degrees of freedom was ensured, and massive condensation was avoided by expanding mixtures containing a few percent of the van der Waals molecule constituents in a helium carrier gas. Infrared laser irradiation of the molecular beam using a low-power cw CO_2 laser resulted in photodissociation of a large fraction of the van der Waals complexes. In these experiments the laser-induced change in molecular beam composition was monitored as a function of laser wavelength and power.

A. Apparatus

A schematic of the molecular beam instrument is shown in Figure 1. Four levels of pumping are used so that low background pressures required for van der Waals molecule spectroscopy and mass spectrometry are maintained, despite the high throughput of the supersonic nozzle. Quartz nozzle sources were constructed by sealing one end of a quartz tube (0.8 cm OD, 0.2 cm ID) and then gently grinding until a pinhole of the desired size was formed. Flat nickel utility pinholes mounted on the end of a stainless steel pipe were also used as nozzle sources. The metal nozzles generally provided more van der Waals molecule intensity but were less durable and dependable than the quartz nozzles.

The source chamber (at the far left in Figure 1) is pumped by an unbaffled 4-inch Pennwalt Stokes booster pump backed by a Leybold-Heraeous E150 mechanical pump. Throughput of this configuration is 2800 torr cm^3 sec^{-1} at 10^{-2} Torr. The first aperture downstream of the nozzle is a skimmer (Beam Dynamics Model 2) with a 0.1-cm entrance diameter. Optimum nozzle-skimmer distance is $\sim$1.0 cm. Nozzle position is completely adjustable while all downstream apertures are fixed in optical alignment. Typically, gases at 5 to 10 atm and 300°K are expanded through a 35-μm pinhole while maintaining a background

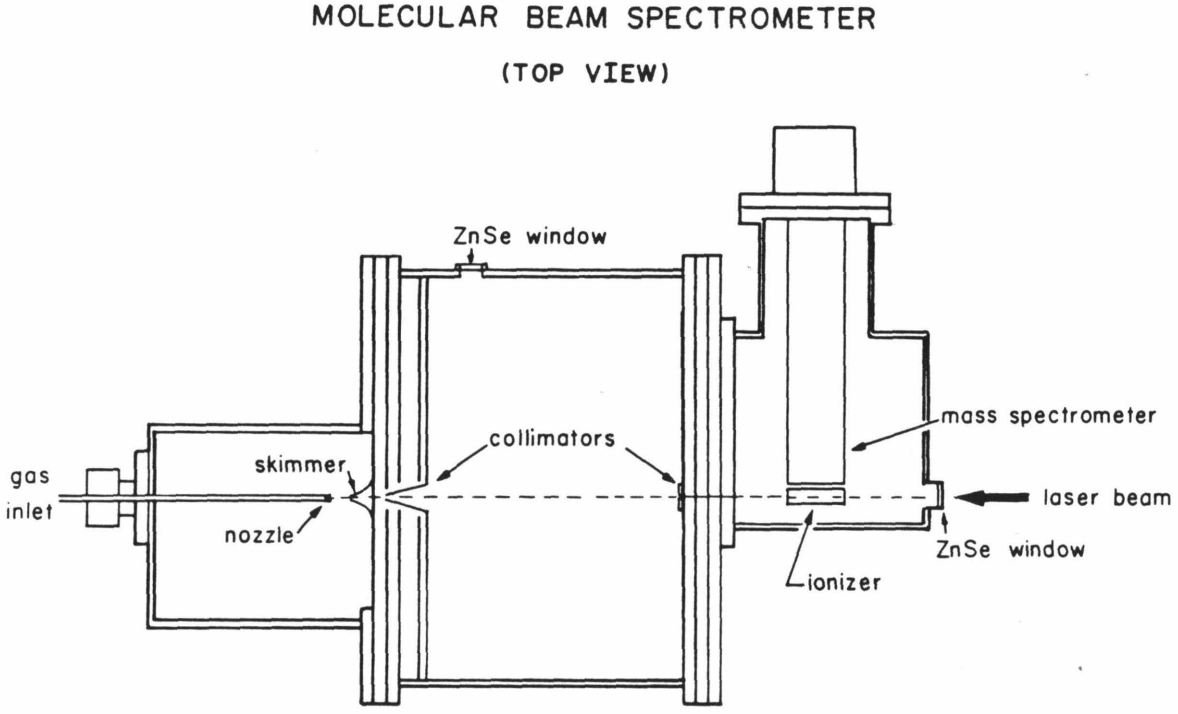

FIGURE 1. Schematic diagram of the molecular beam spectrometer. See Experimental Section for details.

pressure of the order of 10^{-3} Torr in the source chamber. The molecular beam emerging from the skimmer (moving left to right in Figure 1) traverses a 4.8-cm region of differential pumping before encountering a cone-shaped collimator with an entrance diameter of 0.2 cm. Differential pumping is supplied by an unbaffled 6-inch Varian VHS-6 diffusion pump which maintains a pressure in this region of $\sim 10^{-5}$ Torr during operation. Passing through the first collimator, the molecular beam enters the largest vacuum chamber and travels 40.5 cm further to a second collimator. Pressure in the main chamber is maintained at 10^{-6} Torr by an Edwards 160/700 diffusion pump having an internal water-cooled baffle. After the second collimator, the molecular beam enters a fourth vacuum chamber (far right in Figure 1) which houses an Extranuclear quadrupole mass spectrometer equipped with a crossed-beam electron impact ionizer and channeltron particle multipler. The mass spectrometer chamber is pumped by an Edwards CR-760 diffusion pump equipped with internal water and nitrogen-cooled baffles which provide ambient pressures of $\sim 10^{-8}$ Torr during experiments. The second collimator, with a 0.24 cm aperture, defines the diameter of the molecular beam detected by the mass spectrometer. Total distance from the nozzle source to the ionizer of the mass spectrometer is 60 cm corresponding to a molecular flight time of the order of 0.5 msec.

An Apollo Laser Model 550A grating-tuned cw CO_2 laser was used in these experiments. The laser linewidth is estimated by the manufacturer to be $\sim$50 MHz. For most infrared photodissociation studies, the unfocused laser beam was directed into the apparatus through a ZnSe window (supplied by II-VI Incorporated) indicated at the far right in Figure 1. The laser beam and molecular beam were colinear in this configuration and irradiation time of species in the molecular beam was maximized. In one experiment the unfocused laser beam was directed into the apparatus through the auxiliary window (Figure 1, top) and crossed the molecular beam at right angles before being absorbed by a graphite beam stop.

Laser beam quality was monitored with an Optical Engineering Model 22A thermal imaging plate. When optimized (by visual inspection on the imaging plate), the beam profile was nearly Gaussian (FWHM = 6 mm) as determined by measuring the power transmitted through a 1-mm diameter pinhole translated across the beam. However, reproducible variations in mode structure were observed as the laser wavelength was changed. As decribed above, the detected molecular beam is 0.24 cm in diameter and thus only interacts with the central portion of the laser beam.

Measurements of the infrared beam intensity within the largest chamber of the apparatus indicated that 4 to 7% of the total incident laser power was transmitted through the mass spectrometer chamber apertures. This attenuation

was only partly due to losses at optical surfaces. The transmitted power loss was mainly due to the small apertures in the molecular beam apparatus and was thus extremely sensitive to the transverse mode structure of the laser beam. Irradiances were calculated using calibration constants obtained for each set of photodissociation experiments. Power measurements were made with a Laser Precision Corporation Model RkP-345 pyroelectric radiometer. Temporal fluctuations in laser power were less than ±5% during an experiment. Infrared laser wavelengths were measured with an Optical Engineering Model 16A spectrum analyzer.

For infrared photodissociation experiments performed with colinear laser and molecular beams, the laser beam was mechanically chopped (usually 100-150 Hz). The intensity of a given peak in the molecular beam mass spectrum was measured both in the presence and absence of infrared radiation using a two-channel boxcar. Direct electronic division of the two values gave the fractional change in mass spectrometer signal intensity due to laser irradiation. Fine adjustments in laser beam position were made to maximize extent of photodissociation. For the experiment performed with the crossed-beam arrangement, the infrared beam was chopped at 1000 Hz, and resulting changes in mass spectrometer signal were measured using a lock-in amplifier.

Infrared photodissociation spectra were obtained by measuring attenuation of mass spectrometer signals while tuning the CO_2 laser from line to line and maintaining constant laser power. Beam quality and power were optimized with each change of wavelengths by adjusting laser optics. Laser power was then brought to some standard value by adjusting the discharge current in the laser. Most spectra were recorded using 5.0 W total laser power corresponding to irradiances of 4.0 to 6.7 W cm^{-2} (depending on transverse mode structure) transmitted to the molecular beam. The dependence of infrared photodissociation intensity on laser power at fixed laser frequency was also measured. Irradiance was varied in the range of 0 to 11 W cm^{-2} in the power dependence experiments.

B. Characterization of Detected Clusters

As indicated above and in Figure 1, molecular beams were characterized using a quadrupole mass spectrometer equipped with an electron impact ionizer. A typical molecular beam mass spectrum is shown in Figure 2. The crossed-beam ionizer was set to deliver 2.5 mA electron current at 50 eV electron kinetic energy. Considerable fragmentation of van der Waals molecules resulted upon electron impact ionization under these conditions. Careful analysis of mass spectra was needed in order to make unambiguous identification of neutral cluster molecules

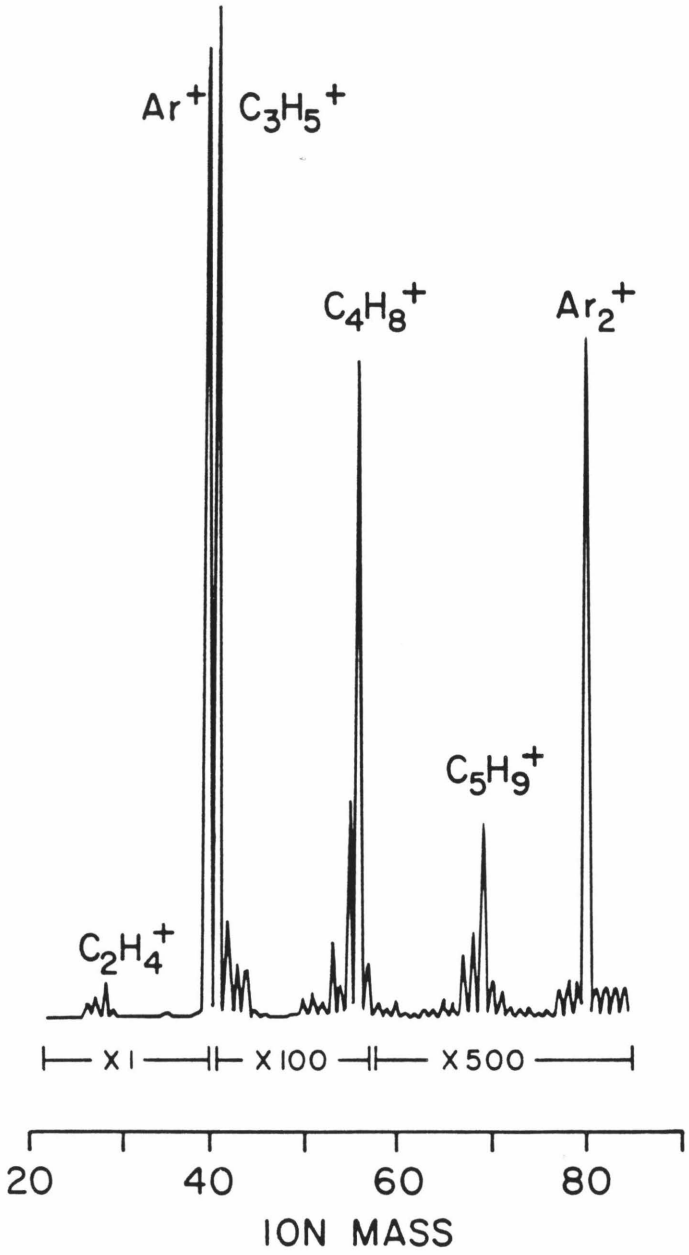

FIGURE 2. Molecular beam mass spectrum indicating formation of ethylene clusters. Note changes in detector sensitivity. Molecular beam formed by expanding 7.7 atm of a mixture of C_2H_4, Ar, and He (0.8:10:90). Nozzle diameter is 50 μm.

present in the molecular beam. Figure 3 shows a plot of mass spectrum ion intensities as a function of source pressure for a C_2H_4-Ar-He (ratio 0.75:20:80) mixture. In Figure 3 both scales are logarithmic. Only those ions not produced by ionization of C_2H_4 or Ar monomers are considered. At low pressures the most abundant species is the parent ion of argon dimer, Ar_2^+ at m/e 80. As the backing pressure is increased, $Ar^+C_2H_4$ is observed. The next group of ions detected as the pressure is increased further are the two at m/e 41 $(C_3H_5)^+$ and m/e 55 $(C_4H_7^+)$. Data points for these two species lie on nearly parallel lines (Figure 3) with slopes 2.6 and 2.3 for $C_3H_5^+$ and $C_4H_7^+$, respectively. The ion notionally identified as ethylene dimer parent ion (m/e 56) shows a higher order pressure dependence than the $C_3H_5^+/C_4H_7^+$ pair. $(C_2H_4)_2^+$ is not formed from ethylene dimer. This result is consistent with reported ion-molecule reactions of ethylene,[32] where it is observed that $C_3H_5^+$ and $C_4H_7^+$ are the principal products of the reaction of $C_2H_4^+$ with C_2H_4.

Data such as those shown in Figure 3 were obtained for all gas mixtures used. Analysis similar to that described above determined identity of molecular beam constituents and optimum source conditions for production of a desired van der Waals cluster. Except as noted, in studies of selected van der Waals molecules the gas mixtures and pressure were adjusted so that large clusters were not present and interfering cluster concentrations

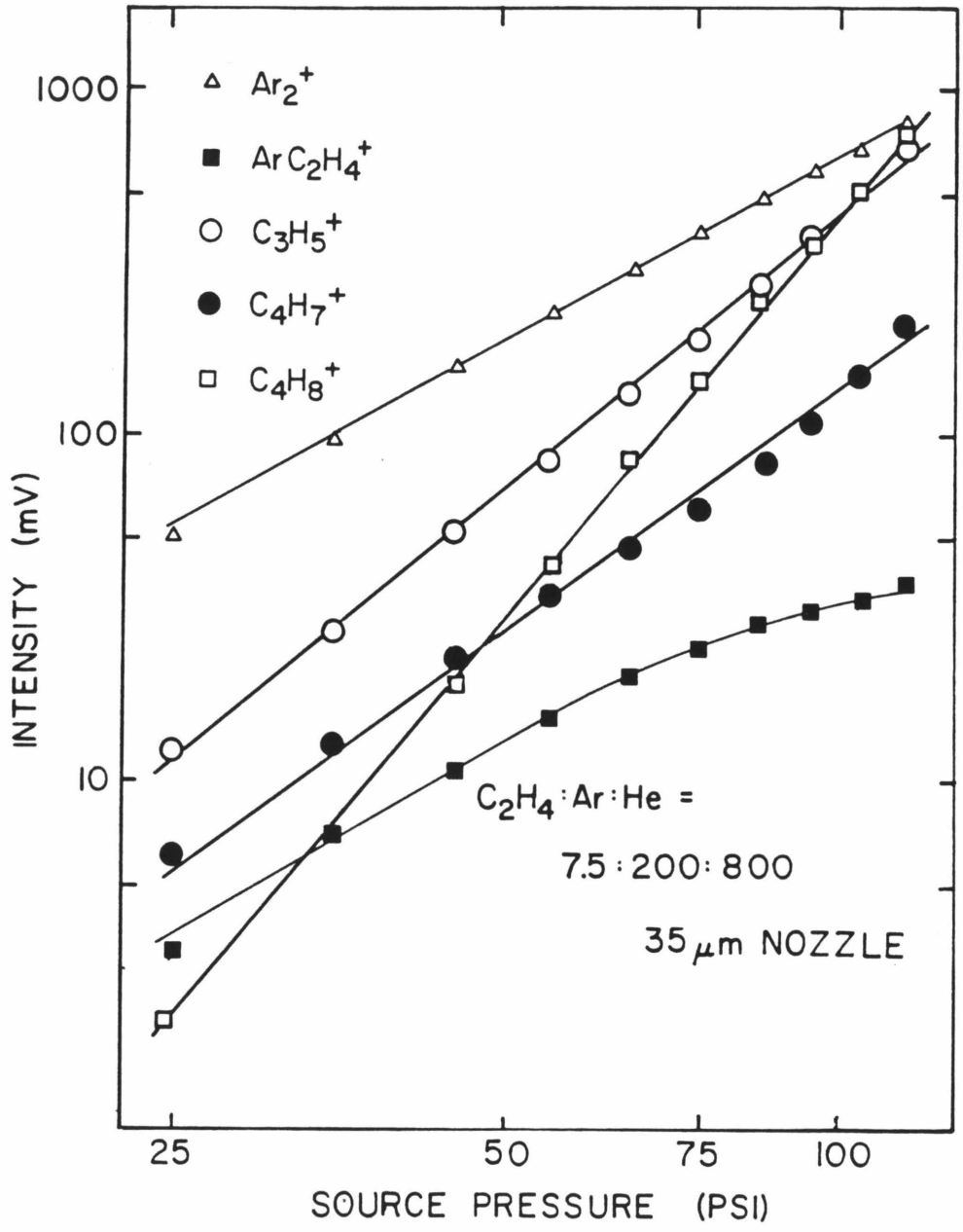

FIGURE 3. Variation of van der Waals molecules mass spectral intensity with source pressure. Both scales are logarithmic. Data for Ar_2^+, $ArC_2H_4^+$, $C_3H_5^+$, $C_4H_7^+$ and $C_4H_8^+$ are included. Gas mixture is 0.75% C_2H_4, 20% Ar and 80% He.

were minimized. Complications occur if different van der Waals clusters present in the molecular beam contribute to the same mass signal. For example, $ArC_2H_4^+$ and fragments of pure ethylene clusters ($C_5H_8^+$) contributed to the mass spectrum signal intensity at m/e 68 observed in molecular beams formed from He-Ar-C_2H_4 mixtures. The intensity of the m/e 68 signals observed in molecular beams formed by expansion of pure ethylene and He-C_2H_4 mixtures was generally about 10% of the intensity of m/e 69 ($C_5H_9^+$) fragments. Accordingly, conditions employed in the study of $Ar \cdot C_2H_4$ were such that the m/e 69 intensity was less than 2% of the m/e 68 signal. A similar situation arose in the study of $Kr \cdot C_2H_4$. In this case, the expansion conditions were adjusted so that ratios of $KrC_2H_4^+$ signals corresponding to isotopic $Kr \cdot C_2H_4$ van der Waals molecules were identical to the relative abundance of naturally occurring Kr isotopes. These considerations ensure that the $KrC_2H_4^+$, $ArC_2H_4^+$ and $NeC_2H_4^+$ signals measured reflect behavior of species containing only one ethylene molecule. Such a determination with respect to the number of rare-gas atoms present is more difficult. Recent work, presented in Chapter 7, indicates that the data reported here for $ArC_2H_4^+$, and presumably for $KrC_2H_4^+$, are due to photodissociation of clusters which contain at least two noble gas atoms.

The problem of maximizing production of mixed bimolecular clusters and cooling their internal degrees of

freedom while minimizing other cluster concentrations is somewhat of an art form. It has proved useful[33] to think in terms of a kinetic scheme such as:

$$Ar + Ar + He \longrightarrow Ar_2 + He$$
$$Ar_2 + C_2H_4 \longrightarrow Ar \cdot C_2H_4 + Ar$$
$$Ar \cdot C_2H_4 + C_2H_4 \longrightarrow (C_2H_4)_2 + Ar$$

Insofar as this picture is correct, the He carrier gas is important because it can provide cooling collisions that only rarely produce clusters containing He. In a fluorescence excitation study of van der Waals complexes of tetrazine and noble gases, addition of a few percent argon to helium carrier gas containing a trace of tetrazine inhibited formation of helium complexes and only Ar complexes were observed.[34]

The role of Ar in the expansion is to provide the seed reaction for cluster formation, in effect catalyzing the condensation process. Ethylene-containing clusters are formed by exchange reactions with Ar_2. It is empirically observed that when Ar is not in the mixture, the formation of ethylene dimer is inhibited. If this is overcome by raising the source pressure or the concentration of ethylene in the expansion mixture, large ethylene clusters are produced before the dimer experiences enough collisions to be rotationally cooled. It is especially important to

optimize source parameters in van der Waals dissociation experiments because individual states are not resolved in the spectroscopy.

C. Molecular Beam Velocities

A knowledge of molecular beam velocity and hence the period of time molecules are irradiated is necessary for interpretation of photodissociation intensities. Velocities were calculated using a supersonic expansion model, since our apparatus is not equipped to measure directly molecular beam velocity distributions. We assume that the molecules in the beam achieve the terminal velocity of the expansion[35] given by

$$V_T = (2C_pT_s/M)^{\frac{1}{2}} , \qquad (1)$$

where C_p is the heat capacity of the expanding gas, T_s is the source temperature, and M is the molecular weight. Since expansions of gas mixtures were used in these experiments, the molecular weight is replaced by an effective mass:

$$M_e = \sum_i m_i F_i \quad . \qquad (2)$$

F_i is the mole fraction and m_i is the mass of a component of the expansion mixture. Similarly, the heat capacity in eq. (1) is replaced by an effective heat capacity:

$$C_{p_e} = k \sum_i (1 + \frac{N_i}{2}) F_i \ . \qquad (3)$$

In eq. (3), k is Boltzmann's constant and N_i is the number of relevant degrees of freedom in an expansion component. N_i includes only translational and rotational degrees of freedom since vibrational degrees of freedom are not expected to participate strongly in the cooling process.

The heat of formation of van der Waals molecules is neglected in this analysis, since only a small fraction of molecules are allowed to condense. Also, the high pressure expansion conditions will minimize the slip between rare gas atoms and van der Waals molecules. This velocity analysis is borne out in velocity measurements of Janda et al.[36] Irradiation times were determined from the 60-cm flight distance and calculated velocities.

III. RESULTS

Infrared photodissociation was observed for all ethylene-containing van der Waals molecules studied. Identities of the clusters along with ion fragments monitored and calculated irradiation times are listed in Table I. Also tabulated are gas mixtures and source conditions

TABLE I. Experimental Conditions for Production of Ethylene-Containing Clusters in Molecular Beams.

Cluster	Gas Mixture	Nozzle Diam. (m)	Pressure (psi)	Irradiation Time (ms)	Ion Detected
$(C_2H_4)_2$	0.7% C_2H_4 + 20% Ar + 80% He	35	51.5	0.57	$C_3H_5^+$
$(C_2H_4)_3$	0.7% C_2H_4 + 20% Ar + 80% He	35	51.5	0.57	$C_4H_8^+$
$(C_2H_4)_5$	11% C_2H_4 + 39% Ar + 50% He	25	290.0	0.75	$C_{10}H_{20}^+$
$(C_2H_4)_7$	11% C_2H_4 + 39% Ar + 50% He	25	290.0	0.75	$C_{14}H_{28}^+$
$C_2H_4 \cdot C_2F_4$	0.7% C_2H_4 + 0.5% C_2F_4 + 20% Ar + 80% He	35	111.0	0.58	$C_3H_4F^+$ a)
$Ne \cdot C_2H_4$	0.5% C_2H_4 + 89.5% Ne + 10% He	35	215.0	0.76	$^{20}NeC_2H_4^+$
$Ar \cdot C_2H_4$	0.3% C_2H_4 + 20% Ar + 80% He	35	215.0	0.57	$ArC_2H_4^+$
$Kr \cdot C_2H_4$	0.5% C_2H_4 + 22% Kr + 78% He	50	65.0	0.79	$KrC_2H_4^+$ b)

a) Identical results obtained when monitoring $C_3H_3F_2^+$. These ions are major products of the reaction of $C_2H_4^+$ with C_2F_4.[37]

b) Sum of all Kr isotopes.

used to produce the complexes. Figure 4 shows infrared photodissociation spectra of ethylene dimer and ethylene trimer. Data for this figure as well as for all spectra shown below were obtained using coaxial laser and molecular beams. Note that the spectra are plotted with logarithmic ordinates. The reason for this choice is presented in the discussion section. The solid lines shown in the spectra are nonlinear least-squares fits of a lineshape function described in the discussion section. Both spectra shown in Figure 4 consist of a single symmetric band, centered at $\sim$ 952 cm^{-1}, and both exhibit the same width. The photodissociation cross section of ethylene trimer is larger than that for $(C_2H_4)_2$ at all laser wavelengths shown. Only 6.7 W cm^{-2} was used to obtain data shown in Figure 4, yet it was possible to dissociate 25% of the dimer and 50% of the trimer.

Figure 5 shows photodissociation spectra of large ethylene cluster, notionally $(C_2H_4)_5$ and $(C_2H_4)_7$ which have nearly identical photodissociation bandshapes and photodissociation cross sections. Spectra obtained monitoring $(C_2H_4)_5$ and $(C_2H_4)_7^+$ are thought to be typical of large clusters and not due solely to $(C_2H_4)_5$ and $(C_2H_4)_7$. These spectra exhibit essentially the same width as ethylene dimer and trimer spectra.

Irradiation of ethylene clusters in the crossed laser beam-molecular beam configuration yielded the same wavelength dependence observed in the colinear-geometry experi-

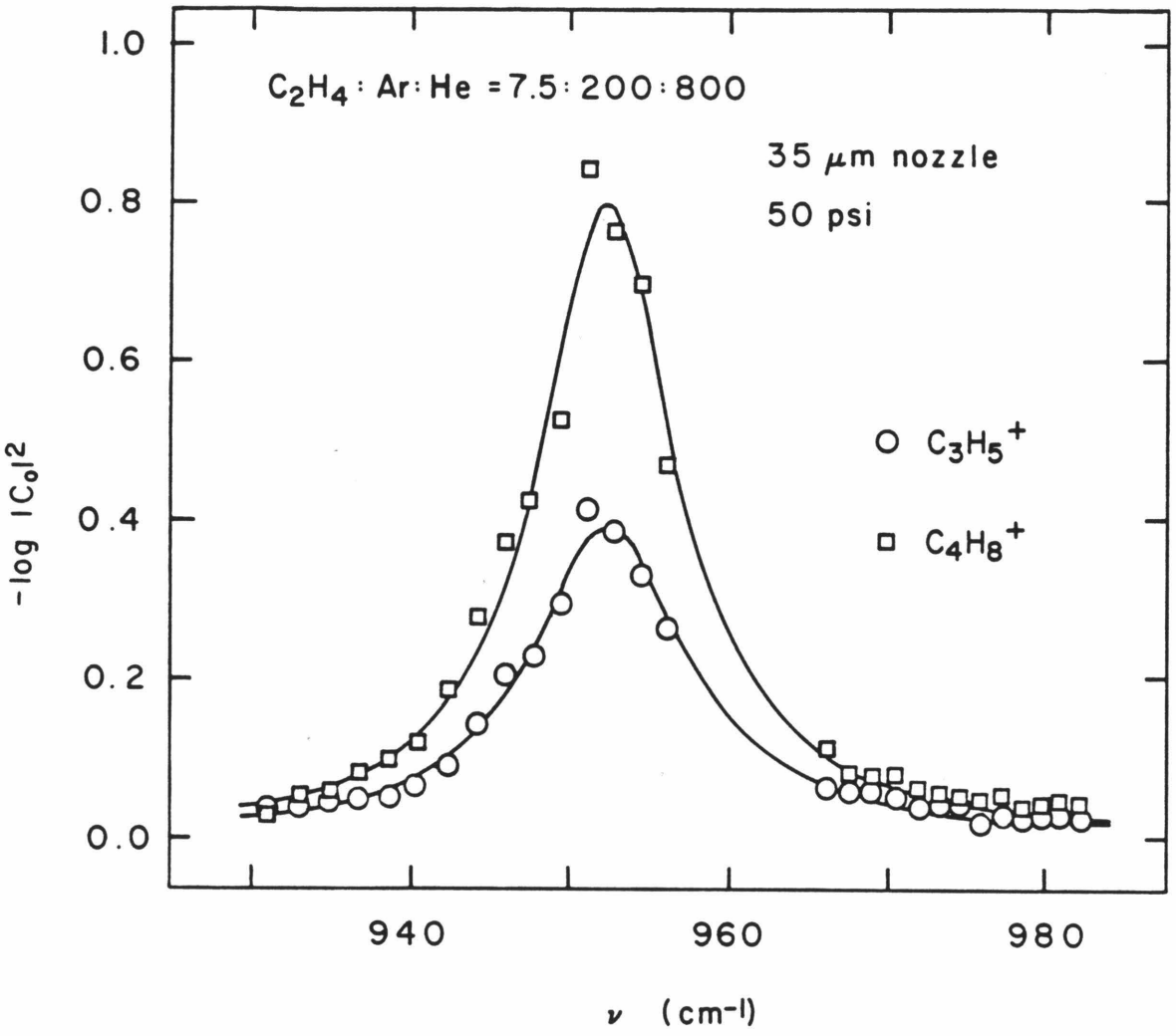

FIGURE 4. Infrared photodissociation spectra of $(C_2H_4)_2$ and $(C_2H_4)_3$. The solid lines are least-squares best fits of Eq. (6). The dimer is detected as $C_3H_5^+$ and the trimer is detected as $C_4H_8^+$. No photodissociation of either species is observed at CO_2 laser wavelengths > 1000 cm^{-1}. Laser intensity is 6.7 W cm^{-2}. Molecular beam conditions are listed in Table I. $|C_0|^2$ is the fraction of undissociated van der Waals molecules.

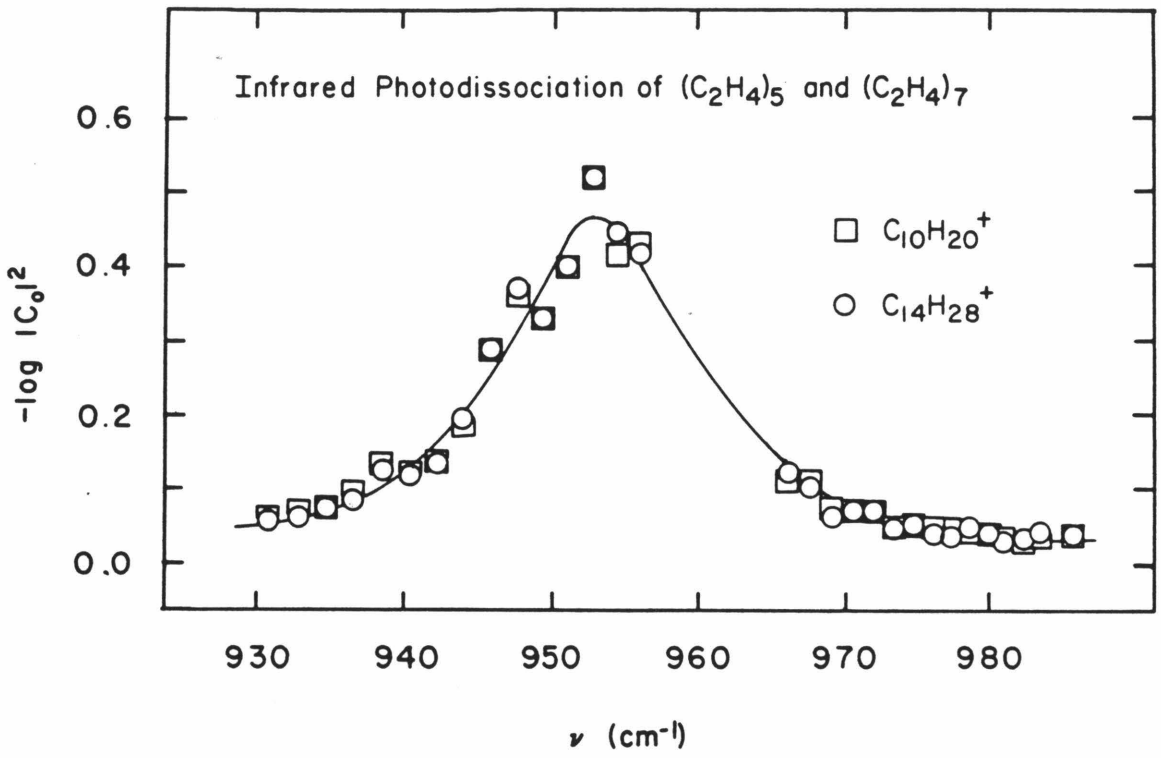

FIGURE 5. Infrared photodissociation spectra of large clusters detected as $(C_2H_4)_5^+$ and $(C_2H_4)_7^+$. The solid lines are least-squares best fits of Eq. (6). No photodissociation of either species is observed at CO_2 laser wavelengths >1000 cm^{-1}. Laser intensity is 6.7 W cm^{-2}. Molecular beam conditions are listed in Table I.

ments. In the crossed-beam experiment photodissociation yield of ethylene trimer was only ~0.005 at 953 cm^{-1} due to the short irradiation time. Relative cross sections for dissociation of $(C_2H_4)_3$ and $(C_2H_4)_2$ are identical for both types of experiments. This indicates inhibition of cluster formation caused by heating of the expansion by the laser beam does not occur. Consideration of the relative probabilities for photon absorption and quenching collisions in the expansion also vitiates expansion heating as a cause of cluster loss. Observed infrared photochemistry is the result of excitation and decomposition of isolated van der Waals molecules.

Changes in laser intensity in the range of 1 to 10 W cm^{-2} do not alter photodissociation bandwidths. Furthermore, the width and position of photodissociation profiles are independent of expansion conditions as ethylene concentration is varied from 0.5% to 5% and stagnation pressure is varied from 65 to 115 psi.

Figure 6 shows the laser power dependence of the logarithm of the fraction of undissociated van der Waals molecules. Data are shown for $(C_2H_4)_2$ and $(C_2H_4)_3$. The laser wavelength is fixed at a frequency close to the peaks of the photodissociation spectra. Similar data were obtained for all of the van der Waals clusters listed in Table I. In each case, semilog plots of power dependence data points lie on straight lines suggesting a Beer's Law-type relationship.[31]

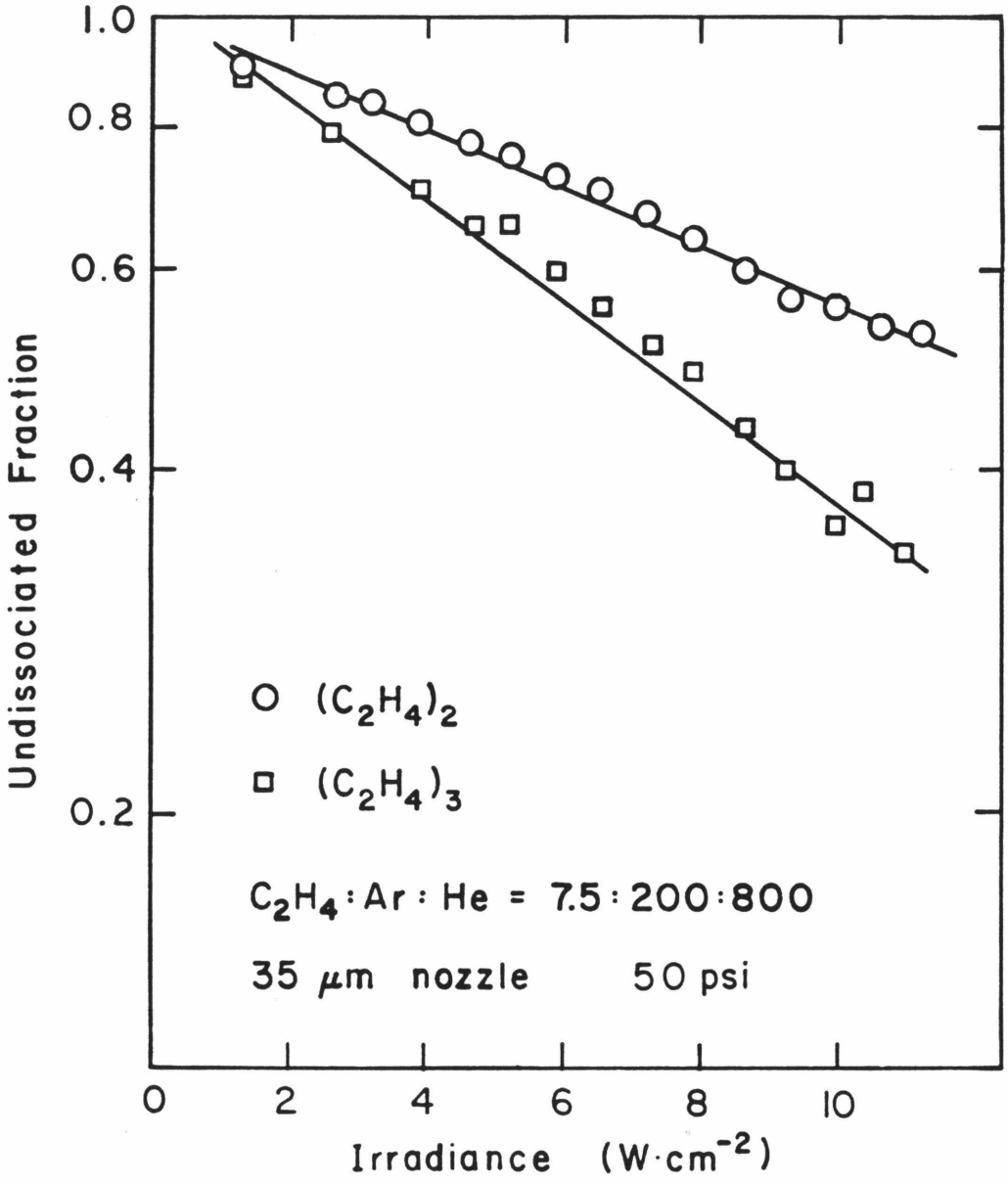

FIGURE 6. Measured power dependence of infrared photodissociation of $(C_2H_4)_2$ and $(C_2H_4)_3$. Ordinate is logarithmic. Laser wavelength is nearly identical to λ_{max} for infrared photodissociation spectra of these van der Waals molecules.

The wavelength dependence for $C_2F_4 \cdot C_2H_4$ photodissociation is shown in Figure 7. Data for ethylene dimer are also shown for comparison. The spectra exhibit characteristic width, position, and photodissociation efficiency. The $C_2F_4 \cdot C_2H_4$ spectrum is narrower and shifted to the blue compared to pure ethylene clusters.

Qualitative differences appear in the spectra of complexes of ethylene and noble gas atoms shown in Figure 8. As in the pure ethylene cluster spectra, a broad symmetric peak is observed near 950 cm^{-1} in the spectra observed for $KrC_2H_4^+$ and $ArC_2H_4^+$. However, in the spectra shown in Figure 8 a second broad feature of lower intensity is discernible near 970 cm^{-1}. For $KrC_2H_4^+$ this appears as a broad shoulder of the main peak, while it is clearly resolved in the $ArC_2H_4^+$ data. The $NeC_2H_4^+$ data are still more enticing. Unfortunately, the signal-to-noise ratio in the NeC_2H_4 experiments is quite low since it is difficult, even in strong expansion to synthesize $Ne \cdot C_2H_4$ clusters in detectable concentrations. Results presented in Chapter 7 indicate that the broad envelope in the $C_2H_4Ar^+$ data is due to $Ar_n \cdot C_2H_4$, with $n \geq 2$, while the underlying structure is due to $Ar \cdot C_2H_4$. Presumably this occurs for $C_2H_4Kr^+$ as well.

No dissociation was detected at energies higher than 1000 cm^{-1} for any of the van der Waals molecules listed in Table I. Therefore, data for only half of the CO_2 laser wavelength range are presented. Resolution of the spectra

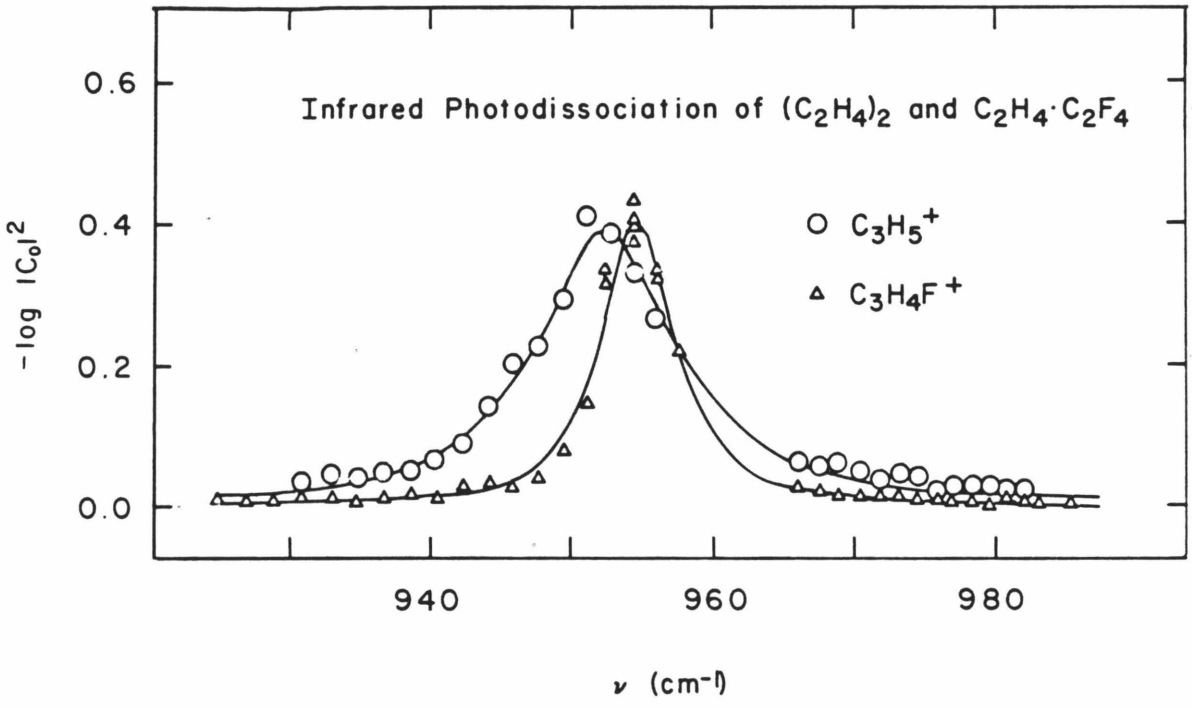

FIGURE 7. Infrared photodissociation spectra of $(C_2H_4)_2$ and $C_2H_4 \cdot C_2F_4$. $(C_2H_4)_2$ data as in Figure 1. The solid curves are least-squares best fits of Eq. (6). $C_2H_4 \cdot C_2F_4$ is monitored using $C_3H_4F^+$. No photodissociation at CO_2 laser wavelengths > 1000 cm^{-1} is observed. Laser intensity is 6.7 W cm^{-2}. Molecular beam conditions are listed in Table I.

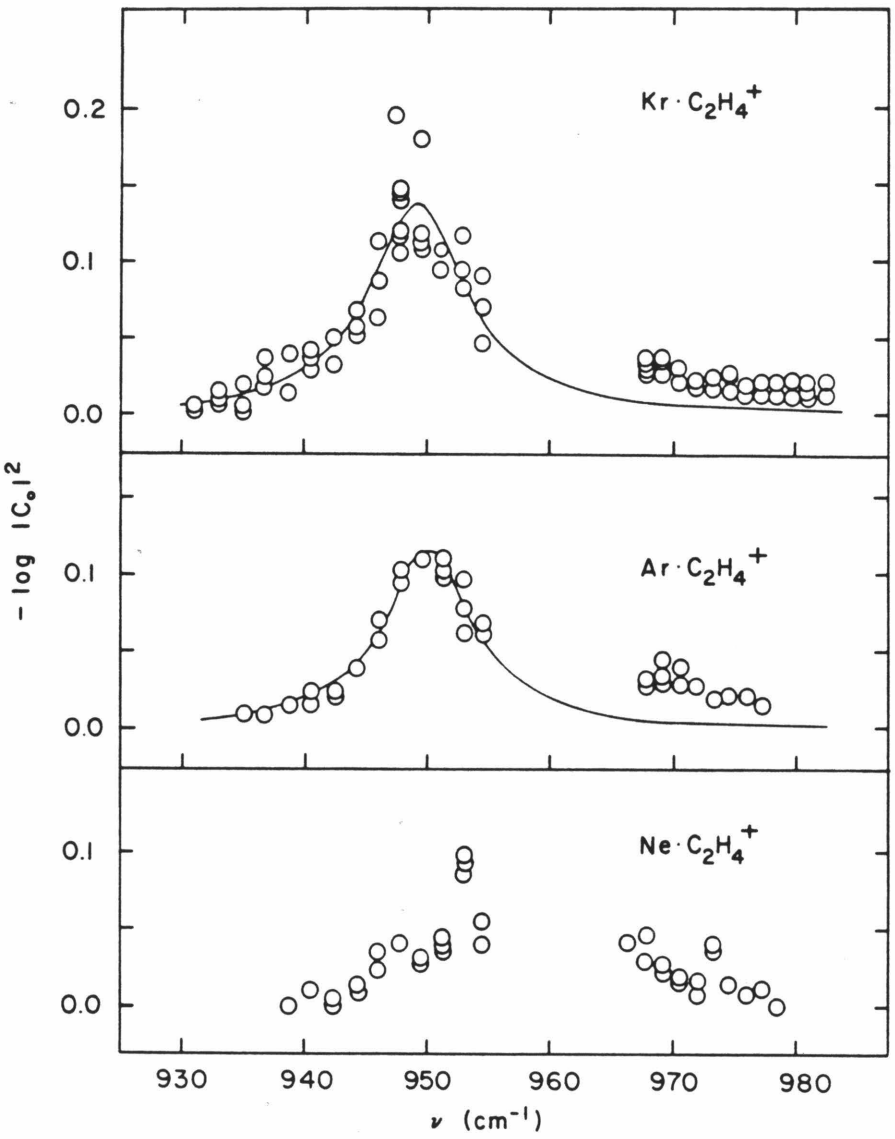

FIGURE 8. Infrared photodissociation spectra observed monitoring of $KrC_2H_4^+$, $ArC_2H_4^+$ and $NeC_2H_4^+$. The solid curves are least-squares best fits of Eq. (6) to data obtained at frequencies less than 960 cm^{-1}. No photodissociation at CO_2 laser wavelengths > 1000 cm^{-1} is observed. Laser intensity is 4.0 W cm^{-2}. Molecular beam conditions are listed in Table I.

is limited by the discrete tunability of the CO_2 laser. The large gap from 955 cm^{-1} to 965 cm^{-1} in all of the spectra presented corresponds to weakly populated or forbidden transitions of the $00^01\text{-}10^00$ band of CO_2. Scatter in the data is mainly due to changes in laser mode structure and hence changes in irradiance along the molecular beam with tuning.

IV. DISCUSSION

The broad, symmetric bandshapes observed in spectra obtained in this study are characteristic of lifetime-broadened transitions. Linewidths are determined by rates of predissociation of the vibrationally excited states of the van der Waals molecules. This interpretation requires that the nature of the initially prepared state and broadening mechanisms be understood. Furthermore, homogeneity of the observed spectra must be well established. These points are taken up individually in the discussion below. Together, these considerations lead to a simple model and lineshape formula for the photodissociation process which are in excellent agreement with our observations. By comparing vibrational predissociation lifetimes of similar molecules some of the criteria that govern intramolecular vibrational energy transfer can be determined. In addition to vibrational predissociation rates, transition moments

for infrared absorption can be extracted from data presented.

A. Vibrational Transitions in Ethylene Clusters

The ethylene molecule has four modes of vibration (ν_4, ν_7, ν_8 and ν_{10}) which are within or near the frequency range of the CO_2 laser. The vibrational modes and frequencies of ethylene and perfluoroethylene are listed in Table II for convenience. All other modes are not relevant to this experiment since they are higher in energy and far removed from the observed absorption frequencies. The ν_4 mode is neither infrared nor Raman active. Consistent with this we see no dissociation of ethylene clusters for laser frequencies near 1027 cm^{-1}. For all molecules studied there was efficient dissociation near 950 cm^{-1}. This corresponds to strongly allowed excitation of the ν_7 mode in ethylene. In this mode the hydrogen atoms are moving together above and below the equilibrium plane. Motion of the nearly degenerate infrared inactive ν_8 mode is similar except that opposite ends of the molecule are out of phase. This mode becomes weakly infrared active as the ethylene molecule is perturbed by van der Waals bonding. In general, this perturbation is weak and ν_8 absorption is expected to be insignificant compared to ν_7 absorption. C_2F_4 has no modes (Table II) which absorb in the range of the CO_2 laser. We thus conclude that for Ar, Kr, Ne, and

TABLE II. Fundamental Frequencies of C_2H_4 and C_2F_4.

		C_2H_4 [a]		C_2F_4 [b]
Mode	Symmetry	Frequency (cm^{-1})	Description	Frequency (cm^{-1})
ν_1	A_{1g}	3019.3	R	1872
ν_2		1623.3		778
ν_3		1342.4		394
ν_4	A_{1u}	1027.0	Inactive	190
ν_5	B_{1g}	3272.3	R	1340
ν_6		1236.0		551
ν_7	B_{1u}	949.2	IR,s	406
ν_8	B_{2g}	940.0[c]	R,w	508
ν_9	B_{2u}	3105.5	IR	1337
ν_{10}		825.9[c]	w	218
ν_{11}	B_{3u}	2989.5	IR	1186
ν_{12}		1443.5		558

[a] Ref. 38, except as noted.

[b] Ref. 39.

[c] Ref. 40.

C_2F_4 bound to ethylene the laser photon is absorbed by a mode similar to ν_7 in free ethylene. Due to symmetry requirements, the absorbing mode in ethylene dimer must be an infrared active combination of the ν_7 motion of each partner. The nature of this combination is discussed more fully below.

Except for $C_2F_4 \cdot C_2H_4$, the observed absorption band center is shifted only slightly from the ν_7 fundamental of free ethylene. It thus seems justified that the vibrational mode excited in cluster-bound ethylene be considered as only slight perturbed. The excited state of the complex can then be considered to be a discrete state imbedded in a dissociative continuum. See Chapter 5 for a discussion of an electrostatic mechanism for the frequency shifts.

B. Nature of the Lineshape for Cluster Excitation

It is crucial to the arguments of this study and of other similar studies that the nature of observed spectral broadening be unambiguously determined. The reported experiments have the advantage that changes in initial population are observed directly. When the ethylene dimer is irradiated with 11 W/cm^2 of laser flux, 50% of the initial population is lost from the molecular beam even though the laser linewidth is $\sim$50 MHz. In a plot of fraction dissociated versus laser irradiance, as shown in Figure 6, a Beer's Law relationship is seen with no

leveling off of the fraction dissociated at the highest laser irradiance available to us. It is clear that the narrow laser bandwidth is interacting with the whole ensemble of molecules. The transition must be dominated by homogeneous broadening.

Unfortunately, our experiment gives no direct measurement of rotational or translational temperature, although similar experimental conditions are known to produce rotational temperatures of less than 1 K .[34] Such a measurement would be useful in light of the fact that vibrational predissociation spectra of $(N_2O)_2$[16] and $(CO_2)_x$[41] are plainly inhomogeneous. In comparing our experimental conditions to those of Gough et al.[16,41] we note that since a large fraction of ethylene dimer is dissociated, it is possible to use very dilute (down to 0.5%) mixtures of ethylene behind the nozzle. This allows for very efficient rotational cooling. Using 10% ethylene mixtures comparable to those used by Gough et al.[16] in their N_2O study leads to formation of large fractions of higher polymer. Under these conditions, it would be likely that ethylene dimer is not effectively cooled.

In molecular beam electric resonance experiments of large van der Waals molecules similar in complexity to ethylene dimer, e.g. $BF_3 \cdot CO$,[42] no van der Waals hot bands could be observed even though relatively mild expansion conditions, P_o = 800 Torr, were used. Finally, when ethylene concentration was varied from 0.5% to 5% and P_o

was varied from 4.3 atm to 7.7 atm, no change in the dimer lineshape was observed. All of the above observations support the claim that the observed lineshapes for $(C_2H_4)_2$ and $C_2H_4 \cdot C_2F_4$ are dominated by homogeneous broadening.

For $(Ar)_nC_2H_4$ and $(Kr)_nC_2H_4$ there are clear features to the high energy side of the main peak. These features cannot be ascribed to rotational structure due to a thermal distribution of initial state rotational levels. The width of such an inhomogeneous rotationally broadened transition measured between maxima of the P and R branches is given by $(8kTB)^{\frac{1}{2}}$. Assuming a structure analogous to that of $Ar \cdot C_2H_2$,[43] $Ar \cdot C_2H_4$ at 1 K would have an absorption bandwidth of approximately 1.7 cm^{-1}. Larger $(Ar)_nC_2H_4$ clusters would be still narrower. Conversely, the $Ar \cdot C_2H_4$ rotational temperature calculated from the observed spectrum, assuming rotational inhomogeneity, is greater than 100 K, which is unreasonable. Together with the efficient dissociation observed, these considerations indicate that the main parts of these spectra are essentially homogeneous.

C. Broadening Mechanism

The most satisfying explanation of the observed linewidth is that the lifetime of the initially excited state is limited by the rate of vibrational predissociation. For each of the molecules in this study this would imply a vibrational predissociation rate of greater

than 10^{12} sec^{-1}. These rates are one to two orders of magnitude faster than any observed by Levy et al.[5-15] in their study of van der Waals molecules containing I_2. Even for $H_2 \cdot I_2$, where the I_2 and van der Waals bond-stretching motions are of similar frequency, the predissociation rate is only 5×10^{10} sec^{-1}.[15] The observed widths of the ethylene spectra are also an order of magnitude greater than those of Gough et al. for $(N_2O)_2$[16] and $(CO_2)_2$.[41] Are such fast predissociation rates reasonable?

First, it is useful to consider the molecule $Ar \cdot C_2H_4$ as a prototypical ethylene cluster. In this case it is possible to make a reasonable estimate of the molecular structure by comparison with $Ar \cdot C_2H_2$.[43] $Ar \cdot C_2H_2$ is a "T-shaped" molecule with Ar located 3.2 Å from the acetylene molecular axis. The dipole moment of $Ar \cdot C_2H_2$ is 0.02 Debye, indicating that acetylene bond angles are unaffected by Ar. This supports the above supposition that monomer vibrational modes are only weakly affected by formation of a weak bond. Another interesting aspect of $Ar \cdot C_2H_2$ is that the vibrational potential for bending of the "T" is very flat. This may indicate that even in the ground vibrational state of the molecule the bending amplitude is such that there is direct interaction between the hydrogen atoms and the Ar atom.

The Ar-ethylene interaction should be much the same as Ar-acetylene, resulting in a "T-shaped" configuration with Ar above the plane defined by the hydrogen atoms.

There are three normal modes of motion associated with the weak bond: a stretch, and bends parallel and perpendicular to the carbon axis. It is of interest to speculate how these weak modes interact with the vibrationally excited ν_7 mode of ethylene.

The change of vibrational amplitude upon excitation of ν_7 can be determined by comparing root mean square bending angles, β, given by:

$$\langle\beta^2\rangle^{\frac{1}{2}} = (h/2\pi\nu_b m_b)^{\frac{1}{2}} (v_b + 1/2)^{\frac{1}{2}} \qquad (4)$$

in the ground and excited states. ν_b is the ν_7 bending frequency, v_b is the vibrational quantum number, and m_b is an effective bending reduced mass (units of gm cm^2). Herzberg[44] gives the equation for the frequency of the ν_7 mode which defines m_b:

$$4\pi^2\nu_7^2 = \frac{m_C + m_H}{2m_C m_H \ell_2^2 \cos^2(\alpha/2)} k_b = \frac{k_b}{m_b} \qquad (5)$$

The bending force constant is k_b, m_H and m_C are hydrogen and carbon masses, ℓ_2 is the C-H bond length and α is the H-C-H angle. Putting in numbers leads to the result that

the rms amplitude due to zero point motion of ν_7 is 7°, while the rms amplitude of the first excited level is 13°. Corresponding displacements of the hydrogen atoms from the molecular plane are 0.14 Å and 0.24 Å, respectively.

The substantial out-of-plane bending amplitude for ν_7 excitation may provide anharmonic terms necessary to efficiently couple vibrational energy out of ν_7 into the dissociative pathway. Comparing the symmetry of ν_7 with that of the weak bond vibrational modes, it would appear that only the stretch is a likely mode for the excitation enegy. This would certainly be true if the molecule was rigid. However, the average position of Ar is expected to be well off to one side of the equilibrium position above the center of the C-C bond because of large amplitude zero point motion. Data presented in Chapter 7 show that ArC_2H_4 is indeed a hindered internal rotor. This opens the additional possibility of direct coupling of ν_7 with weak bending modes. The end result in either case is rapid dissociation leaving the ethylene fragment in a high rotational state.

The arguments applied to $Ar \cdot C_2H_4$ would apply in an analogous fashion to $(C_2H_4)_2$. Unfortunately, the structue of $(C_2H_4)_2$ is not known. Possibilities are a "T-shaped" structure or a parallel structure, and there ae theoretical calculations in the literature supporting both geometries[45,46]. It is unlikely that any but the very best calculation would give a reliable structure or bond energy

for this molecule. Recent molecular beam electric deflection experiments[47] using ions of m/e 41 to detect $(C_2H_4)_2$ beams indicate that the dipole moment of the complex is less than 0.1 D. This supports a centrosymmetric parallel configuration. However, similar experiments were also unable to detect a dipole moment for $Ar \cdot C_2H_4$. This indicates that the quadrupole moment of C_2H_4 may be too weak to induce an observable dipole moment in $(C_2H_4)_2$ no matter what structure is favored. In either case, an argument for the nature of coupling ν_7 to the weak modes of $(C_2H_4)_2$ and other van der Waals molecule studies would be analogous to those presented for $Ar \cdot C_2H_4$.

Up to this point it has been argued that spectral broadening in these complexes is due to predissociation rather than other types of intramolecular energy redistribution. There are two nondissociative broadening mechanisms conceivable: 1) Energy transfer to the weak modes, but creation of a long-lived orbiting complex; and 2) vibrational dephasing within covalently bound modes. With regard to the possibility of high enegy internal rotation, note that the radial van der Waals potential is highly anisotropic with respect to internal rotation. The equilibrium bond length of $(C_2H_4)_2$ with respect to ethylene centers of mass changes by more than half an Angstrom as the ethylene rotates.[45] This type of anisotropy would certainly couple bending and stretching degrees of freedom. Several hundred wavenumbers of excitation deposited in such

an orbiting resonance would result in a subpicosecond rotational period and rapid coupling to dissociative modes.

Intramolecular energy transfer within bound ethylene modes is also unlikely. The ν_7 and ν_8 modes of ethylene are close in energy but are of different symmetry, and remain so in the reduced symmetry of ethylene clusters. The coupling might be expected to be low on this basis. Experiment argues against such fast dephasing processes. The spectrum of ethylene in an Ar matrix at 10°K exhibits linewidths of less than 0.25 cm^{-1}, determined by site inhomogeneity rather than matrix-induced dephasing.[48] The special case of $(C_2H_4)_2$ is considered below.

All of the above evidence gives strong support to the conclusion that the observed homogeneous linewidths are due to vibrational predissociation on the subpicosecond time scale.

D. Absorption Profile and Intensities

A model for vibrational excitation followed by predissociation, which for some circumstances leads to purely lifetime broadened absorption, is a two-level system in which the upper state undergoes unimolecular decay. In our experiments the v = 0 and v = 1 states of the ethylene ν_7 mode correspond to the states of the two level system. Derivation of an exact lineshape equation from this model is described in Chapter 4. In the present study, uni-

molecular dissociation rates of vibrationally excited van der Waals molecules are more than 5 orders of magnitude faster than rates of stimulated absorption and stimulated emission. Spontaneous emission in the infrared is even slower. Thus it is possible to make simplifying approximations to the lineshape function (see Chapter 4) from which we obtain eq. (6):

$$|C_o(\omega,t)|^2 = \exp\left\{-\omega_R{}^2\tau t \frac{\tau^{-2}}{4(\omega - \omega_o)^2 + \tau^{-2}}\right\} . \qquad (6)$$

$|C_o(\omega,t)|^2$ is the fraction of undissociated van der Waals molecules, t is the irradiation time, ω is the laser frequency, ω_R is spacially averaged the Rabi frequency (see Chapter 4), τ is the dissociation rate of molecules in the excited state, and ω_o is the band center. Note that ω and ω_o in eq. (6) are in units of angular frequency. Eq. (6) is the exponential of a scaled Lorentzian curve. Typically, $\omega_R{}^2\tau t < 1$ implying that $|C_o(\omega,t)|^2$ is nearly Lorentzian but is slightly narrower than the simple Lorentzian lineshape reported in our previous communication.[31]

Solid lines drawn in the infrared photodissociation spectra (Figures 4, 5, 7 and 8) are results of a nonlinear, least-squares fit of eq. (6) to the data points.

predissociative lifetimes are calculated from the fitted spectra using eq. (7).

$$\tau(\text{sec}) = \frac{1}{2\pi c[\text{FWHM}(\text{cm}^{-1})]} \qquad (7)$$

Values of ω_o and τ for each ethylene containing van der Waals molecule studies are listed in Table III.

The spectra of $(C_2H_4)_2$ and $C_2H_4 \cdot C_2F_4$ fit this lineshape function with remarkable consistency. While agreement with a lineshape is not usually strong enough evidence to assert homogeneity, the lineshape of these transitions does serve as additional evidence that inhomogeneous effects are not observed.

Note that in the case of each noble gas-ethylene cluster a reasonable fit of eq. (6) to the entire spectrum is not possible. However, statistically reasonable fits are obtained for ArC_2H_4 and KrC_2H_4 data if only points occurring in the P branch of the CO_2 ($00^01\text{-}10^00$) laser emission are used. This is consistent with the discussion in the previous sections and, for the purpose of comparing spectral linewidths, we ignore the high frequency portions of the rare gas-ethylene spectra. Values of ω_o and τ for $(Ar)_nC_2H_4$ and $(Kr)_nC_2H_4$ listed in Table III were calculated in this way. Results in Chapter 7 suggest that these are

TABLE III. Parameters Obtained from Lineshape Fit to Photodissociation Spectra and Photodissociation Power Dependence Data[a)]

Cluster	ω_0 (cm^{-1})	τ (psec)	$\langle\mu\rangle^2$ (10^{-3} D^2)
$(C_2H_4)_2$	952.3 ± 0.5	0.44 0.05	96.0 ± 18.0
$(C_2H_4)_3$	952.3 ± 0.5	0.50 0.07	141.0 ± 33.0
$(C_2H_4)_5$	953.2 ± 0.9	0.33 0.05	100.0 ± 19.0
$(C_2H_4)_7$	953.2 ± 0.9	0.33 0.05	100.0 ± 19.0
$(Ar)_nC_2H_4$[b)]	950.0 ± 0.5	0.59 0.13	43.0 ± 16.0
$(Kr)_nC_2H_4$	949.1 ± 0.7	0.55 0.14	39.0 ± 15.0
$C_2H_4 \cdot C_2F_4$	954.7 ± 0.2	0.89 0.10	43.2 ± 3.3

a) The errors tabulated are three standard deviations.

b) These results apply to clusters which contain at least two rare gas atoms. See Chapter 7 for further investigation of $Ar \cdot C_2H_4$ and $Ne \cdot C_2H_4$.

representative of clusters with n > 1. Unfortunately, the signal-to-noise ratio in the $Ne \cdot C_2H_4$ experiment was very low. However, intriguing and reproducible features in the $Ne \cdot C_2H_4$ spectrum suggest that the broadening mechanism is significantly weaker for $Ne \cdot C_2H_4$ than for any of the other molecules which were studied. See Chapter 7 for a closer look at $Ne \cdot C_2H_4$.

Eq. (6) predicts that the logarithm of the undissociated fraction of clusters decreases linearly with increasing laser power since ω_R^2 is proportional to laser intensity. This is in excellent agreement with the observed power dependence of infrared photodissociation shown in Figure 5. The Rabi frequency, ω_R is also a function of the transition moment $\langle \mu \rangle$ for infrared absorption by the two-level system. Results obtained from photodissociation wavelength dependence combined with power dependence data allow determination of $\langle \mu \rangle$ for the van der Waals cluster studied. The square of the transition moment is proportional to absorption probability. Values of $\langle \mu \rangle^2$ are listed in Table III.

Among clusters with three or fewer ethylenes, transition probabilities calculated using eq. (4) are proportional to the number of ethylene molecules in the cluster. The average contribution per ethylene is $(4.5 \pm 1.2) \times 10^{-2}$ D^2 corresponding to a transition moment of 0.21 D. The transition moment for the $v = 0 \rightarrow v = 1$ infrared absorption by the ν_7 mode in ethylene monomer is

0.188 D.[49] The excellent agreement with observed photodissociation bandshapes and power dependences as well as consistency of the various transition moments leads us to conclude that eq. (6) and the underlying model adequately characterize the photodissociative behavior or $(Ar)_nC_2H_4$, $(Kr)_nC_2H_4$, $(C_2H_4)_2$, $(C_2H_4)_3$ and $C_2H_4 \cdot C_2F_4$.

E. Comparison with Theoretical Models

Recent detailed theoretical treatments of vibrational predissociation in simple model systems have led to qualitative generalizations which may guide comparison of predissociation rates. For example, Beswick and Jortner[19] present approximate relations for vibrationally predissociative lifetimes of molecules of the type AB·X. AB is a well-characterized, vibrationally excited diatomic and X represents a rare gas atom or simple molecule. An energy gap law predicts that close matching of the high molecular frequency and the low stretching frequency of the van der Waals bond enhances vibrational predissociation rates. Furthermore, with other parameters fixed, the predissociation rate is expected to increase with decreasing mass of X or as the van der Waals bond energy is decreased. Theoretical treatments of vibrational predissociation in hydrogen-bonded complexes by Ewing[25] indicate that internal degrees of freedom in the van der Waals molecule constituents can enhance vibrational

predissociation rates by six orders of magnitude. In particular, enhancement compared to V → T processes is observed when a V → V channel is operative. Ewing[24] has derived a momentum gap rule which states that overlap of the initially excited bound state and continuum wave functions determines the predissociation rate.

Although no theoretical treatment exists for molecules as complicated as ethylene clusters, some features of calculations with simpler systems are borne out in trends in the observed lifetimes listed in Table III. The bonding between C_2F_4 and ethylene is expected to be stronger than interactions in other bimolecules studied. Indeed, the ethylene absorption frequency in $C_2H_4 \cdot C_2F_4$ is shifted to the blue by 5 cm^{-1}. Also, C_2F_4 is the most massive partner used in construction of ethylene complexes. Insofar as the previous discussion is correct, both of these factors contribute to the observed extension of the $C_2H_4 \cdot C_2F_4$ lifetime compared to other clusters. Rates do not vary significantly as the internal degrees of freedom of van der Waals partners are changed in the series of clusters studied. This implies that the same efficient predissociation channel is operative in all of the molecules studied, and that energy transfer rates depend mainly on the mode excited in ethylene. For example, C_2F_4 has several vibrational frequencies (Table II) below 949 cm^{-1} which might be candidates for acceptor modes. the slow dissociation rate of $C_2H_4 \cdot C_2F_4$ relative to other van der

Waals molecules studied suggests that such acceptor modes are not coupled to ν_7. The C_2F_4 fragment of $C_2H_4^* \cdot C_2F_4$ decomposition is not expected to be vibrationally excited.

The dynamics of ethylene dimer predissociation are of special interest because of degeneracies introduced by symmetry. Exactly analogous is the decomposition of dimers of the type AB·BA. Beswick and Jortner[22] have shown that strong intramolecular coupling of degenerate bound states in such molecules can lead to linewidths dominated by dephasing rather than decomposition lifetimes. In the case of the ethylene dimer in D_{2h} symmetry, nearly degenerate symmetry adapted wave functions can be constructed from symmetric and antisymmetric combinations of the ν_7 normal mode motion of monomeric ethylene. Designating the van der Waals partners arbitrarily as A and B, and the localized ν_7 motions are A_7 and B_7, corresponding dimer wave functions with one quantum of ν_7 excitation are

$$|(+)\nu_7\rangle = 2^{-\frac{1}{2}}(|A_7(1)B_7(0)\rangle + |A_7(0)B_7(1)\rangle)$$

and

$$|(-)\nu_7\rangle = 2^{-\frac{1}{2}}(|A_7(1)B_7(0)\rangle - |A_7(0)B_7(1)\rangle)$$

Nearly degenerate vibrational states obtained from inspection of Table II are

$$(+)\nu_8 = 2^{-\frac{1}{2}}(|A_8(1)B_8(0)> + |A_8(0)B_8(1)>)$$

and

$$(-)\nu_8 = 2^{-\frac{1}{2}}(|A_8(1)B_8(0)> - |A_8(0)B_8(1)>)$$

We assume that only such discrete states carry oscillator strength from the ground state. Consideration of dipole moment derivatives indicates that optical transitions from the ground state to only $(+)\nu_7$ and $(+)\nu_8$ are allowed, and we expect that absorption by the $(+)\nu_8$ mode will be weak compared to the $(+)\nu_7$ mode. Assuming that $(+)\nu_7$ motion is excited, we need to consider whether energy flow into the other three nearly degenerate modes can compete with transitions into the dissociative continuum. Using the Morse potential coupling term derived by Beswick and Jortner,[22] the only nonzero matrix elements couple the discrete state $(+)\nu_7$ and $(+)\nu_8$. However, widths due to coupling between discrete states compete with the width due to decomposition only in special cases. Calculations for such a case,[22] collisionally excited $F_2 \cdot F_2$, predict widths of less than 4×10^{-3} cm^{-1} due to coupling of discrete states. The ethylene dimer width must be dominated by

vibrational predissociation since the observed width is much larger than 4 x 10^{-3} cm^{-1} and is not dramatically different than widths observed for other clusters.

Calculated vibrational predissociation rates are dramatically affected by slight changes in molecular parameters.[19,26] In contrast, lifetimes listed in Table III vary by only a factor of three through the series of seven ethylene clusters studied. This is an extremely small range of lifetimes compared to those calculated for simpler molecules, perhaps reflecting a narrow range of bond energies and frequencies among the dimeric species studied. In addition, observed predissociation rates are considerably faster than those generally calculated for theoretical models.

Photodissociation spectra of pure ethylene clusters (Figures 4 and 5) all show maxima blue-shifted compared to ν_7= 949.2 cm^{-1} in ethylene monomer (Table II). This trend in wavelength shifts is observed but is more marked in condensed ethylene. Liquid C_2H_4 exhibits ν_7 = 961 cm^{-1} and in the crystal ν_7 = 970 cm^{-1}.[50] One expects the infrared frequency of absorption band maxima in ethylene clusters to increase with increasing cluster size until a limiting value characteristic of the liquid or solid is reached. However, in the homologous series $(C_2H_4)_2$, $(C_2H_4)_3$, $(C_2H_4)_5$ and $(C_2H_4)_7$ photodissociation bands are shifted, at most, by 5 cm^{-1} relative to the monomer fundamental. The anticipated progression towards 970 cm^{-1} is not observed.

Photodissociation efficiencies do not scale with the number of molecules constituting pure ethylene clusters beyond $(C_2H_4)_3$, implying that photodissociation spectra of large clusters may not mimic absorption spectra.

$(C_2H_4)_5$ and $(C_2H_4)_7$ exhibit nearly identical photodissociation spectra with transition probabilities comparable to ethylene dimer. Assuming that all constituents of large clusters can be excited locally, this suggests that excitation at only a few sites will lead to decomposition on the time scale of our experiment. For example, fast predissociation may be detected only when an ethylene molecule at the cluster "surface" is activated by infrared excitation. Decomposition following excitation of molecules embedded in the cluster may require time-consuming multiple bond cleavage or extensive energy redistribution.

V. SUMMARY

Vibrational predissociation of van der Waals molecules has been observed. Absorption of a single infrared photon (950 cm^{-1}) by a slightly perturbed normal mode of ethylene is sufficient to photodissociate such weakly bound complexes. Use of relatively low laser power (less than 10 W cm^{-2}) avoids saturation. Infrared photodissociation spectra (925-1080 cm^{-1}) are characterized by lifetime broadened homogeneous lines. Observed wavelength

dependences and power dependences show excellent agreement with a lineshape derived from a a two-level-plus- decay model. Predissociative lifetimes lie in the range of 0.3 psec for large ethylene clusters to 0.9 psec for $C_2H_4 \cdot C_2F_4$. These correspond to 9-26 vibrational periods prior to dissociation.

Low-power infrared irradiation removes large fractions of clusters from the molecular beam in all of the experiments presented in this study. Photodissociation spectra of clusters in molecular beams are simplified due to supersonic cooling and generally consist of single homogeneously broadened absorptions. This suggests that infrared lasers may be used to modulate van der Waals molecule intensity for phase-sensitive detection in other molecular beam experiments. An isotope separation scheme based on infrared photodissociation of van der Waals molecules in molecular beams may prove feasible. For example, in a recent study of $Ar \cdot BCl_3$ photodissociation,[51] using the technique explored here, 50% of the ^{11}B containing van der Waals molecular were removed from the molecular beam without effecting species containing ^{10}B. Efficient selective photodissociation of ^{10}B species was also observed.

Qualitative aspects of simple theoretical models applied to ethylene clusters are useful in comparing predissociation lifetimes. However, observed rates are much greater than these models would imply, and the range

of predissociation rates expected as molecular parameters are varied is not observed. This suggests that among the dimeric species studied, predissociation rates are controlled by the nature of the vibration initially excited in ethylene. This may reflect a narrow range of van der Waals bond-types and available predissociation channels. Alternatively, theory developed thus far may not prove applicable to the more complex polyatomic species containing ethylene.

Absolute magnitudes of infrared transition moments are obtained. The transition moment per ethylene unit is roughly constant over the series $(C_2H_4)_2$, $(C_2H_4)_3$, $(Ar)_nC_2H_4$, $(Kr)_nC_2H_4$ and $C_2H_4 \cdot C_2F_4$. The molecular beam technique used in this study appears to be an excellent general method for measuring infrared transition intensities.

Larger ethylene clusters, $(C_2H_4)_5$ and $(C_2H_4)_7$ exhibit infrared photodissociation behavior similar to the dimer. It is inferred that present experiments sample only a fraction of ethylene molecules constituting larger clusters. Excitation of a C_2H_4 unit which is bound to many other ethylene molecules may not yield cluster dissociation on the time scale of the experiment.

ACKNOWLEDGEMENTS

The authors gratefully acknowledge J. L. Beauchamp for his ideas, advice, and the use of his CO_2 laser. Thanks are also due to D. D. Smith for providing the curve-fitting routines. Robert Altman, Harvard University, kindly measured electric deflection of $(C_2H_4)_2$ and $Ar \cdot C_2H_4$ to set an upper limit for the dipole moments of these species. Dr. Heinz Frei, University of California at Berkeley, generously supplied prepublication matrix isolation spectra of C_2H_4 in Ar. It is a pleasure to acknowledge W. C. Schuelke for work in constructing our apparatus.

This work was supported by the Research Corporation and the Division of Chemical Sciences, Office of Basic Energy Sciences, U. S. Department of Energy under contract no. DE-AS03-76SF00767. Acknowledgement is made to the Donors of the Petroleum Research Fund, administered by the American Chemical Society, for partial support of this research.

REFERENCES

1. W. Klemperer, Ber. Bunsenges. Phys. Chem. 78, 1281 (1974).
2. M. S. Child, Faraday Discuss. Chem. Soc. 62, 307 (1977).
3. C. A. Coulson and G. N. Robertson, Proc. Royal Soc. (London), Ser. A 342, 289 (1975).
4. J. S. Lassegues and P. V. Huong, Chem. Phys. Lett. 17, 444 (1972).
5. R. E. Smalley, L. Wharton and D. H. Levy, J. Chem. Phys. 64, 3266 (1976).
6. M. S. Kim, R. E. Smalley, L. Wharton and D. H. Levy, J. Chem. Phys. 65, 1216 (1976).
7. R. E. Smalley, L. Wharton and D. H. Levy, J. Chem. Phys. 66, 2750 (1977).
8. G. Kubiak, P. H. Fitch, L. Wharton and D. H. Levy, J. Chem. Phys. 68, 4477 (1978).
9. D. H. Levy, J. Chem. Phys. 68, 2524 (1978).
10. K. E. Johnson, L. Wharton and D. H. Levy, J. Chem. Phys. 69, 2719 (1978).
11. W. Sharfin, K. E. Johnson, L. Wharton and D. H. Levy, J. Chem. Phys. 71, 1292 (1979).
12. J. E. Kenny, D. V. Brumbaugh and D. H. Levy, J. Chem. Phys. 71, 4757 (1979).
13. J. A. Blazy, B. M. DeKoven, T. D. Russell and D. H. Levy, J. Chem. Phys. 72, 2439 (1980).
14. J. E. Kenny, K. E. Johnson, W. Sharfin and D. H. Levy, J. Chem. Phys. 72, 1109 (1980).

15. J. E. Kenny, T. D. Russell and D. H. Levy, J. Chem. Phys. 73, 3607 (1980).

16. T. E. Gough, R. E. Miller and G. Scoles, J. Chem. Phys. 69, 1588 (1978).

17. M. A. Hoffbauer, W. R. Gentry and C. F. Giese, Laser-Induced Processes in Molecules, edited by K. L. Kompa and S. D. Smith (Springer-Verlag, Heidelberg, 1979).

18. H. S. Kwok, M. F. Vernon, D. J. Krajnovich, Y. R. Shen and Y. T. Lee, Lawrence Berkeley Laboratory Report No. 10566; H. S. Kwok, M. F. Vernon, D. J. Krajnovich and Y. T. Lee, Lawrence Berkeley Laboratory Report No. 10288.

19. J. A. Beswick and J. Jortner, J. Chem. Phys. 68, 2277 (1978).

20. J. A. Beswick and J. Jortner, J. Chem. Phys. 69, 512 (1978).

21. J. A. Beswick, G. Delgado-Barrio and J. Jortner, J. Chem. Phys. 70, 3895 (1979).

22. J. A. Beswick and J. Jortner, J. Chem. Phys. 71, 4737 (1979).

23. J. A. Beswick and G. Delgardo-Barrio, J. Chem. Phys. 73, 3653 (1980).

24. G. Ewing, J. Chem. Phys. 71, 3143 (1979).

25. G. Ewing, J. Chem. Phys. 72, 2096 (1980).

26. G. Ewing, Chem. Phys. 29, 253 (1978).

27. R. Ramaswamy and A. E. DePristo, J. Chem. Phys. 72, 770 (1980).

28. S. B. Woodruff and D. L. Thompson, J. Chem. Phys. 71, 376 (1979).

29. J. W. Brady, J. D. Doll and D. L. Thompson, J. Chem. Phys. 73, 292 (1980).

30. L. S. Bernstein and C. E. Kolb, J. Chem. Phys. 71, 2818 (1979).

31. M. P. Casassa, D. S. Bomse, J. L. Beauchamp and K. C. Janda, J. Chem. Phys. 72, 6805 (1980).

32. M. T. Bowers, D. D. Elleman and J. L. Beauchamp, J. Phys. Chem. 72, 3599 (1968).

33. K. C. Janda, Ph.D. Thesis, Harvard University (1977).

34. R. E. Smalley, L. Wharton, D. H. Levy and D. W. Chandler, J. Chem. Phys. 68, 2487 (1978).

35. L. D. Landau and E. M. Lifshitz, Fluid Mechanics (Pergamon Press, New York, 1959).

36. K. C. Janda, J. E. Hurst, C. A. Becker, J. P. Cowin, D. J. Auerbach and L. Wharton, J. Chem. Phys. 72, 2403 (1980).

37. A. J. Ferrer-Correia and K. R. Jennings, Int. J. Mass Spectrom. Ion Phys. 11, 111 (1973).

38. R. L. Arnett and B. L. Crawford, Jr., J. Chem. Phys. 18, 118 (1950).

39. D. E. Mann, N. Acquista and E. K. Plyer, J. Res. Natl. Bur. Stand. 51, 69 (1953).

40. J. L. Duncan and E. Hamilton, J. Mol. Struct. 76, 65 (1981).

41. R. E. Miller, Ph.D. Thesis, University of Waterloo (1980).

42. K. C. Janda, L. S. Bernstein, J. M. Steed, S. E. Novick and W. Klemperer, J. Am. Chem. Soc. 100, 8074 (1978).

43. R. L. DeLeon and J. S. Muentor, J. Chem. Phys. 72, 6020 (1980).

44. G. Herzberg, Infrared and Raman Spectra (Van Nostrand and Reinhold, New York, 1966).

45. K. Suzuki and K. Iguchi, J. Chim. Phys. 75, 779 (1978).

46. R. Lochmann and P. Hobza, Int. J. Quant. Chem. 15, 73 (1979).

47. R. Altman, Harvard University (unpublished results).

48. H. Frei, University of California at Berkeley (unpublished results).

49. T. Nakanaga, S. Kondo and S. Saeki, J. Chem. Phys. 70, 2471 (1979).

50. C. Brecher and R. S. Halford, J. Chem. Phys. 35, 1109 (1961).

51. M. P. Casassa, D. S. Bomse and K. C. Janda, J. Phys. Chem. 85, 2623 (1981).

Chapter 3

Isotopic Selectivity in van der Waals Molecule Photodissociation. Infrared Photolysis of $Ar \cdot BCl_3$

IR PHOTOLYSIS OF $ArBC\ell_3$

Michael P. Casassa[a], David S. Bomse, and Kenneth C. Janda*

Arthur Amos Noyes Laboratory of Chemical Physics[b]

California Institute of Technology

Pasadena, California 91125

ABSTRACT

The infrared photodissociation spectrum of $Ar \cdot BC\ell_3$ is reported. Spectra obtained using a cw CO_2 laser are dominated by homogeneous broadening due to vibrational predissociation of excited van der Waals molecules. The predissociation lifetime of $Ar \cdot BC\ell_3$ containing one quantum of vibrational excitation in the $BC\ell_3$ ν_3 mode is between 1 psec and 3 psec. Results presented are discussed in terms of the efficiency and isotopic selectivity of the photodissociation process.

INTRODUCTION

In recent studies of the infrared photodissociation of van der Waals molecules, ethylene clusters formed in supersonic molecular beams were photodissociated using a low power cw CO_2 laser.[1,2] The object of these experiments was to characterize intramolecular vibrational energy flow in weakly bound molecules. The large fractional dissociation and simplified spectra observed in these studies suggest that an isotope separation scheme based on infrared photodissociation of van der Waals molecules would be both highly selective and efficient.

The isotopic selectivity and quantum efficiency of photochemical processes are of fundamental interest, though

certainly not the only practical considerations in designing laser isotope separation schemes.[3] In both cw[4] and pulsed[5] enrichment studies, loss of selectivity often occurs by isotope scrambling due to reactions of excited intermediates or thermal heating. Selectivity is also diminished if spectra of different isotopes overlap. This is often the case in multiphoton infrared photodissociation spectra which are generally broader than corresponding single photon infrared absorption spectra. Multiphoton excitation, which is the key photochemical process in many enrichment studies, represents an inefficient use of laser power. The cross section for multiphoton excitation is typically two orders of magnitude smaller than the cross section for the first absorption step.[6] Overall quantum efficiency is also reduced by collisional quenching of reactive intermediates.

In contrast to covalently bound molecules, van der Waals molecules undergo rapid bond cleavage upon single infrared photon absorption by a constituent of the complex.[1,2,7,8] Consistent with this simple mechanism, observed photodissociation spectra exhibit frequencies and cross sections characteristic of the uncomplexed species. Supersonic molecular beams provide a collisionless environment in which molecules exist in their lowest rotational and vibrational states. Thus, cluster photodissociation spectra are Doppler-free and, in the case of ethylene clusters,[2] are dominated by homogeneously broadened absorption lines. Linewidths determined by vibrational

predissociation lifetimes are of the order of 10 cm^{-1} or less.[2,9]

In this paper we present a molecular beam study of infrared photodissociation of $Ar \cdot BC\ell_3$ using a low power cw CO_2 laser. In addition to characterizing vibrational predissociation for this species, we have examined the isotopic selectivity and efficiency of the photodecomposition process.

EXPERIMENTAL SECTION

The apparatus for studying infrared photodissociation of van der Waals molecules has been described in detail in another publication.[2] Briefly, $Ar \cdot BC\ell_3$ and other van der Waals clusters are formed by supersonic expansion of mixtures of the constituent gases in a large excess of helium. A quadrupole mass spectrometer positioned 60 cm from the nozzle source is used to monitor molecular beam composition. Uniform infrared irradiation along the molecular beam is provided by an unfocused cw CO_2 laser directed through the ionizer of the mass spectrometer and propagating colinearly with the molecular beam. The laser beam is chopped and the intensity of a given peak in the molecular beam mass spectrum is measured both with and without laser irradiation using a two-channel boxcar. The fractional change in mass spectrometer signal intensity due to photo-

dissociation of van der Waals molecules is recorded as a function of laser power and wavelength.

Characterization of molecular beams containing $BC\ell_3$ clusters is complicated by chlorine isotopes, and because electron impact ionization of $Ar \cdot BC\ell_3$ and pure $BC\ell_3$ clusters leads to extensive fragmentation. The most prominent ions observed are $BC\ell_2^+$ and $BC\ell_3^+$ which evidently arise from $BC\ell_3$ monomers and polymers. No parent $Ar \cdot BC\ell_3^+$ is detected, nor are any fragment ions containing both argon and boron observed. Ionic species definitely attributable to parent clusters containing Ar and $BC\ell_3$ are $Ar^{35}C\ell^+$ and $Ar^{37}C\ell^+$ observed at m/e 75 and 77, respectively. Relative intensities of these two fragments are consistent with chlorine isotope natural abundances. The photodissociation results described below are also consistent with the assignment of these ions to $Ar \cdot BC\ell_3$.

RESULTS AND DISCUSSION

A photodissociation spectrum obtained by measuring the fractional attenuation of $Ar^{35}C\ell^+$ signal intensity as a function of laser wavelength is shown in Figure 1. In this example, the molecular beam was formed by expansion of a 0.5% $BC\ell_3$ - 25% Ar - 75% He mixture at 7 atm pressure through a 50 μm nozzle. These expansion conditions result in a 0.62 msec irradiation time.[10] The data shown were

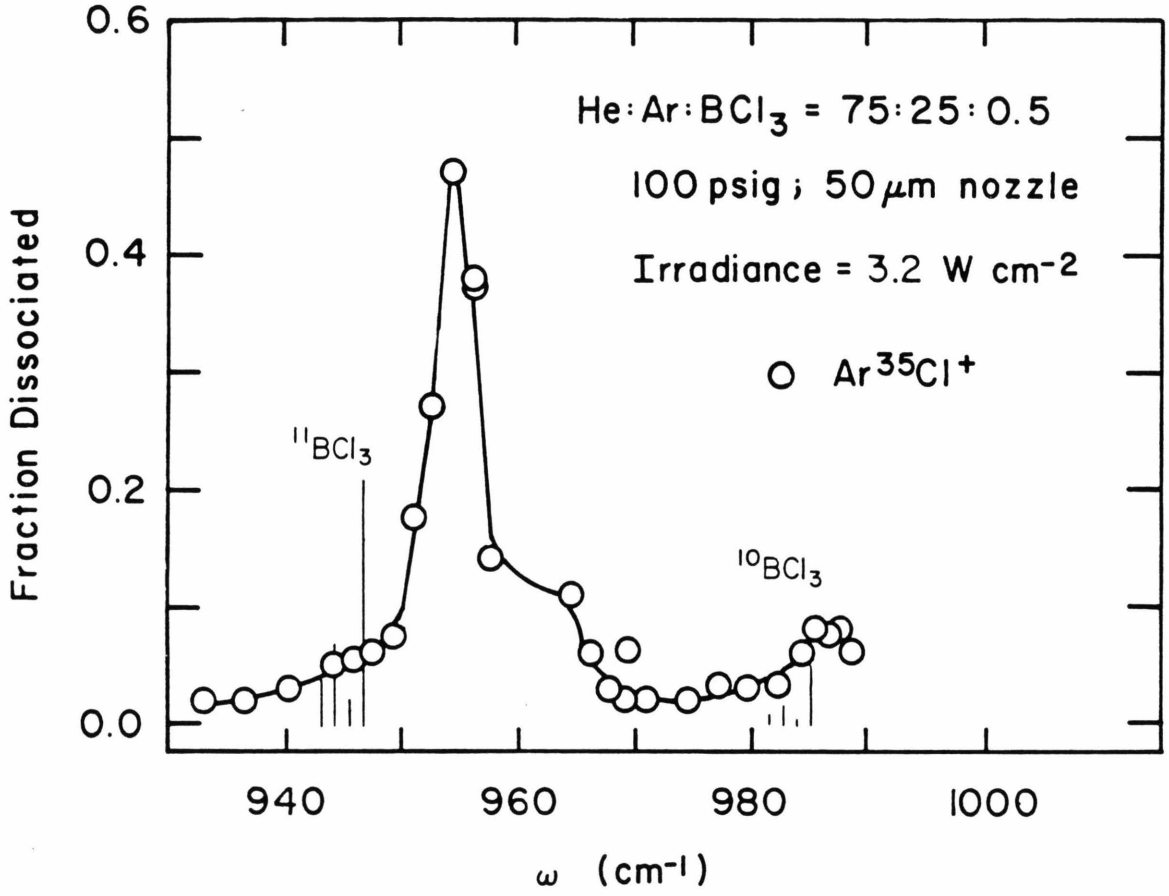

FIGURE 1. Infrared photodissociation spectrum of $Ar \cdot BC\ell_3$. $Ar \cdot BC\ell_3$ is detected as $Ar^{35}C\ell^+$. The line spectrum represents absorption by $BC\ell_3$ dissolved in solid argon at 75.8 K.[12] Note that widths of the matrix absorption lines are less than 0.1 cm^{-1}.

obtained with 2.4 W total laser power which after losses at surfaces and apertures provided 3.2 W cm^{-2} in the molecular beam.

A strong feature is observed at 954 cm^{-1} which we attribute to selective photodissociation of $Ar \cdot {}^{11}BC\ell_3$. The band position corresponds to the ν_3 in-plane-bending fundamental of free ${}^{11}BC\ell_3$.[11] Results of ethylene cluster photodissociation experiments indicate that the frequency shift caused by van der Waals bonding should not be significant.[1,2] The irregular shape of the band may be due to dissociation of chlorine isotopic variants of $Ar \cdot BC\ell_3$. Similarly, $Ar \cdot {}^{10}BC\ell_3$ photodissociation is expected to occur close to the gas phase ν_3 absorption frequency of ${}^{10}BC\ell_3$ (994 cm^{-1});[11] thus dissociation of $Ar \cdot {}^{10}BC\ell_3$ contributes to the weak feature observed at 987 cm^{-1}. Unfortunately, both resolution and range of the spectrum are limited by the discrete tuning capability of the CO_2 laser.

To our knowledge, infrared absorption by the ν_3 mode of the chlorine isotope variants of $BC\ell_3$ has never been accurately measured in the gas phase. High resolution spectra of $BC\ell_3$ dissolved in solid argon have been reported.[12] For a given boron isotope, there are several lines, spaced by approximately 1.3 cm^{-1} due to chlorine isotope shifts, exhibiting widths of less than 0.1 cm^{-1}. These lines, reproduced in Figure 1, approach the unperturbed gas phase $BC\ell_3$ absorption frequencies with increasing lattice temperature, presumably because the lattice expands and the

$BC\ell_3$ is less perturbed. Results presented here indicate that the gas phase limit is achieved at low temperatures if the bonding interaction is limited to a single argon atom.

Figure 2 shows the variation of the logarithm of the undissociated fraction of molecules with laser power at fixed wavelength. Data shown were obtained by measuring the fraction of the total $Ar^{35}C\ell^+$ ion intensity surviving irradiation with the laser tuned to 954.55 cm^{-1}, close to the ν_3 fundamental of $^{11}BC\ell_3$. The plot of the raw data is nonlinear and at the highest laser power attained approaches a limiting value of 42%. Note that $Ar^{35}C\ell^+$ arises from ionization of six isotopic variants of $Ar \cdot BC\ell_3$. Data such as shown in Figures 1 and 2 thus represent a sum of photodissociation probabilities of six distinct species. 20% of the $Ar^{35}C\ell^+$ ion intensity is due to $Ar \cdot {}^{10}BC\ell_3$ and is insensitive to 954.55 cm^{-1} irradiation. The additional 22% not dissociated by 954.55 cm^{-1} radiation must be due to isotopic and rotational inhomogeneity. Still, the homogeneous widths of the underlying absorptions must be of the same order as the inhomogeneous structure since it is possible to induce 72% attenuation of the $Ar \cdot {}^{11}BC\ell_3$ flux with 9.5 W cm^{-2} irradiation at 954 cm^{-1}. Data presented indicate that the homogeneous broadening is comparable to the chlorine isotope shifts but much less than the separation of boron isotope absorption frequencies.

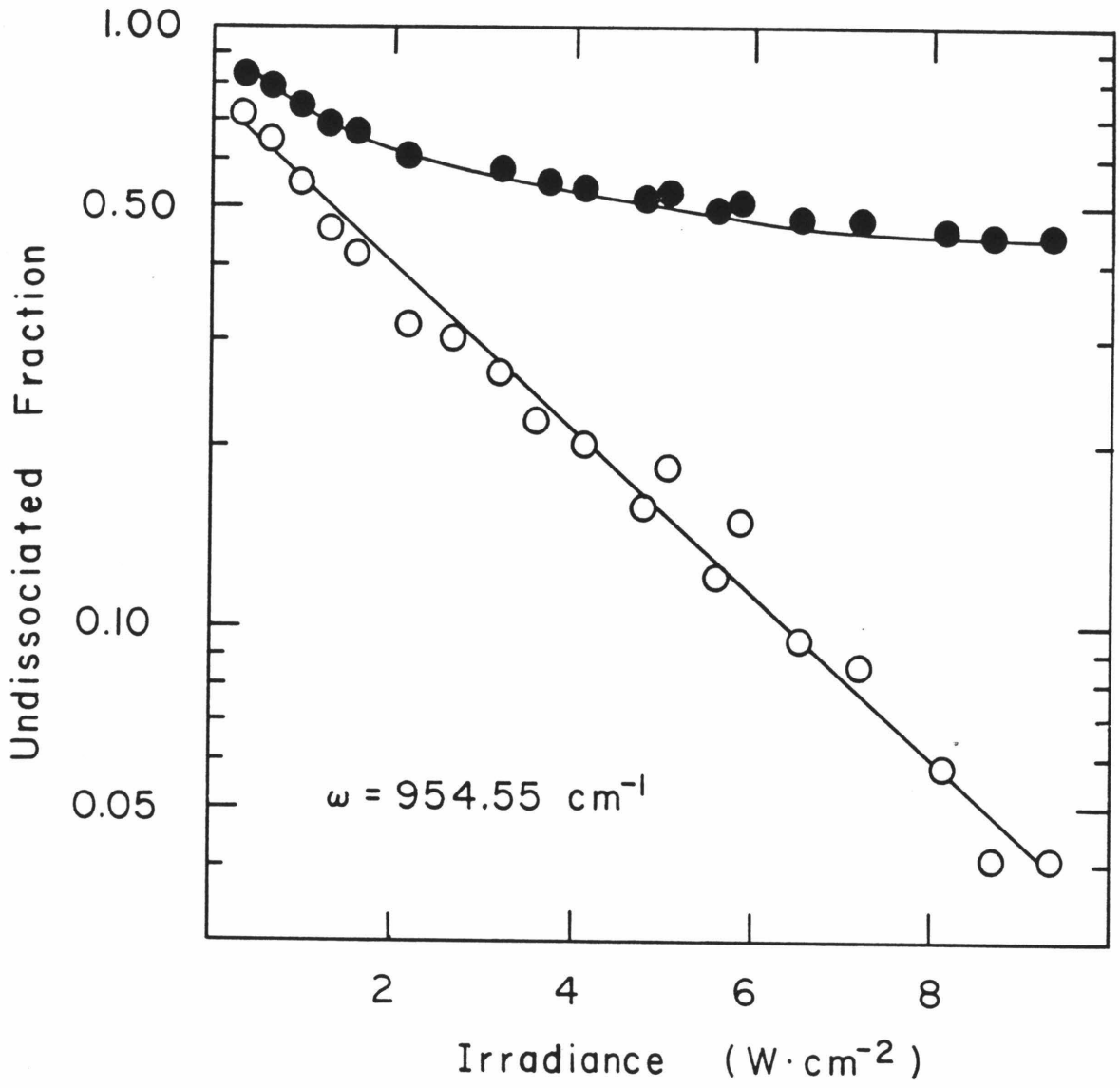

FIGURE 2. Power dependence of the photodissociation yield. Expansion conditions are identical to those used in generating Figure 1. The nonlinear plot corresponds to measured fractional attenuation of total $Ar^{35}Cl^+$ ion intensity. The linear plot is generated by assuming that 42% of the $Ar^{35}Cl^+$ signal is insensitive to 954.55 cm^{-1} radiation and treating this as background.

A simple two-level-plus-decay model yields a lineshape formula for homogeneous photodissociation under our experimental conditions:[2]

$$|C_o(\omega,t)|^2 = \exp\left[-\omega_R{}^2\tau t \ \frac{\tau^{-2}}{4(\omega-\omega_o)^2 + \tau^{-2}}\right]. \qquad (1)$$

$|C_o(\omega,t)|^2$ is the fraction of van der Waals molecules in the molecular beam which survive irradiation for a time t, by light with angular frequency ω. Laser power and the infrared transition moment enter equation (1) through the Rabi frequency ω_R. The complex has a resonant absorption at frequency ω_o and excited state vibrational predissociation lifetime τ. Note that equation (1) confirms the intuitive prediction that the extent of photodissociation at ω_o increases with increasing lifetime (and concomitant line narrowing). Consideration of equation (1) indicates that inhomogeneity such as observed in these experiments can be washed out by increasing the laser fluence.

Attributing the full width of the dissociation spectrum to predissociative broadening, the minimum lifetime of Ar·BCℓ_3 containing one quantum of ν_3 excitation is determined to be 1.2 psec. This corresponds to 34 vibrational periods. Alternatively, the minimum width must certainly be larger than the separation of CO_2 laser lines which

corresponds to a maximum vibrational predissociation lifetime of 2.7 psec.

Results presented are consistent with a highly efficient, isotopically selective photodissociation process. The quantum yield is near unity since the vibrational predissociation process is extremely fast, and intensities are comparable to single photon infrared absorption intensities. Isotopic selectivity is limited only by the overlap of absorptions by different isotopic species and hence depends on the vibrational predissociation rate. Equipment used to implement selective dissociation is relatively energy efficient and inexpensive.

The feasibility of this technique as a practical method for isotope separation is most limited by the intrinsically small scale of the method. Although it may be possible to remove 70% of the $Ar \cdot {}^{10}BC\ell_3$ from the molecular beam, this is only a fraction of the total ${}^{10}BC\ell_3$ concentration in the beam. The van der Waals dimer concentrations in our expansions are typically a few percent of the total parent gas concentration. Thus, the separation of one mole of ${}^{10}BC\ell_3$ from a natural isotopic mixture would require several years of constant irradiation, recirculation, and fragment collection under present operating conditions (105 PSI behind a 35 μm nozzle) of our apparatus. However, the throughput of such a device could easily be increased by a factor of 100 by using larger pumps, nozzles and apertures. This would decrease the required time to several days.

SUMMARY

We have reported a one photon infrared dissociation spectrum for $Ar \cdot BC\ell_3$. The predissociation lifetime of the ν_3 excited state is between one and three picoseconds. The homogeneous spectral widths are of the same magnitude as chlorine isotopic shifts, but much less than the boron isotope shift. The implications of these findings to laser isotope separation using van der Waals molecules are discussed.

ACKNOWLEDGEMENT

The authors thank J. L. Beauchamp for providing the CO_2 laser used in the experiment.

This work was supported by the Research Corporation and the Division of Chemical Sciences, Office of Basic Energy Sciences, U. S. Department of Energy, under contract no. DE-AS03-76SF00767. Acknowledgement is made to the Donors of the Petroleum Research Fund, administered by the American Chemical Society, for partial support of this research.

NOTES AND REFERENCES

a. National Science Foundation Predoctoral Fellow.

b. Contribution Number 6396.

1. M. P. Casassa, D. S. Bomse, J. L. Beauchamp and K. C. Janda, J. Chem. Phys. 72, 6805 (1980).

2. M. P. Casassa, D. S. Bomse and K. C. Janda, J. Chem. Phys. 74, 5044 (1981).

3. V. S. Letokhov and C. B. Moore in Chemical and Biochemical Applications of Lasers, Vol. III, edited by C. B. Moore (Academic Press, New York, 1979).

4. T. J. Manuccia and M. D. Clark, J. Chem. Phys. 68, 2271 (1978).

5. R. V. Ambartsumyan, V. S. Letokhov, E. A. Ryabov and N. V. Chekalin, JETP Lett. 20, 273 (1974).
R. V. Ambartsumyan, Yu. A. Gorokhov, V. S. Letokhov and G. N. Makarov, JETP Lett. 21, 171 (1975).
J. L. Lyman, R. J. Jensen, J. Rink, C. P. Robinson and S. D. Rockwood, Appl. Phys. Lett. 27, 87 (1975).
J. L. Lyman and S. D. Rockwood, J. Appl. Phys. 47, 595 (1976).
S. Bittenson and P. L. Houston, J. Chem. Phys. 67, 4819 (1977).
C. T. Lin and T. D. Z. Atvars, J. Chem. Phys. 68, 4233 (1978).
A. Hartford, Jr. and S. A. Tuccio, Chem. Phys. Lett. 60, 431 (1979).

6. E. R. Grant, P. A. Schultz, A. A. Sudbø, M. J. Coggiola, Y. R. Shen and Y. T. Lee, Multiphoton Processes, Proc. Int. Conf., 1977, 359 (1978).

7. M. A. Hoffbauer, W. R. Gentry and C. F. Giese, Laser-Induced Processes in Molecules, edited by K. L. Kompa and S. D. Smith (Springer-Verlag, Heidelberg, 1979).

8. T. E. Gough, R. E. Miller and G. Scoles; J. Chem. Phys. 69, 1588 (1978).

9. K. E. Johnson, W. Sharfin and D. H. Levy, J. Chem. Phys. 74, 163 (1981), and references contained therein.

10. Molecular beam velocities are calculated using effective masses and heat capacities for each expansion mixture and the known expansion conditions as in reference 2.

11. L. P. Lindeman and M. K. Wilson, J. Chem. Phys. 24, 242 (1956).

12. W. B. Maier, II and R. F. Holland, J. Chem. Phys. 72, 6661 (1980).

13. Natural abundances ^{10}B=19.78%, ^{11}B=80.22%, Handbook of Chemistry and Physics, edited by R. C. Weast, 52nd edition (Chemical Rubber Co., Cleveland, 1971).

Chapter 4

Homogeneous Photodissociation and Photodesorption Lineshapes

PHOTODISSOCIATION AND PHOTODESORPTION LINESHAPES

Michael P. Casassa[a], Francis G. Celii, and Kenneth C. Janda

Contribution No. 6577 from the Arthur Amos Noyes Laboratory of Chemical Physics, California Institute of Technology, Pasadena, California 91125

Abstract

Photodissociation lineshapes are derived based on two-level-plus-decay models. The simplest model involves only dissociative decay of the upper level and applies to laser-induced vibrational predissociation of van der Waals molecules. A more general model which includes quenching processes that compete with dissociation is presented in a form applicable to laser-induced desorption. Both models yield insightful lineshape expressions with explicit dependence on laser power and frequency, irradiation time, absorption strength, and phenomenological rate constants. Implications of the lineshape formulae for several recent experiments as well as feasibility of studying more complex systems are discussed.

[a]National Science Foundation Predoctoral Fellow.

I. INTRODUCTION

Van der Waals molecule photodissociation spectroscopy has developed in recent years as an elegant technique for studying intramolecular vibrational energy flow. Well characterized photodissociation spectra include, for example, those of iodine[1] and ethylene containing clusters,[2] and pure clusters of CO_2[3] and HF.[4] Using narrow band lasers, excitation can be localized in covalent constituents of weakly bound complexes. Subsequent intramolecular vibrational energy flow leads to dissociation since van der Waals bond energies are generally smaller than the quanta of vibrational excitation. Excitation spectra, simplified by narrow distributions of initial states produced upon formation of clusters in molecular beams, exhibit widths and time evolution which may be interpreted in terms of molecular rate processes. Rates are also amenable to detailed theoretical approach[5-7] since the excitation is well defined, and in many cases, the structures and relevant potentials for van der Waals clusters are known. The precise relationship of observed line profiles and time evolution of excitation spectra to molecular rate processes has not appeared in the literature, but is crucial to the interpretation of experiments.

Laser induced desorption of molecules from surfaces is currently an active research area, though still in its nascent stage. It is anticipated that energy transfer rates

for surface processes might be extracted from desorption experiments analogous to van der Waals molecule photodissociation spectroscopy. Additional nondissociative processes occurring at surfaces would, however, influence desorption lineshapes and intensities. Analysis of laser-induced desorption spectra would of necessity include consideration of these various rates.

Two models are discussed in detail. The first--the pure case--applies to an ensemble of non-interacting, predissociating clusters. In this paper we present line-shape formulae, based on ensembles of simple two-level-systems, which may be used in modeling photodissociation spectra to unambiguously extract rates for decay processes. This model is appropriate for molecules isolated in molecular beams and has been employed in the interpretation of ethylene cluster photodissociation experiments.[2] The second model--the mixed case--is more general and may be applied to an ensemble of interacting species in which decomposition must compete with quenching of excited states. A layer of molecules physisorbed on a surface constitutes such an ensemble. The dependences of vibrational state populations and photodissociation yield on laser power, wavelength and irradiation time, as well as phenomenological rate constants for decomposition, quenching and pure dephasing, are explicit. Detailed

lineshape formulae are reduced to simpler expressions valid for conditions generally employed in photodissociation experiments. Finally, results of photodissociation experiments performed to date and feasibility of studying more complicated chemical processes, in particular, that of laser-induced desorption, are discussed in terms of the models presented.

II. MODEL

An insightful model characterizing vibrational predissociation induced by light absorption consists of an ensemble of two-level systems interacting with a radiation field, in which upper state population has the option of decaying into a dissociative continuum. In the simplest conceivable situation--the pure case--members of the ensemble are completely independent and the two levels are coupled exclusively by the light. Time evolution of population, and hence photodissociation spectra, are then completely coherent, depending only on rates of up- and down-pumping and the predissociation rate for isolated molecules. Van der Waals molecules formed in supersonic expansion of gases conform to this simplest model.

A more general situation--the mixed case--ought to include nondissociative decay pathways for the excited state, perhaps ultimately serving to repopulate the ground state, as well as the possibility of decay of phase coherence in the ensemble. The system of interest here is a collection of infrared-absorbing molecules weakly bound to a surface. Upon absorption of a photon, surface-adsorbate complexes may either decompose, release a photon to the radiation field, or lose energy to the infinite heat reservoir of the solid. Decomposition of complexes may occur by ejection of the adsorbed species, chemisorption, or chemical reaction.

We start the description of this problem with standard expressions from time dependent quantum mechanics. Our approach and notation closely parallel those given by Lamb et al.[8]

The state function for a two-level system evolving in time can be written as a linear superposition of the two time-independent eigenfunctions with time-dependent coefficients.

$$\psi(\underset{\sim}{r},t) = c_a(t)\phi_a(\underset{\sim}{r}) + c_b(t)\phi_b(\underset{\sim}{r}) \quad . \tag{1}$$

ϕ_a and ϕ_b are eigenfunctions of the Hamiltonian for the unperturbed molecule, representing the upper and lower levels, respectively, of the two-level system. The complete

time dependence of the system is contained in the c_i. If the upper state is predissociative, then c_a will contain a corresponding exponential decay. In the presence of a perturbation, the time dependence of the c_i can be deconvoluted into factors due to the perturbation interaction and the inherent time evolution of stationary states,

$$c_i(t) = C_i(t)_e^{-i\omega_i t} \quad , \tag{2}$$

where ω_i is the energy of the i^{th} state in units of angular frequency. The mathematical development of lineshape formulae is simplest using interaction picture probability amplitudes, C_i, in the pure case, and Schrodinger picture probability amplitudes, c_i, in the mixed case.

Pure Case

In the situation that members of the ensemble are completely noninteracting, the populations of states in the ensemble correspond to the isolated molecule probability amplitudes. If initially $|C_a(0)|^2 + |C_b(0)|^2 = 1$, then the fraction of the molecules remaining in the ensemble at some later time is given by

$$F_p(t) = |C_a(t)|^2 + |C_b(t)|^2 \quad . \tag{3}$$

The time evolution of C_a and C_b in the presence of a perturbation in the simplest two-level-plus-decay model,[2,9] is given by

$$\dot{C}_a = -\frac{i}{\hbar} V_{ab} C_b e^{-i(\omega_b-\omega_a)t} - \frac{\gamma_D}{2} C_a , \tag{4a}$$

$$\dot{C}_b = -\frac{i}{\hbar} V_{ba} C_a e^{-i(\omega_a-\omega_b)t} . \tag{4b}$$

The first equation includes $\frac{-\gamma_D}{2}$ so that $|C_a|^2$ decays exponentially with rate constant γ_D in the absence of radiation. The matrix elements for coupling of the states by the radiation field are given in the rotating wave approximation[8] by

$$V_{ab} = -\frac{1}{2}\mu \cdot E_o e^{-i\omega t} = V_{ba}^* . \tag{5}$$

Here μ is the transition moment, E_o is the electric field intensity, and ω is the angular frequency of the light. Substituting eq. (5) into eqs. (4) gives the rate equations

$$\dot{C}_a = \frac{i\omega_R}{2} e^{i\Delta\omega t} C_b - \frac{\gamma_D}{2} C_a , \tag{6a}$$

$$\dot{C}_b = \frac{i\omega_R}{2} e^{-i\Delta\omega t} C_a , \tag{6b}$$

where $\Delta\omega = \omega_a - \omega_b - \omega$ and $\omega_R = \frac{\mu \cdot E_o}{h}$ is the Rabi frequency. Solution of eqs. (6) subject to initial conditions $C_a(0) = 0$ and $C_b(0) = 1$ yields

$$C_a(t) = \frac{i\omega_R}{z} \exp(i\Delta\omega t/2) \exp(-\gamma_D t/4) \sin(zt/2), \quad (7a)$$

$$C_b(t) = \left[\left(\frac{\gamma_D/2 + i\Delta\omega}{z}\right) \sin(zt/2) + \cos(zt/2)\right] \times \exp(-i\Delta\omega t/2) \exp(-\gamma_D t/4) \quad , \quad (7b)$$

where

$$z = [(\Delta\omega - i\gamma_D/2)^2 + \omega_R^2]^{1/2} \quad .$$

The populations of the individual states are irradiation at frequency ω for the t are

$$|C_a(\omega,t)|^2 = \frac{\omega_R^2}{|z|^2} \left(\cosh^2 \frac{yt}{2} - \cos^2\right) \frac{xt}{2} \exp(\gamma_D t/2), \quad (9a)$$

$$|C_b(\omega,t)|^2 = \left\{\frac{\Delta\omega^2 + (\gamma_D/2)^2}{|z|^2} \left(\cosh^2 \frac{yt}{2} - \cos^2 \frac{xt}{2}\right) + \frac{2}{|z|^2}\left[\left(\frac{\gamma}{2} x + \Delta\omega y\right) \sin \frac{xt}{2} \cos \frac{xt}{2} + \left(\frac{\gamma}{2} y + \Delta\omega x\right) \times \sinh \frac{yt}{2} \cosh \frac{yt}{2}\right] + \left(\cosh^2 \frac{yt}{2} - \sin^2 \frac{xt}{2}\right)\right\} \times \exp(-\gamma_D t/2) \quad , \quad (9b)$$

where x and y are the real and imaginary parts of z. Explicit expressions for x and y appear in Ref. 2. The fraction of the total initial population remaining at time t is given by eq. (3). However, the exact solution is unnecessarily cumbersome and does not directly yield physical insight into long-time observations. In the case that $\omega_R < \gamma_D$, eq. (3) can be reduced to a simpler form

$$F_p(\omega,t) = \exp\left[-\omega_R^2\,\gamma_D^{-1}t \cdot \frac{\gamma_D^2}{4(\omega-\omega_o)^2 + \gamma_D^2}\right] . \qquad (10)$$

Equation (10) is the exponential of a Lorentzian multiplied by a factor proportional to laser power, irradiation time, decomposition lifetime and the square of the absorption transition moment. The width of the Lorentzian term (FWHM) is related to the decomposition rate by

$$\gamma_D(\mathrm{sec}^{-1}) = 2\pi c \cdot \mathrm{FWHM}\ (\mathrm{cm}^{-1}) \quad . \qquad (11a)$$

The full width at half minimum of eq. (10) is given by

$$\mathrm{FWHM}' = \left[\frac{\omega_R^2\,\gamma_D^{-1}t}{\ln 2 - \ln[1 + \exp(-\omega_R^2\,\gamma_D^{-1}t)]} - 1\right]^{\frac{1}{2}} \gamma_D, \qquad (11b)$$

where FWHM' is to be distinguished from the width of the Lorentzian term (FWHM) appearing in eq. (11a). Equations (10), (11), and associated restrictions apply to most photodissociation experiments performed to date.

Mixed Case

In order to include interaction between molecular systems and repopulation or feeding processes, a density matrix approach to the problem of time evolution of the ensemble is more appropriate than the isolated molecule approach used for the pure case. The equations of motion for the isolated molecule Schrödinger picture probability amplitudes are obtained from eqs. (2) and (6):

$$\dot{c}_a = -(i\omega_a + \gamma/2)\, c_a - \frac{i}{\hbar} V_{ab}\, c_b \quad , \tag{12a}$$

$$\dot{c}_b = -i\omega_b\, c_b - \frac{i}{\hbar} V_{ba}\, c_a \quad . \tag{12b}$$

Equations of motion for the corresponding density matrix elements, defined as $\rho_{nm} \equiv c_n\, c_m^*$ are easily derived from eqs. (12):

$$\dot{\rho}_{aa} = -\gamma\rho_{aa} - \frac{i}{\hbar}(V_{ab}\rho_{ba} - V_{ba}\rho_{ab}) \quad , \tag{13a}$$

$$\dot{\rho}_{bb} = +\frac{i}{\hbar}(V_{ab}\rho_{ba} - V_{ba}\rho_{ab}) \quad , \tag{13b}$$

$$\dot{\rho}_{ab} = -[i(\omega_a-\omega_b) + \gamma/2]\rho_{ab} + \frac{i}{\hbar}V_{ab}(\rho_{aa}-\rho_{bb}) \quad , \tag{13c}$$

$$\dot{\rho}_{ba} = \dot{\rho}_{ab}^* \quad . \tag{13d}$$

Equations (13) are completely equivalent to eqs. (4) though solution[10] is somewhat more complicated. The utility of the density matrix formalism is in that eqs. (13) are easily modified to phenomenologically include other decay and feeding terms. For example, suppose that γ is actually composed of a sum of nondissociative quenching rates, γ_Q, as well as decomposition rates, γ_D. Excited state population which is quenched should reappear incoherently in the ground state population. Another incoherent effect due to intermolecular interactions is increased rate for loss of ensemble phase coherence. This appears as more rapid decay (greater than $\gamma/2$) of the off-diagonal density matrix elements. Although the formalism presented here is designed specifically to deal with the problem of laser-induced desorption, eqs. (13) may be further modified to apply to different or more complicated physical systems.[11] Simple modifications include, for example, additional coherent and incoherent feeding and decay paths for both states.

Recasting eqs. (13) to include these effects produces

$$\dot{\rho}_{aa} = -(\gamma_Q + \gamma_D)\rho_{aa} - \frac{i}{\hbar}\left[V_{ab}\,\rho_{ba} - V_{ba}\,\rho_{ab}\right] , \tag{14a}$$

$$\dot{\rho}_{bb} = \gamma_Q\rho_{aa} + \frac{i}{\hbar}\left[V_{ab}\,\rho_{ba} - V_{ba}\,\rho_{ab}\right] , \tag{14b}$$

$$\dot{\rho}_{ab} = -\left(i\omega_o + \frac{\gamma_T}{2}\right)\rho_{ab} + \frac{i}{\hbar}\,V_{ab}\,(\rho_{aa} - \rho_{bb}) , \tag{14c}$$

$$\dot{\rho}_{ba} = \dot{\rho}_{ab}^{\,*} , \tag{14d}$$

where $\omega_o = \omega_a - \omega_b$. $\frac{\gamma_T}{2}$ is the total phase relaxation rate defined such that

$$\gamma_T = \gamma_Q + \gamma_D + 2\gamma_{PD} \quad , \tag{15}$$

where γ_{PD} is the rate for "pure" dephasing. In NMR parlance, $\gamma_Q + \gamma_D$ can be associated with $1/T_1$ and $\frac{\gamma_T}{2}$ with $1/T_2$. V_{ab} is again given by eq. (5). The initial conditions are taken to be $\rho_{aa} = \rho_{ab} = \rho_{ba} = 0$ and $\rho_{bb} = 1$ as are appropriate for molecules in a supersonic molecular beam, or on a cold surface.

Solution of eqs. (14) is accomplished by an iterative procedure, as used in Lamb's semiclassical laser theory,[8] whereby it is noted that the population difference, $\rho_{aa} - \rho_{bb}$, is slowly varying compared to ρ_{ab}. The first order solution of eq. (14) is then

$$\rho_{ab}(t) = \frac{-i}{2}\,\omega_R\,(\rho_{aa} - \rho_{bb})\,\frac{e^{-i\omega t}}{i(\omega_o - \omega) + \gamma_T/2} \quad . \tag{16}$$

Substitution of eq. (16) into (14a) and (14b) yields

$$\dot{\rho}_{aa} = -(\gamma_D + \gamma_Q + L)\,\rho_{aa} + L\rho_{bb} \quad , \tag{17a}$$

$$\dot{\rho}_{bb} = (\gamma_Q + L)\,\rho_{aa} - L\rho_{bb} \quad , \tag{17b}$$

where

$$L = \frac{\omega_R^2 \gamma_T}{4(\omega-\omega_o)^2 + \gamma_T^2} \quad . \tag{18}$$

Integration of eqs. (17) is performed by the Laplace transform method to give second order solutions for ρ_{aa} and ρ_{bb}.

The fraction of population remaining at time t is

$$F_m(t) = \rho_{aa} + \rho_{bb}$$

$$= \exp\left[-(L + (\gamma_Q + \gamma_D)/2)t\right]$$

$$X\left[\frac{L + (\gamma_Q + \gamma_D)/2}{z'} \sinh(z't) + \cosh(z't)\right] \tag{19}$$

where

$$z' = \left[\left(L + \frac{\gamma_Q + \gamma_D}{2}\right)^2 - L\gamma_D\right]^{\frac{1}{2}} \tag{20}$$

In the case that $\omega_R < \gamma_Q + \gamma_D$, eq. (16) simplifies to

$$F_m(\omega,t) = \exp\left(-L \cdot \frac{\gamma_D}{\gamma_Q + \gamma_D}\right) \tag{21}$$

Substituting eq. (19) into eq. (21) yields a form of $F_m(t)$

which can be compared to eq. (10) (the isolated two level solution):

$$F_m(\omega,t) = \exp\left(-\omega_R^2\ \gamma_T^{-1}\ t\frac{\gamma_T^2}{4\Delta\omega^2 + \gamma_T^2}\cdot\frac{\gamma_D}{\gamma_Q + \gamma_D}\right) \quad . \qquad (22)$$

The width of the Lorentzian is increased by the added decay and dephasing processes as compared to eq. (10). Eq. (22) also includes a scaling factor $\gamma_D/(\gamma_Q + \gamma_D)$: if the quenching rate overwhelms decomposition processes, the ensemble remains intact. In the absence of pure dephasing and quenching eq. (22) reduces to eq. (10).

III. DISCUSSION

The pure case two-level-plus decay model is applicable to many recent vibrational predissociation studies since these have involved coherently excited van der Waals molecules formed in molecular beams. There is a substantial, growing body of experimental and theoretical literature devoted to these well-defined systems. The mixed-case formalism is appropriate for photochemical systems of increased complexity and has been presented in a form

describing laser-induced desorption of physisorbed molecules. Due to the increased difficulty of studying such systems, there are, unfortunately, relatively few examples of laser-induced desorption for comparison. In both the pure and mixed cases, photodissociation profiles and yields depend explicitly on decomposition rates. Physical details, such as coupling mechanisms and product distributions are intimately related to these rates but may remain unspecified in modeling photodissociation spectra.

In the discussion below, we consider the interpretation of spectral profiles and intensities observed in several van der Waals molecule experiments, and those anticipated in surface experiments. In light of the models presented, extraction of lifetimes from spectral data generally requires consideration of factors such as irradiation time, power, and the possibility of saturation. The same considerations apply in determining feasibility of lifetime measurements or optimizing experimental conditions. For more complicated photochemical systems, these considerations must also include competing rate processes.

Ethylene containing clusters

The pure case two-level-plus-decay model is in excellent agreement with the observed power and wavelength dependence of infrared photodissociation yields for ethylene dimer.[2] Lifetimes and transition probabilities for a series

of ethylene containing clusters have been obtained. The success of the model for $(C_2H_4)_2$ dissociation makes this an attractive system for exploring the nature of the lineshape in different regimes of power and irradiation time.

In one set of $(C_2H_4)_2$ photodissociation experiments, dimers were formed in supersonic expansions and detected 60 cm downstream with a mass spectrometer. Colinear excitation with a cw CO_2 laser provided low-power (6.7 W cm^{-2}) uniform irradiation of the beam with moderate fluences (3.7 mJ cm^{-2}) due to a long irradiation time (0.57 msec). The irradiation time corresponds to the flight time from the nozzle to the detector. Plots of fractional dissociation vs. laser frequency exhibit symmetric, nearly Lorentzian line-shapes close to the ν_7 out-of-plane bending frequency of free ethylene. Photodissociation spectra are homogeneously broadened. A Lorentzian fit to these raw data, however, leads to an error in the lifetime.

Eq. (10) and associated restrictions are appropriate for interpreting the experiment described. Note that eq. (10) is the exponential of a scaled Lorentzian. Thus, a plot of the logarithm of the undissociated fraction of molecules exhibits Lorentzian shape with width directly associated with the predissociation rate using eq. (11a). In addition, the transition moment for infrared absorption is readily determined from absolute fractional dissociation data using eq. (10), since μ appears in the scaling factor as part of the Rabi frequency.

The departure of eq. (10) from Lorentzian behavior increases with the scaling factor $\omega_R^2 \gamma_D^{-1} t$ and is not readily observable for $\omega_R^2 \gamma_D^{-1} t < 1$. For the ethylene dimer experiment described, $\omega_R^2 \gamma_D^{-1} t = 0.389$, and the width of a least-squares Lorentzian fit to the raw data yields a predissociation rate which is only 11% greater than obtained using eq. (10). In comparison, ethylene trimer has an absorption probability 1.5 times that of the dimer. Experimental conditions identical to those which yield $\omega_R^2 \gamma_D^{-1} t = 0.389$ for $(C_2H_4)_2$ give $\omega_R^2 \gamma_D^{-1} t = 0.795$ for the trimer. In the latter case a simple Lorentzian fit implies a dissociation rate which is high by 24%. Though these discrepancies are consistent with eqs. (11), the relative quality of statistical fits to experimental data is not sufficient to obviate use of either functional form. This is illustrated in Figure 1, which shows nearly identical least-squares Lorentzian fits to ethylene trimer dissociation spectra for fractional dissociation (solid line) and logarithm of the undissociated fraction (dashed line) as functions of laser frequency. Arrows indicate widths of the two fitted curves which differ by 24%. The statistical quality of the Lorentzian fit to the raw data shown in Figure 1 (solid line) is misleading and alone lends no justification to interpreting its width as a lifetime.

As laser power and irradiation time are increased, the lineshape, eq. (10), exhibits increasingly non-Lorentzian shape. At some point, saturation dramatically affects the

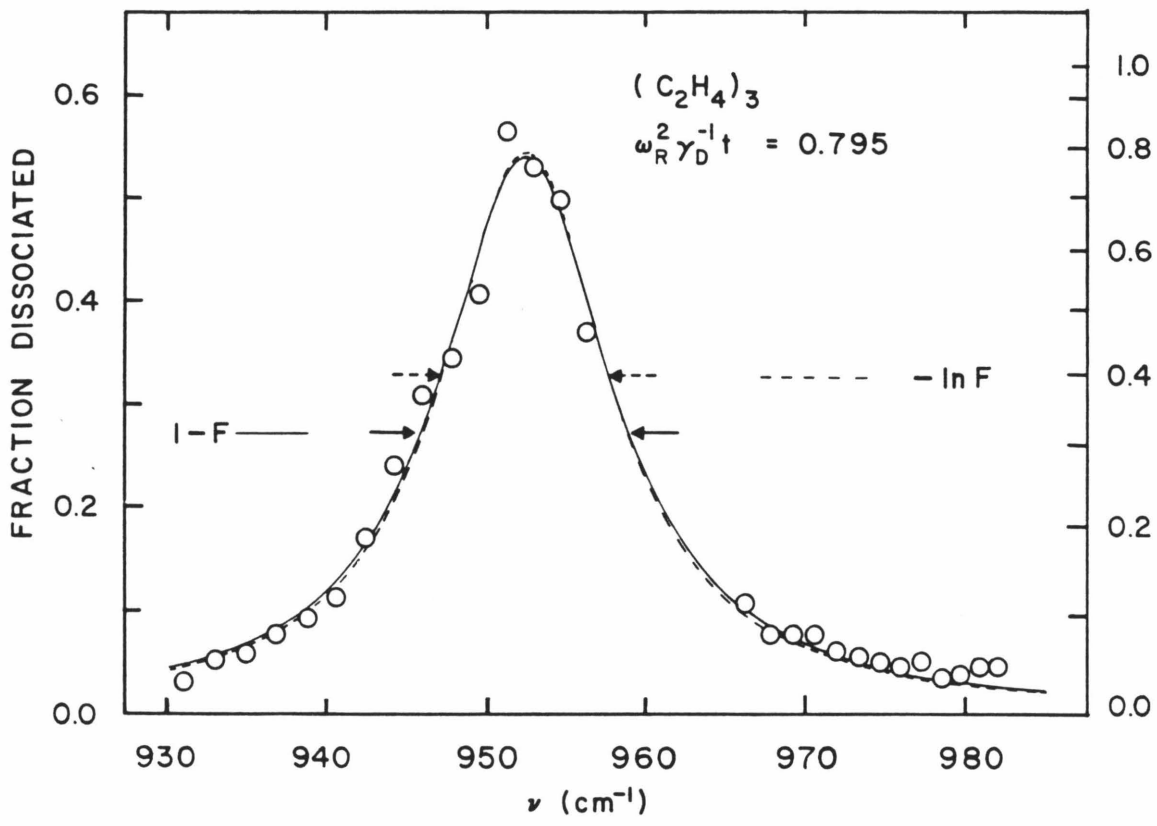

FIGURE 1. Photodissociation profiles for $(C_2H_4)_3$. The solid and broken lines are nonlinear least-squares fits of a Lorentzian and Eq. (10), respectively, to experimental measurements (circles). Arrows indicate widths of the profiles at half maximum on their respective scales.

profile, appearing as a plateau of complete attenuation of van der Waals molecule intensity. Such a situation is easily accessible for $(C_2H_4)_2$ dissociation and is depicted in eq. (10) with parameters determined in the dimer experiment described above. The broad, intense spectrum is obtained from eq. (10) using the same measured predissociation lifetime and transition moment, but with shorter irradiation time, t = 10 μsec, and higher power so that the fluence is 0.5 J/cm^2 — conditions attainable with a TEA CO_2 laser. Lifetimes can be extracted from saturated spectra using the same procedure described above for the low-fluence experiment. Note, however, that detailed analysis of pulsed laser photodissociation profiles is complicated considerably by temporal and spatial variations in laser power not included in the models presented here.

The width of the profile predicted for the pulsed laser experiment is an order of magnitude greater than observed using the cw laser. Inspection of eq. (11b) shows that the broadening varies with the product $\omega_R^2 t$ and is therefore dependent on laser fluence for a given molecule. We have dubbed this effect <u>fluence broadening</u> in order to distinguish it from power broadening and interaction-time broadening. The power-broadened width of a transition is given by the Rabi frequency, while the interaction time broadening is given by the reciprocal irradiation time. These widths (2×10^{-2} cm^{-1} and 5×10^{-7} cm^{-1}, respectively, for the pulsed laser experiment depicted in Figure 2 are

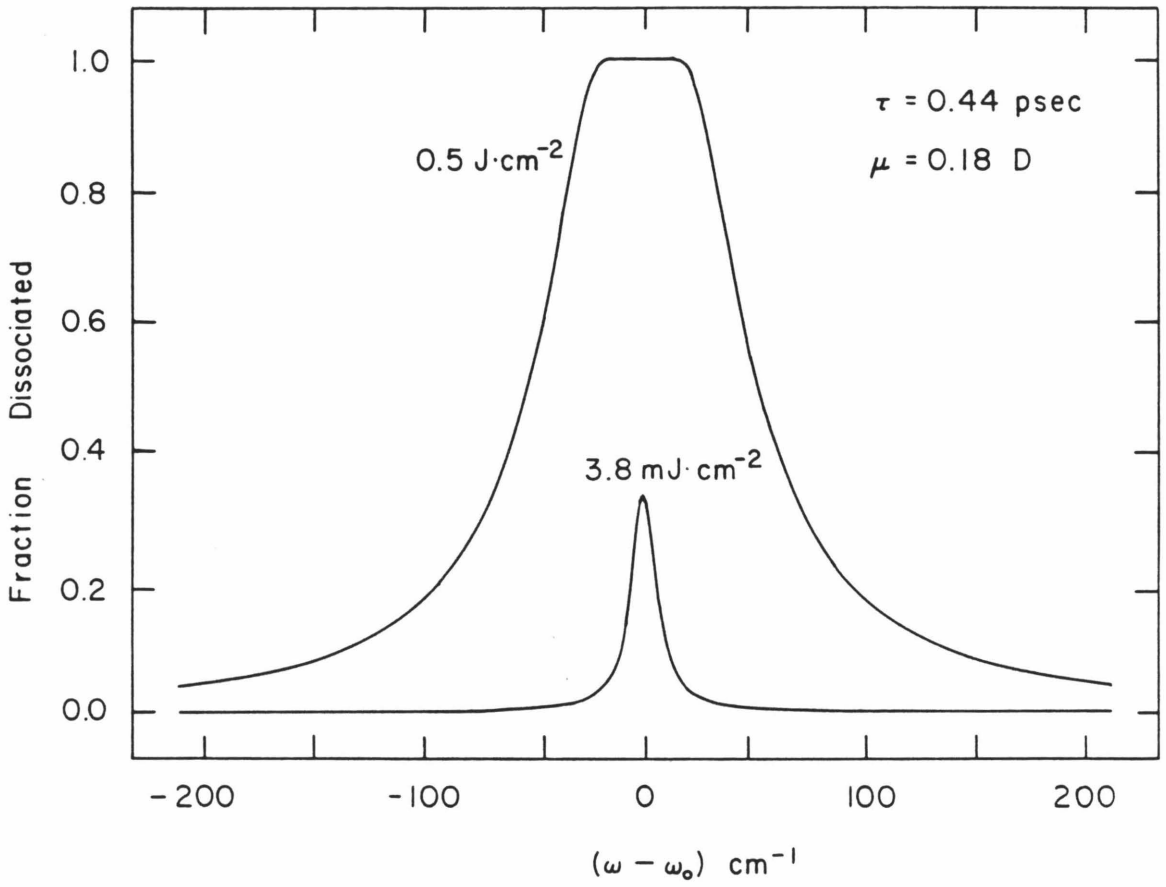

FIGURE 2. Photodissociation profiles for $(C_2H_4)_2$ calculated using Eq. (10) for pulsed laser (0.5 J cm^{-2}) and cw laser (3.8 mJ cm^{-2}) experiments.

insignificant compared to the lifetime and fluence broadened width.

The infrared photodissociation spectrum of ethylene dimer consists of an isolated, homogeneously broadened line. Because of this simplicity, fluence and saturation effects on the profile do not appreciably complicate extraction of the photodissociation rate from the spectrum. If the predissociative lifetime were somewhat longer, it is conceivable that inhomogeneous structure would begin to emerge, obscuring the saturation plateau and fluence broadening, and perhaps lead to an incorrect assessment of the nature of the broadening mechanism.

$\underline{He \cdot I_2}$

Vibrational predissociation of $He \cdot I_2$[12] is representative of a series of iodine-rare gas clusters which have been investigated thoroughly with innovative experiments reported by Levy and co-workers.[1] In these experiments, $He \cdot I_2$ formed in molecular beams is pumped optically to an electronically and vibrationally excited state of iodine. Fluorescence observed is emitted exclusively from uncomplexed I_2, and therefore fluorescence intensity is proportional to the fraction of irradiated molecules which predissociate. Spectral lines are significantly narrower than observed in the ethylene experiments, so that the possibility of observing saturation and fluence effects is more acute. Individual

bands are inhomogeneous and consist of overlapping homogeneously broadened rotational lines. In the analysis,[12] the rotational lines were assumed to be Lorentzian, with width corresponding to the predissociation rate, and a convolution procedure was employed to determine lifetimes.

Are conditions employed in the $He \cdot I_2$ experiments such that the choice of a Lorentzian as a functional form is valid? Two of many $He \cdot I_2$ transitions measured are $He \cdot I_2$ $X(\upsilon=0) \rightarrow B(\upsilon=12)$ and $X(\upsilon=0) \rightarrow B(\upsilon=25)$, which have squared transition moments of $\sim 2 \times 10^{-3}$ D^2 and $\sim 2 \times 10^{-2}$ D^2, respectively.[13] Measured widths yield lifetimes of 221 and 43 psec. The single mode laser power was approximately 0.3W focused to a 0.2 mm beam waist. Assuming a velocity of 2×10^5 cm/sec, the irradiation time in the crossed beam configuration is in the order of 10^{-7} sec. Each molecule then experiences a fluence of ~ 0.1 mJ cm^{-2}. The conditions yield scaling factors, $\omega_R^2 \gamma_D^{-1} t$, of 0.33 and 0.65 for the 0-12 and 0-25 transitions, respectively, so that lineshapes are quite similar to Lorentzian profiles. However, on the basis of eq. (11b), measured widths, and the approximate conditions, actual predissociation lifetimes are $\sim$9% and $\sim$17% larger than reported.

This discussion by no means vitiates results or significance of the $He \cdot I_2$ experiment. Discrepancies calculated certainly represent an upper limit and are reduced to 3% and 6% by simply decreasing the estimated product, $\omega_R^2 t$, by a factor of 3. Improved interpretation of the data would

require more precise knowledge of conditions employed, perhaps consideration of spatial variations of laser power and irradiation time, but would probably not change lifetimes reported by more than ten percent.

We emphasize that such considerations will be crucial to extraction of lifetimes in the case that any one of four factors--laser power, irradiation time, transition moment, and lifetime--is increased. For example, it would be trivial to completely remove $He \cdot I_2$ from a molecular beam using colinear excitation. In general, the prospect is excellent for observing large attenuation of cluster intensity in molecular beams using visible lasers and molecules with moderately allowed electronic transitions. Measuring absolute fractional attenuation--as in the ethylene experiments--permits direct determination of transition moments, which are important in line shape analysis, as well as straightforward assignment of spectra to particular clusters. The visible laser induced fluorescence technique is complimentary in that it is extremely sensitive and can be used to probe product state distributions as well a excitation spectra. Combination of the two techniques would seem to be ideal for fully characterizing vibrational predissociation of van der Waals molecules over a wide range of vibrational excitation.

$(CO_2)_2$

The first infrared laser induced vibrational predissociation spectrum was reported by Gough, Miller and Scoles for $(N_2O)_2$.[14] Similar experiments have since been performed with pure CO_2 clusters using an F-center laser oscillating near the (101) and (021) combination bands of CO_2.[3] In these experiments, the molecular beam was directed into a bolometer which produces a signal proportional to the energy imparted to the detector surface by collisions with molecules. The observed signal includes contributions from all degrees of freedom of all molecular beam components. Laser-excited predissociation of clusters scatters fragments out of the field of view of the detector and reduces bolometer signal by an amount which is assumed to be proportional to the fractional dissociation of van der Waals molecules.

The $(CO_2)_2$ photodissociation spectrum exhibits a broad, nearly symmetric band, near the (101) absorption frequency of CO_2, with full width at half maximum of 2.3 cm^{-1} providing a lower limit of 2.3 psec for the lifetime. The slight asymmetry suggests inhomogenity in the band and consequently longer lifetimes. In order to provide an upper limit, Miller has modeled the rotational structure and obtained a similar profile composed of $\sim 10^5$ rotational lines with no broadening mechanism imposed other than the 1 MHz bandwidth of the laser. However, the finite flight time of particles from the

irradiation region to the detector further limits the life-time to less than 3×10^{-4} sec.

The lineshape expression, eq. (10), together with dissociation yield data can considerably reduce the uncertainty in the CO_2 dimer lifetime. We have obtained dimer spectra similar to those described by Miller using an F-center laser in the colinear arrangement and monitoring fractional attenuation of $(CO_2)_2$ intensity in the molecular beam mass spectrum.[15] The maximum fractional dissociation observed is 0.6% using laser intensity of approximately 0.16 W/cm^2 and an irradiation time of 0.82 msec. Using eq. (10) and assuming complete homogeneity, these conditions yield 0.6% dissociation if the lifetime is 4.0 psec accounting for the full width of the observed spectrum. If the band is substantially inhomogeneous, it would be impossible to dissociate 0.6% of the total population at a given frequency, because the laser linewidth is extremely narrow. An intermediate degree of inhomogeneity may exist such that the laser probes subensembles to varying extent at different laser frequencies. An estimate of the minimum homogeneous width which is consistent with observations is 0.6% of the observed width. This corresponds to a maximum predissociation lifetime of 700 psec. With improved characterization of the CO_2 dimer spectrum and modeling, it should be possible to further reduce the uncertainty in the $(CO_2)_2$ predissociation lifetime to one order of magnitude.

Laser-Induced Desorption

The use of radiation to effect desorption of adsorbed species is a topic which encompasses a wide range of experiments. Included are cases in which species bound to semiconductor surfaces are desorbed with bandgap excitation,[16] or where the radiation enhances desorption by surface heating.[17] The subset of particular interest in this paper consists of the case in which coherent radiation directly excites vibrations within an adspecie to induce resonant desorption. The problem is conceptually similar to the case of van der Waals molecule vibrational predissociation[18] with one partner of the van der Waals complex being replaced by a surface. The adspecie subsequently desorbs upon coupling of the excited localized molecular vibration to the weak substrate-adsorbate bond. Unfortunately, a solid surface, particularly of a metal, is not strictly analogous to the other van der Waals partners previously discussed. The presence of additional fast decay channels not present in the gas phase experiments may serve to quench desorption. Electron-hole pair excitation[20] and phonon emission[21] are examples of such quenching mechanisms which must be considered when dealing with excited species in close proximity to a solid surface.

Relatively few experiments have demonstrated resonant desorption of condensed species.[22-24] Resonant molecular absorption of radiation followed by local heating has been

advanced as the mechanism for the evaporation of thick C_5H_5N layers on KCl or Ni.[24] A similar explanation for the case of CH_3F multilayers on NaCl (100) seems reasonable, as the wavelength dependence of the desorption yield mimics the solid-phase CH_3F adsorption spectrum.[23] An additional broad (~ 25 cm^{-1}) desorption feature for CH_3F on a NaCl film[23] has been interpreted as indicative of the layer bound directly to the surface. As there are few data with which to compare computed results, our discussion thus deals with the feasibility of future experiments. The mixed-case formalism presented here can be used to estimate the probability of desorption given reasonable rates for the different decay processes.

Vibration-vibration interactions coupling a high frequency (localized adatom) mode with low frequency surface (phonon) modes has been modeled,[20b,21] yielding rates of 10^{10}-10^{11} sec^{-1}. The rate of electron-hold pair excitation has also been considered[20] for the case of vibrationally excited CO bound to Cu and was computed to lie in the range of 10^{9}-10^{10} sec^{-1}. The 0.2 to 3.5 psec lifetimes of similar systems derived from IR reflection-absorption lineshapes[25] have been explained by invoking energy loss to charge oscillation in the CO-metal bond.[26] These results seem to indicate that, in general, rates of energy transfer to the metal may not be as fast as is commonly speculated.

We consider the example of a molecule which absorbs radiation from a low power (10 mW) cw laser at ~ 3100 cm^{-1}

(8.9 kcal/mole), with one-tenth the absorption strength ($\langle\mu\rangle$ = 0.01 D) of CO on Cu (100).[27] A model system would be $CH_4(\nu_3 = 1)$ adsorbed on a metal surface, or $NH_3(\nu_1 = 1)$ on an inert (e.g., sapphire) substrate. A glancing angle of incidence is used to interact with the component of molecular vibration normal to the surface,[28] which also serves to lower the laser power density. The mixed-case lineshape expression, eq. (22), is used to examine the dependence of the peak desorption signal ($\omega = \omega_o$) as a function of the experimentally determined irradiation time, t, and the system dependent rates, γ_D, γ_Q, and γ_{PD}. A more detailed account will be presented elsewhere,[29] but some important results are summarized here.

Figure 3 demonstrates that desorption may be induced, even with quenching rates faster than 10^{13} sec^{-1}, if the ensemble of molecules on the surface can be irradiated for a sufficiently long time. The fraction remaining on the surface after the indicated irradiation time, t, is plotted vs. the quenching rate, on a logarithmic scale. The assumed desorption rate is 10^{12} sec^{-1}, consistent with gas-phase rates, γ_{PD} is assumed negligible, and the example system parameters result in a Rabi frequency (ω_R) of 1.47×10^5 sec^{-1}. The maximum value of t, set by the cleanliness of the vacuum chamber, could probably not be greater than $\sim$ 3 hrs (10^4 sec).

Figure 4 examines the desorption response of the model system upon change of various molecular parameters. The

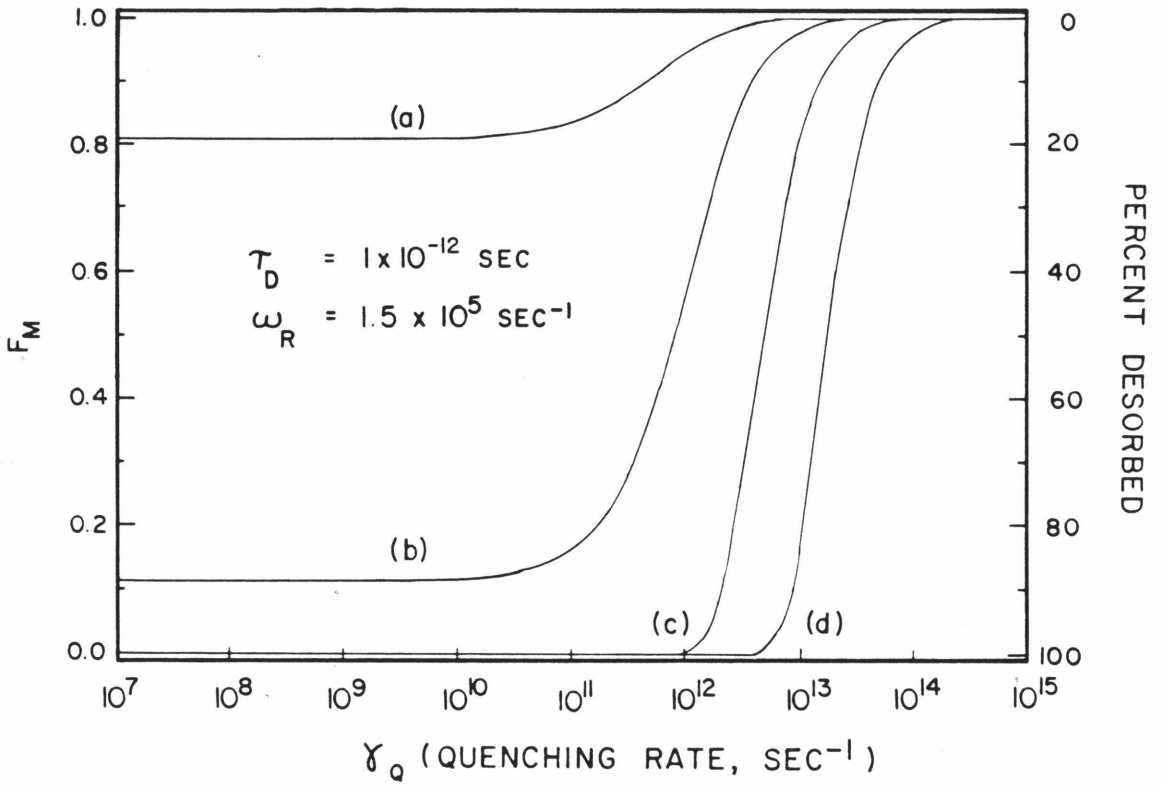

FIGURE 3. Fraction of adspecies remaining on the surface for a range of quenching rates. The irradiation time is: (a) 10; (b) 10^2; (c) 10^3; (d) 10^4 sec. Other parameters are given in the text.

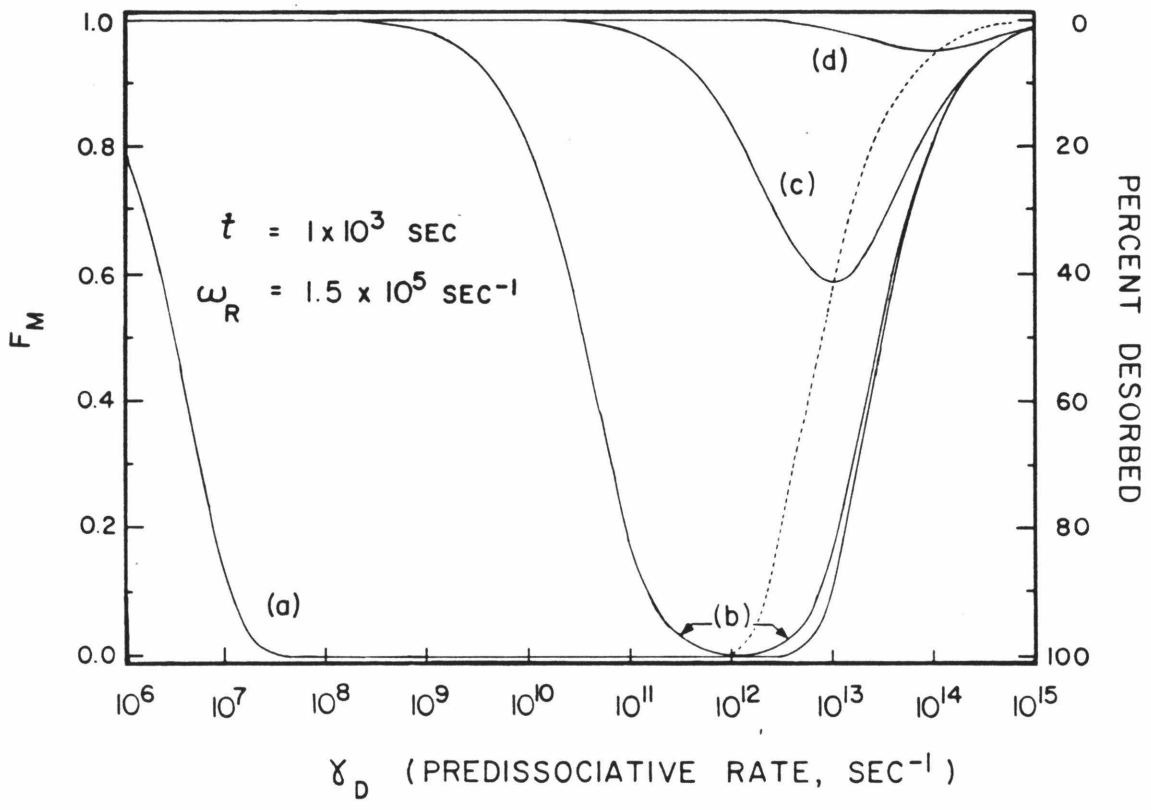

FIGURE 4. Fraction of adspecies remaining on the surface for a range of desorption rates. The quenching rate is: (a) 10^{10}; (b) 10^{12}; (c) 10^{13}; (d) 10^{14} sec^{-1}. Other parameters are given in the text.

fraction of adspecies remaining on the surface is plotted vs. the logarithm of the desorption rate, for various quenching rates. The Rabi frequency and dephasing rate are as set previously, while the irradiation time is fixed at 1000 sec. A variety of predissociative rates lead to observable attenuation of the overlayer, including cases with quenching rates of 10^{13} sec^{-1}.

The key to experiments of the type described lies with the term $\omega_R{}^2 t$ in eq. (22). Even with a low-power laser, desorption may be observed since t can be made large, and the product $\omega_R{}^2 t$ overwhelms the quenching rate γ_Q. Note that $\omega_R{}^2 t$ scales linearly with both the laser fluence and the square of the transition dipole moment. Desorption induced with a cw CO_2 laser may occur more readily than for the case calculated. Assuming the lower energy of vibration remains greater than the adsorbate-substrate bond strength, the higher available power and generally stronger absorption strengths of fundamentals in this spectral region would increase $\omega_R{}^2 t$ by a factor of 10-100, which would facilitate desorption over a wide range of dynamic rates. We conclude that resonant laser-induced photodesorption of weakly-bound adspecies should be an observable phenomenon.

Acknowledgement

This work was supported by the Division of Chemical Sciences, Office of Basic Energy Sciences, U. S. Department of Energy. One of us (FGC) thanks the Exxon Corporation for summer fellowship support.

REFERENCES

1. K. E. Johnson, W. Sharfin and D. H. Levy, J. Chem. Phys. 74, 163 (1981), and references contained therein.
2. M. P. Casassa, D. S. Bomse and K. C. Janda, J. Chem. Phys. 74, 5044 (1981).
3. R. E. Miller, T. E. Gough and G. Scoles, J. Phys. Chem., 85, 4041 (1981).
4. J. M. Lisy, A. Tramer, M. F. Vernon and Yuan T. Lee, J. Chem. Phys. 75, 4733 (1981).
5. J. A. Beswick, G. Delgado-Barrio and J. Jortner, J. Chem. Phys. 70, 3895 (1979).
6. G. Ewing, J. Chem. Phys. 72, 2096 (1980).
7. S. B. Woodruff and D. L. Thompson, J. Chem. Phys. 71, 376 (1979).
8. M. Sargent III, M. O. Scully and W. E. Lamb, Jr., Laser Physics (Addison-Wesley, Reading, Massachusetts, 1974).
9. J. C. Hemminger, R. Cavanagh, J. M. Lisy and W. Klemperer, J. Chem. Phys. 67, 4952 (1977).
10. K. E. Jones, A. Nichols and A. H. Zewail, J. Chem. Phys. 69, 3350 (1978).
11. W. G. Breiland, M. D. Fayer and C. B. Harris, Phys. Rev. A 13, 383 (1976).
12. K. E. Johnson, L. Wharton and D. H. Levy, J. Chem. Phys. 69, 2719 (1978).

13. J. Tellinghuisen, J. Quant. Spectrosc. Radiat. Transfer 19, 149 (1978), and A. Chutjian and T. C. James, J. Chem. Phys. 51, 1242 (1969).

14. T. E. Gough, R. E. Miller, G. Scoles, J. Chem. Phys. 69, 1588 (1978).

15. M. P. Casassa, F. G. Celii and K. C. Janda, unpublished results.

16. D. Lichtman, Y. Shapiro, in "The Chemistry and Physics of Solid Surfaces", Vol. II (eds., R. Vanselow, S. Y. Tong), CRC Press, Cleveland (1979).

17. J. P. Cowin, D. J. Auerbach, C. Becker, L. Wharton, Surf. Sci. 78, 545 (1978).

18. This analogy has also been utilized by Ewing (ref. 19) to extract photodesorption rates.

19. D. Lucas and G. E. Ewing, Chem. Phys. 58, 385 (1981).

20. a) B. N. J. Persson and M. Persson, Surf. Sci. 97, 609 (1980). b) T. Korzeniewski, E. Hood and H. Metiu, J. Vac. Sci. Tech. 20, 594 (1982).

21. H. Metiu, W. E. Palke, J. Chem. Phys. 69, 2574 (1978).

22. N. V. Karlov, R. P. Petrov, Yu. N. Petrov and A. M. Prokhorov, JETP Lett. 24, 258 (1977); see, however, B. Davies, M. Poliakoff, R. P. Smith and J. J. Turner, Chem. Phys. Lett. 58, 28 (1978).

23. J. Heidberg, H. Stein, E. Riehl and A. Nestmann, Z. Phys. Chem. Neue Folge 121, 145 (1980).

24. T. J. Chuang and F. A. Houle, J. Chem. Phys. 76, 3828 (1982).

25. See Table 1, ref. 26, and associated references therein.

26. B. N. J. Persson and M. Persson, Solid State Commun. 36, 175 (1980).

27. S. Andersson, Surf. Sci. 89, 477 (1979).

28. R. G. Greenler, J. Chem. Phys. 44, 310 (1966).

29. F. G. Celii, M. P. Casassa and K. C. Janda, submitted to Surf. Sci.

Chapter 5

Infrared Photodissociation of Hydrogen-Bonded Clusters: $C_2H_4 \cdot HF$ and $C_2H_4 \cdot HCl$

Infrared Photodissociation and Hydrogen-Bonded Clusters: $C_2H_4 \cdot HF$ and $C_2H_4 \cdot HCl$

Michael P. Casassa,[a] Colin M. Western, Francis G. Celii, David E. Brinza and Kenneth C. Janda[b]

Arthur Amos Noyes Laboratory of Chemical Physics,[c]
California Institute of Technology
Pasadena, California 91125

ABSTRACT

Infrared photodissociation spectra of $C_2H_4 \cdot HF$, $C_2H_4 \cdot HCl$ and $C_2H_4 \cdot NO$ formed in molecular beams are reported. Parameters determined are absorption frequencies, ω_o, initial-state lifetimes, τ, transition moments, $\langle\mu\rangle^2$:

	ω_o cm^{-1}	τ psec	$\langle\mu\rangle^2$ 10^{-3} D^2
$C_2H_4 \cdot HF$	974.8(1)	1.57(19)	44.2(28)
$C_2H_4 \cdot HCl$	964.3(1)	3.27(16)	51.9(34)
$C_2H_4 \cdot NO$	951.5(5)	0.72(10)	50.9(48)

---

[a] Atlantic Richfield Foundation Fellow and Proctor & Gamble Fellow

[b] Alfred P. Sloan Fellow

[c] Contribution No. 6827.

All are blue-shifted relative to the 949 cm^{-1} monomer ν_7 absorption frequency. While the frequency for $C_2H_4 \cdot HF$ is close to that observed in an Ar matrix, the frequency for $C_2H_4 \cdot HCl$ is shifted 6.8 cm^{-1} further than that observed in a matrix. The results are discussed in terms of the bonding interaction and the photodissociation mechanism.

INTRODUCTION

Spectroscopy of van der Waals molecules has been applied to understanding the nature of weak interactions between molecules for many years. Recently, van der Waals clusters have served as model systems for studying vibrational energy transfer within molecules.[1] They are attractive for this purpose because a single vibrational quantum in a covalently bound partner in a van der Waals complex is generally larger than the weak bond energy and can lead to dissociation. Ideally, factors which control the rate and direction of vibrational energy flow, as well as the fragmentation mechanism, can be determined.

Experimental studies of vibrational predissociation of van der Waals molecules were first performed by Levy and coworkers on HeI_2.[2] Since then vibrational predissociation spectra have been obtained for many clusters, both in the visible and the infrared.[3-6] Lifetimes inferred from spectral widths range from subpicosecond for ethylene

dimer[4,5] to greater than 10 nsec for HF dimer.[6] Theoretical workers have examined the relative importance of factors affecting vibrational predissociation rates. These studies show that rates are strongly dependent on the nature of the interaction between van der Waals partners and on the availability of internal degrees of freedom to absorb excess energy.[7]

Several experiments on vibrational predissociation of ethylene-containing clusters have been reported. Spectral widths observed for $(C_2H_4)_2$, $(C_2H_4)_3$ and $C_2H_4 \cdot C_2F_4$ all indicate similar lifetimes (less than 1 psec) for clusters excited with one quantum in the ν_7 out-of-plane C-H bending mode.[4] (Spectra of Ar- and Kr-containing clusters also exhibited broad widths but closer examination has revealed additional structure in the case of $Ar \cdot C_2H_4$. This work will be presented in a future publication.) Excitation of the ν_{10} in-plane bending mode leads to significantly longer decay times.[5] Scattering experiments[5,8] have shown that the fragments of ethylene dimer and trimer dissociation carry most of the excess energy as rotation and are scattered isotropically. These results imply that the same efficient decay mechanism operates in each of these clusters and that predissociation may be indirect.

Here we report photodissociation spectra of $C_2H_4 \cdot HF$ and $C_2H_4 \cdot HCl$ obtained by exciting the ν_7 mode of the C_2H_4 partner. Lifetimes measured are significantly longer than previously observed for other ethylene-containing clusters.

The absorption frequencies are strongly blue-shifted compared to the other ethylene complexes. These observations are discussed in terms of differences in the bonding interaction and the decay mechanism. We also report the photodissociation spectrum of $C_2H_4 \cdot NO$, which is similar to those obtained for the nonhydrogen-bonded ethylene clusters.

EXPERIMENTAL

The molecular beam apparatus used in obtaining photodissociation spectra of $C_2H_4 \cdot HF$, $C_2H_4 \cdot HCl$ and $C_2H_4 \cdot NO$ has been described previously.[4] Van der Waals molecules were synthesized in seeded supersonic expansions. Clusters were detected 60 cm downstream from the skimmed gas jet, using a quadrupole mass spectrometer equipped with an electron impact ionizer. The molecular beam was irradiated over the entire flight path by a counterpropagating, unfocused cw infrared laser beam. This arrangement ensured that the van der Waals complexes were bathed in a uniform radiation field for a period of approximately 0.5 msec, corresponding to the flight time from the source to the detector. Photodissociation, induced by mechanically chopped laser light, was detected as modulation of cluster intensities in the mass spectrum.

Two modifications greatly improved the experimental procedure. The first improvement was to measure the molecular beam intensity by counting ions, rather than measuring ion current. Under computer control, ion counts were accumulated in two channels corresponding to the laser-on and laser-off phases of the chopper blade. Periodically, the molecular beam was blocked and background counts were accumulated. These three count totals determine the absolute fraction of van der Waals molecules dissociated by the infrared laser. Uncertainty in this result was mainly due to statistical counting errors so that statistical error analysis of the measurement was straightforward. For low cluster intensities, or weak dissociation signals, a counting time corresponding to a time constant of several minutes was required to keep statistical uncertainties to an acceptable level.

The second improvement was to measure laser power inside the molecular beam apparatus, eliminating artifacts caused by variation of laser mode structure with wavelength and power. This was done by moving a mirror into the path of the molecular beam to deflect the laser beam into a calibrated thermoelectric detector before and after each dissociation measurement. The mirror also served to block the molecular beam for molecular beam background measurements.

The experiments were performed with a cw CO_2 laser, although for some experiments the same laser was operated as

an N_2O laser by using a different gas mixture. Both lasers are discreetly tunable with the N_2O laser filling in some of the gaps in the tuning curve of the CO_2 laser.

Spectra were taken by monitoring the photodissociation of the mass peaks $(C_2H_4HF)^+$, $(C_2H_4HCl)^+$ and $(C_2H_4NO)^+$ as a function of laser wavelength and power. For some expansion conditions, these spectra did not reflect photodissociation of the simplest dimeric species, but rather photodissociation of large clusters. To ensure that spectra of dimeric species were obtained, the dependences of the spectra and the mass peak intensities on the expansion conditions were thoroughly investigated.

RESULTS

Figures 1-3 show the photodissociation spectra obtained for HF, HCl and NO mixtures under a variety of expansion conditions. All three show significant changes with concentration but each converges on a single peak with a fixed intensity at the lowest concentration. Experiments with lower concentrations were not feasible because of the low count rates. Furthermore, the spectra taken at the lowest concentration did not show a pressure dependence over a range of source pressure of about 5-15 atm. This leads us to believe that these limiting spectra are mainly due to the mixed dimers with little contribution from higher polymers.

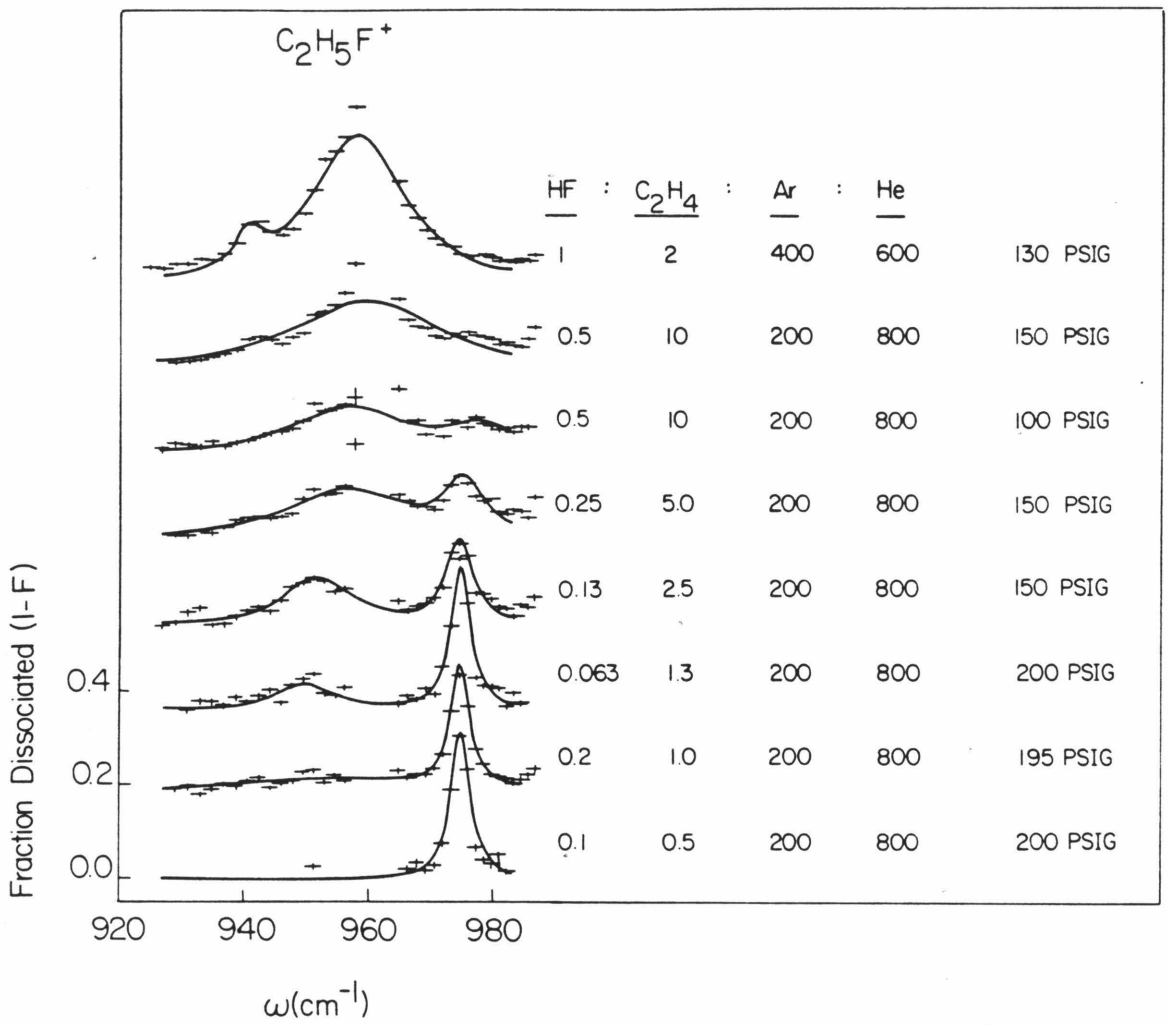

FIGURE 1. Photodissociation spectra of $(C_2H_4)_m(HF)_n$ clusters observed at m/e 48 ($C_2H_5F^+$) for a variety of expansion conditions. The lowermost spectrum best represents $C_2H_4 \cdot HF$. Solid curves are best non-linear least-squares fits of the line shape formula described in the text. Data points shown are averages of several measurements, taken over a range of powers and scaled using the fitted parameters to a laser fluence of $2.4 mJ/cm^2$. Error bars correspond to ± σ. Where spectra appears to consist of more than one peak, fitted curves are weighted superpositions of line shape formulas,

$$F = \sum_i X_i F_i \quad ,$$

where the mole fractions, X_i, are adjustable parameters constrained by

$$\sum_i X_i = 1 \quad .$$

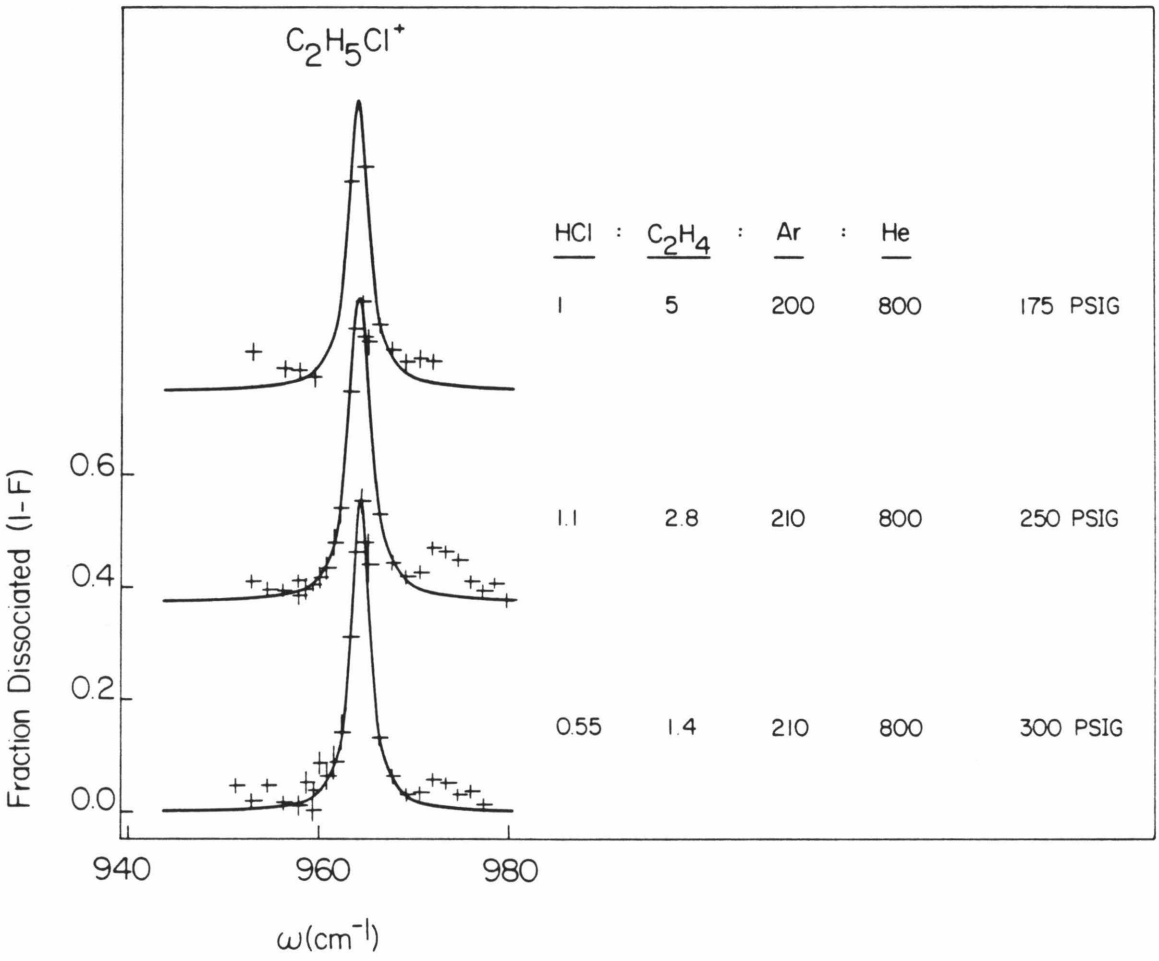

FIGURE 2. Photodissociation spectra of $(C_2H_4)_m(HCl)_n$ observed at m/e 64 ($C_2H_5Cl^+$) with a laser fluence of 3.7 mJ/cm^2. The lowermost spectrum best represents $C_2H_4 \cdot HCl$. See Figure 1 and the text for details of the data manipulation and curve fitting.

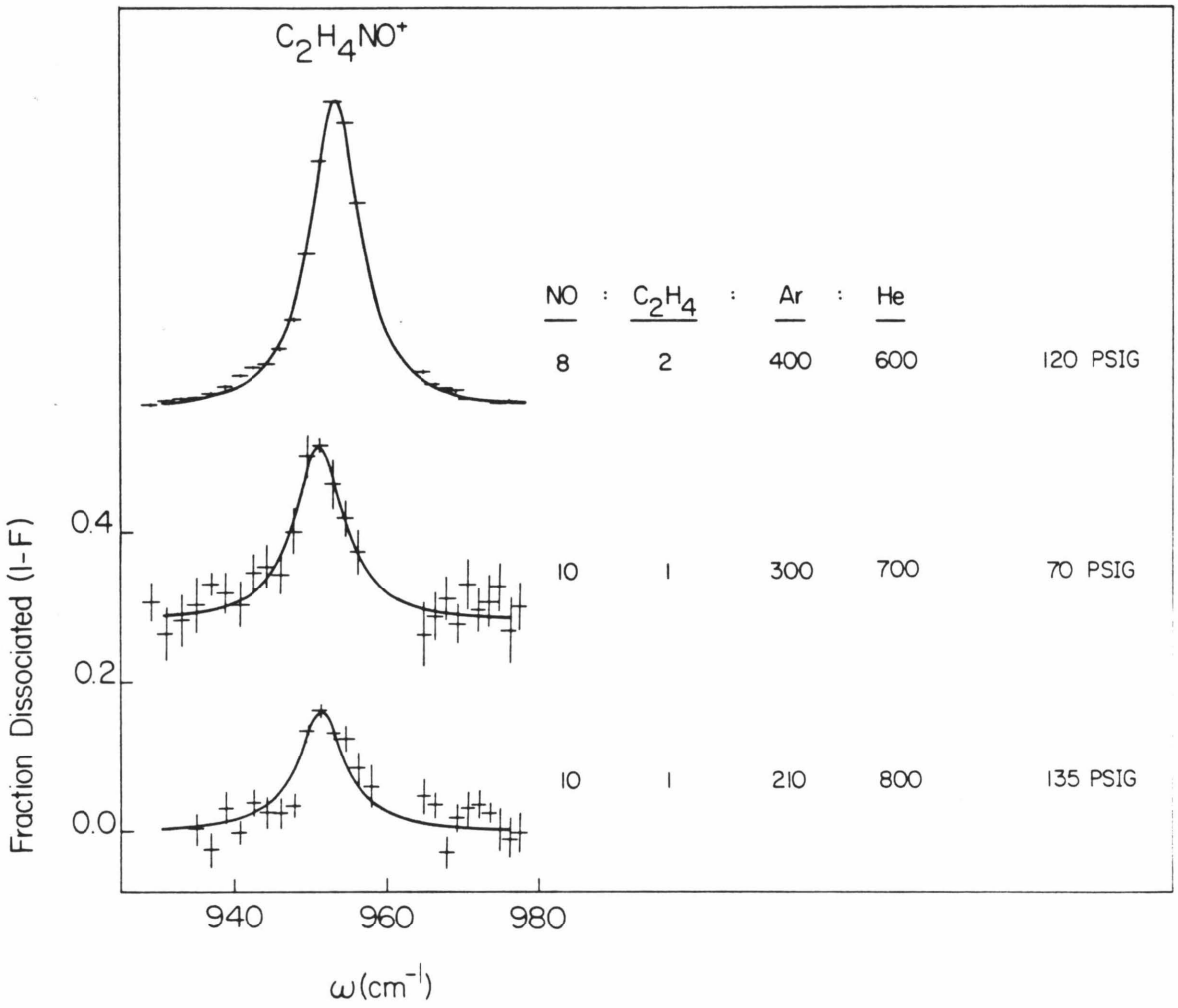

FIGURE 3. Photodissociation spectra of $(C_2H_4)_m(NO)_n$ observed at m/e 58 ($C_2H_4NO^+$) with a laser fluence of 1.9 mJ/cm^2. The lowermost spectrum best represents $C_2H_4 \cdot NO$. See Figure 1 and the text for details of the data manipulation and curve fitting.

It should be noted that the pressure dependence of molecular beam intensities, which has also been used as a diagnostic tool for determination of cluster sizes contributing to a given mass,[4,5] was of limited use in this work. The mass peaks used in these experiments always showed a smooth pressure dependence, $\sim P^2$, regardless of the gas mixture used. The mass spectrum did, however, serve to reject obviously unsuitable mass peaks and to aid minimization of the concentration of unwanted species such as $(C_2H_4)_n$. For example, the pressure dependence of m/e 66 (notionally $C_2H_4H^{37}Cl^+$) was of higher order than that of m/e 64 ($C_2H_4H^{35}Cl$) so m/e 66 was not used for photodissociation spectra of the dimer.

The line shape found in previous experiments on ethylene were successfully described by a formula derived from a two-level-with-decay model.[9] In order to apply the model, it must be demonstrated that observed spectra are homogeneous. The discussion given in our previous paper[4] on this point applies here, and furthermore, Gentry and coworkers have verified experimentally that ethylene cluster spectra are homogeneous.

The lineshape formula is:

$$F(\omega,t) = \exp\left[\frac{-\omega_R^2\,\gamma t}{4(\omega-\omega_o)^2 + \gamma^2}\right] \qquad (1)$$

where F is the fraction of molecules remaining undissociatd after irradiation at angular frequency ω for a time t. The central frequency of the transition is ω_o and the decay rate for molecules in the excited state is γ. The lifetime, τ, is simply γ^{-1}. The Rabi frequency, ω_R, is given by:

$$\omega_R = \frac{\underset{\sim}{\mu} \cdot \underset{\sim}{E}}{\hbar} = \frac{\langle \mu \rangle |E| \langle \cos^2\theta \rangle^{1/2}}{\hbar} \qquad (2)$$

where $\underset{\sim}{\mu}$ is the transition dipole moment, $\underset{\sim}{E}$ is the electric field, and θ is the angle between μ and E. The result of averaging $\cos^2\theta$ is:

$$\omega_R^2 = \frac{\langle \mu \rangle^2 |E|^2}{3\hbar^2} \qquad (3)$$

This factor of 3 was not taken into account in our previous work on ethylene clusters, and our reported transition moments were a factor of 3 too small. Our results and those of Gentry are now in agreement.[5]

The irradiation time, t , was calculated using the effective heat capacity and molecular weight of the expansion mixture assuming all the thermal rotational and translational energy is converted to translational energy of the molecular beam.[4]

Values of ω_o, τ and $\langle \mu \rangle^2$ obtained by a nonlinear least-squares fit to the above line shape formula are shown in Table I. The uncertainties shown are 95% confidence

TABLE I. Parameters obtained from line shape fit to photodissociation wavelength and power-dependence data.[a]

Cluster	ω_o (cm^{-1})	τ (psec)	$\langle\mu\rangle^{2}$[b] (10^{-3} D^2)
$(C_2H_4)_2$	952.3(5)	0.44(5)	96.0(18)
$(C_2H_4)_3$	952.3(5)	0.50(7)	141.0(33)
$C_2H_4 \cdot NO$	951.5(5)	0.72(10)	50.9(48)
$C_2H_4 \cdot C_2F_4$	954.7(2)	0.89(10)	46.2(63)
$C_2H_4 \cdot HF$	974.8(1)	1.57(19)	44.2(28)
$C_2H_4 \cdot HCl$	964.3(1)	3.27(16)	51.9(34)
C_2H_4[c]	949.0		35.5(14)

[a] Errors reflect 95% nonlinear confidence limits.

[b] Values for $\langle\mu\rangle^2$ reported in ref. 4 have been multiplied by 3. See text for discussion on this point.

[c] Ref. 16.

limits. In the case of $C_2H_4 \cdot HCl$, the spectrum used shows definite evidence for a higher cluster in the small feature at $\sim$943 cm^{-1} and in a smaller-than-expected dissociation at higher power. To account for this, the least-squares fit was restricted to the 959 - 970 cm^{-1} range and a fourth parameter, x, was introduced corresponding to the mole fraction of $C_2H_4 \cdot HCl$ in the molecular beam. The observed fraction remaining, F_o, is then given by:

$$F_o = xF + 1 - x \qquad (4)$$

For this case x was found to be 0.69(3). In the spectra of $C_2H_4 \cdot HF$ and $C_2H_4 \cdot NO$ there is less evidence for the presence of other species, and exponential power dependence was observed for the full range of power available (1-10 W cm^{-2}). In any case uncertainties in the mole fraction only affect the quoted transition moment, not the center frequency or lifetime.

We can also make tentative assignments of the other peaks in the spectra. All show an intense peak near 950 cm^{-1} at high ethylene concentration, and the hydrogen halide complexes show small peaks of higher frequency than the dimer peak. Earlier work[4] indicated that ethylene polymers absorb around 953 cm^{-1} and are typically more intense than dimer species. In mixtures rich in ethylene where large clusters are formed, most clustered ethylene will be in an experiment similar to that in pure ethylene

clusters, so that the spectrum should approach that of ethylene polymers. This is in fact observed in all three cases. Note, however, that the clusters whose spectra are observed at 950 cm^{-1} must contain at least one HF (or HCl, NO) to be detected on the mass peak which was monitored.

From the spectra taken at low concentrations we see that ethylene bound to one hydrogen halide has a significant frequency shift. We might suppose that ethylene bound to two or more hydrogen halides might have an even greater shift. In the case of $C_2H_4 \cdot HCl$ the mixtures relatively high in HCl do indeed show a peak to the blue of the dimer peak which we can assign to $C_2H_4 \cdot (HCl)_2$ and other polymers rich in HCl. There is some evidence for a similar peak due to $C_2H_4 \cdot (HF)_2$ but, unfortunately, this seems to occur just out of the range of the CO_2 laser.

DISCUSSION

The results of the $C_2H_4 \cdot HF$ and $C_2H_4 \cdot HCl$ experiments are qualitatively different than those of other ethylene clusters. Inspection of Table I shows that lifetimes of nonhydrogen-bonded clusters are grouped below 1 psec, while $C_2H_4 \cdot HCl$ and $C_2H_4 \cdot HF$ are considerably longer lived. Central absorption frequencies in the nonhydrogen-bonded species are all slightly blue-shifted from the monomer absorption frequency. In contrast, $C_2H_4 \cdot HCl$ and $C_2H_4 \cdot HF$ exhibit larger

blue-shifts of 15.3 cm^{-1} and 25.8 cm^{-1}, respectively. However, despite the range of lifetimes and blue-shifts observed, transition moments for ν_7 absorption per ethylene subunit show remarkable similarity for all the clusters listed in Table I. In the discussion below, we consider these observations in terms of the interaction between partners, and their implications for the dissociation mechanism.

A. The Bonding Interaction of $C_2H_4 \cdot HF$ and $C_2H_4 \cdot HCl$

$C_2H_4 \cdot HCl$ and $C_2H_4 \cdot HF$ are unique among ethylene-containing clusters in that their microwave[10] and matrix-isolated infrared spectra[11] have been observed. The microwave spectra show that the axis of the diatom is perpendicular to the ethylene plane in the equilibrium structure, with the hydrogen of the diatom directed toward the π clouds of the C=C bond. The distances between centers of mass of the partners are 3.097 Å for $C_2H_4 \cdot HF$ and 3.67 Å for $C_2H_4 \cdot HCl$.

The ν_7 absorption frequencies of $C_2H_4 \cdot HF$ and $C_2H_4 \cdot HCl$ in matrices[11] are both blue-shifted relative to C_2H_4 but not to the extent observed here. The blue-shifts of matrix-isolated $C_2H_4 \cdot HF$ and $C_2H_4 \cdot HCl$ are 1.8 cm^{-1} and 6.8 cm^{-1} less than the gas phase shifts. This difference is presumably due to some matrix-induced constraint on the $C_2H_4 \cdot HCl$ geometry. While the same forces should act on

$C_2H_4 \cdot HF$, their manifestation may not be as large, since the interaction between C_2H_4 and HF is stronger than that between C_2H_4 and HCl.

A blue shift for the ethylene ν_7 vibration in $C_2H_4 \cdot HF$ and $C_2H_4 \cdot HCl$ is expected on electrostatic grounds alone. The ν_7 motion leads to an electrostatic potential energy increase as the ethylene hydrogens approach the hydrogen-bound proton and a decrease as they move away. Since the electrostatic interaction is roughly proportional to $1/r^2$, the net result is a narrowing of the ν_7 vibrational potential and an increase in frequency. An implicit assumption in this picture is that aside from the electrostatic interaction, the bending force constant is unchanged in hydrogen bonding. This simple picture is supported by the fact that infrared spectra of matrix-isolated $C_2H_4 \cdot HF$ and $C_2H_4 \cdot HCl$ show no measurable shifts of infrared active CH bending or stretching modes in C_2H_4 other than the out-of-plane bend.[11]

Considering only the ν_7 vibration and treating the atoms as point charges, the effective ν_7 potential can be written as:

$$V = \tfrac{1}{2}k_\beta(\beta_1^2 + \beta_2^2) + \sum_{i,j} \frac{q_i q_j}{|\underset{\sim}{r}_{ij}|} \qquad (5)$$

where k_β is the ν_7 bending force constant,[12] β_1 and β_2 are out-of-plane bending angles (constrained to be equal), and i and j are atom indices on the ethylene and hydrogen halide fragments, respectively. The eigenvalues and eigenfunctions of this potential were found using standard techniques[13] given estimates of the parameters in eq. (5). Interatomic distances, r_{ij}, were taken from the structures described above. The atomic charges, q_k, were formal charges deduced from isolated molecule properties or those reported in an ab initio study of $C_2H_4 \cdot HX$ electronic structure.[14] The isolated molecule properties used were the HX dipole moments[15] and C-H bond-dipole moments which reproduced the measured C_2H_4 ν_7 intensity.[16]

For comparison, similar calculations were performed with the electrostatic term of eq. (5) replaced with a pair-wise Lennard-Jones potential, plus a pair-wise charge-induced dipole potential, to approximate the interaction in the nonhydrogen-bonded cluster, $C_2H_4 \cdot NO$. The ArNe and ArHe Lennard-Jones parameters[17] were chosen to model the interactions of NO with C and H, respectively. The polarizability of NO was approximated with that of Ar.[18] The geometry was taken to resemble the structures of the hydrogen-bonded complexes.

Results of these calculations, and parameters used, are listed in Table II. Calculated blue-shifts for $C_2H_4 \cdot HF$ and $C_2H_4 \cdot HCl$ are in qualitative agreement with the observed values. Comparison of shifts calculated using parameters

TABLE II. Parameters used and results of the frequency shift calculation.[a]

Cluster	C_2H_4 q_H	C_2H_4 q_C	HX q_H	HX q_X	R_{cm} (A)	D_e (cm^{-1})	ω_o (cm^{-1})	$\Delta\omega$ (cm^{-1})	$\langle\mu\rangle^2$ $D^2 x10^{-3}$
Isolated molecule properties:									
C_2H_4	.1375	-.2750	--	--	--	--	947.98	--	35.3
$C_2H_4 \cdot HF$	.1375	-.2750	.4130	-.4130	3.097	- 939.28	957.60	9.62	35.0
$C_2H_4 \cdot HCl$	.1375	-.2750	.1786	-.1786	3.670	- 375.49	952.29	4.32	35.2
$C_2H_4 \cdot NO$	.1375	-.2750		b	3.299	- 326.08	948.11	.13	35.3
Ab initio properties:									
C_2H_4	.1631	-.3263	--	--	--	0.00	947.98	--	49.7
$C_2H_4 \cdot HF$	.1770	-.3494	.3894	-.3985	3.097	-1075.27	959.36	11.38	57.6
$C_2H_4 \cdot HCl$	.1720	-.3416	.2167	-.2214	3.670	- 549.70	954.42	6.49	54.8
$C_2H_4 \cdot NO$	.1631	-.3263		b	3.299	- 388.64	947.97	-.01	49.7

[a] The harmonic part of the potential was the same for all calculations and used the following parameters for C_2H_4:[19] k_β = .289 mdyne A/rad^2, R_{C-H} - 1.081 A, R_{C-C} = 1.334 A, <HCH = 117.37°. D_e is the potential minimum and R_{cm} is the distance between the centers of mass of the partners.

[b] These calculations were performed with a pair-wise Lennard-Jones potential with induction forces. The parameters used were: α_{NO}=1.64A^3; NO-C: ε=48.7 cm^{-1}; R_e=3.43 A; NO-H: ε=20.4 cm^{-1}, R_e=3.47 A.

from isolated molecule properties and the ab initio values shows that the calculated shifts are sensitive to the values of the formal charges which in themselves are only an approximation to the true distribution. Thus, calculations with a more detailed charge distribution might reproduce the blue-shifts observed in $C_2H_4 \cdot HF$ and $C_2H_4 \cdot HCl$ without adjusting k_β. The blue-shift calculated for $NO \cdot C_2H_4$ is very slight, but shows that induction and dispersion forces, which would cause a red-shift, can be compensated by valence forces to produce a blue-shift.

The experiments reported here demonstrate that the dissociation energy, D_o, of $C_2H_4 \cdot HF$ must be less than 975 cm^{-1} Assuming a zero-point energy of 50 cm^{-1} for the stretching vibration of the van der Waals bond, this dissociation energy is lower than would be inferred from the published ab initio value of the bond energy, D_e = 1180 cm^{-1},[14] or from the 1075 cm^{-1} bond energy listed in Table II. These exaggerated bond energies, which would preclude dissociation, reflect the approximate character of the calculations.

Infrared transition moments are characteristic of the charge distribution on C_2H_4. If the charge distribution on C_2H_4 is held fixed, and if the influence of the polarizability of the partner is neglected, then only changes in the vibrational motion can affect the transition moment. The calculations using isolated-molecule properties show this effect to be negligible even for strongly bound

clusters. A more pronounced, though still relatively small, change in the transition moment occurs if the C_2H_4 charge density is redistributed upon hydrogen bonding, as shown by the calculations using ab initio parameters. The measured transition moments in Table I are close to the transition moment of ethylene monomer,[16] although we note that all are slightly larger. This may be due to the presence of a polarizable partner in the clusters. For example, if the contribution of the polarizability of NO is included, the transition moments calculated are 13% larger than those listed in Table II.

These considerations imply that the electronic structure of the C-H bonds of C_2H_4 is not strongly perturbed by hydrogen bonding and that the blue-shift is electrostatic in origin. The magnitude of the blue-shift reflects the change in the distribution of electron density in the C=C bond and in the hydrogen halide upon hydrogen bonding.

B. Decomposition Mechanisms

Photodissociation linewidths have implications for the predissociation mechanism but only reflect decay of the initially excited state. The mechanism could, indeed, be indirect involving other states before dissociation. If the mechanism is direct and does not involve excitation of internal degrees of freedom, one might expect $C_2H_4 \cdot HF$ and

$C_2H_4 \cdot HCl$ to exhibit the fastest decay since they are more strongly bound than the nonhydrogen-bonded clusters and consequently offer a smaller momentum or energy gap. In fact, $C_2H_4 \cdot HF$ and $C_2H_4 \cdot HCl$ have the slowest decay rates. The availability of degrees of freedom to absorb excess energy would also affect the measured lifetime regardless of the nature of the dissociation mechanism. However, the variety of degrees of freedom of the passive constituents listed in Table I is not reflected in the range of lifetimes, and no clear trends are apparent.

Another factor which may influence decay rates is the shape of the intermolecular potential. In particular, one may expect hydrogen-bonded clusters to have deeper and narrower wells than the other clusters. The barrier to internal rotation could be substantial and is perhaps as large as the dissociation energy. Velocity-resolved angular distribution experiments[5,8] on $(C_2H_4)_2$ indicate that most of the excess energy appears in the fragments as rotational energy. Excitation of rotation then appears to be important in the decomposition process and on this basis one might expect decay of rigid clusters to proceed slowly.

ACKNOWLEDGEMENTS

The authors thank J. L. Beauchamp for the use of his CO_2 laser and D. S. Bomse for helpful discussions. One of us (M.P.C.) thanks the Shell Companies Foundation for summer fellowship support. This work was supported by the Division of Chemical Sciences, Office of Basic Energy Sciences, U. S. Department of Energy.

REFERENCES

1. For a comprehensive bibliography of work in this field published prior to 1980, see: J. A. Beswick and J. Jortner, Adv. Chem. Phys. 47, 363 (1981).

2. R. E. Smalley, D. H. Levy and L. Wharton, J. Chem. Phys. 64, 3266 (1976).

3. D. H. Levy, Ann. Rev. Phys. Chem. 31, 197 (1980); T. E. Gough, R. E. Miller and G. Scoles, J. Phys. Chem. 85, 4041 (1981); J. Geraedts, S. Stolte and J. Reuss, Z. Phys. A - Atoms and Nuclei 304, 167 (1982); J. M. Lisy, A. Tramer, M. F. Vernon and Y. T. Lee, J. Chem. Phys. 75, 4733 (1981); M. F. Vernon, J. M. Lisy, H. S. Kwok, D. J. Krajnovich, A. Tramer, Y. R. Shen and Y. T. Lee, J. Phys. Chem. 85, 3327 (1981); M. P. Casassa, D. S. Bomse and K. C. Janda, J. Phys. Chem. 85, 2623 (1981); M. F. Vernon, D. J. Krajnovich, H. S. Kwok, J. M. Lisy, Y. R. Shen and Y. T. Lee, J. Chem. Phys. 77, 47 (1982); also see ref. 1.

4. M. P. Casassa, D. S. Bomse and K. C. Janda, J. Chem. Phys. 74, 5044 (1981).

5. M. A. Hoffbauer, K. Liu, C. F. Giese and W. R. Gentry, J. Chem. Phys. 78, 5567 (1983).

6. A. S. Pine and W. J. Lafferty, J. Chem. Phys. 78, 2154 (1983).

7. G. E. Ewing, Chem. Phys. 63, 411 (1981); D. A. Morales and G. Ewing, Chem. Phys. 53, 141 (1980); also see ref. 1.

8. D. S. Bomse, J. B. Cross and J. J. Valentini, J. Chem. Phys. 78, 7175 (1983).

9. M. P. Casassa, F. G. Celii and K. C. Janda, J. Chem. Phys. 76, 5295 (1982).

10. P. D. Aldrich, A. C. Legon and W. H. Flygare, J. Chem. Phys. 75, 2126 (1981); J. A. Shea and W. H. Flygare, J. Chem. Phys. 76, 4857 (1982).

11. L. Andrews, G. L. Johnson and B. J. Kelsall, J. Chem. Phys. 76, 5767 (1982).

12. G. Herzberg, Infrared and Raman Spectra (Van Nostrand Reinhold, New York, 1966).

13. J. W. Cooley, Math. Comput. 15, 363 (1961).

14. A. Hinchliffe, Chem. Phys. Lett. 85, 531 (1982).

15. R. Weiss, Phys. Rev. 131, 659 (1963); E. W. Kaiser, J. Chem. Phys. 53, 1686 (1970).

16. T. Nakanaga, S. Kondo and S. Saeki, J. Chem. Phys. 70, 2471 (1979).

17. G. Scoles, Ann. Rev. Phys. Chem. 31, 81 (1980).

18. A. Dalgarno and E. A. Kingston, Proc. Roy. Soc. (London) A259, 424 (1961).

19. J. L. Duncan and E. Hamilton, J. Mol. Struct. 76, 65 (1981).

Chapter 6

Inhomogeneity in the Infrared Photodissociation Spectra of $(C_2H_4)_2$, $C_2H_4 \cdot HF$ and $C_2H_4 \cdot HCl$

INHOMOGENEITY IN THE INFRARED PHOTODISSOCIATION SPECTRA OF $(C_2H_4)_2$, $C_2H_4 \cdot HF$ AND $C_2H_4 \cdot HCl$

Michael P. Casassa,[a] Colin M. Western, and Kenneth C. Janda[b]

Arthur Amos Noyes Laboratory of Chemical Physics,[c]
California Institute of Technology
Pasadena, California 91125

ABSTRACT

A general inhomogeneous lineshape model for describing predissociation spectra is presented. The model is applicable to systems of noninteracting molecules for which the predissociation rate is greater than the Rabi frequency. The multilevel lineshape formula is used to analyze previously reported results for $(C_2H_4)_2$, $C_2H_4 \cdot HF$ and $C_2H_4 \cdot HCl$. The infrared photodissociation spectra of these van der Waals

---

[a]Atlantic Richfield Foundation Fellow and Proctor & Gamble Fellow.

[b]Alfred P. Sloan Foundation Fellow.

[c]Contribution No._____.

molecules are homogeneous in appearance. However, the broad ν_7 spectrum of $(C_2H_4)_2$ is shown to be significantly affected by orientational inhomogeneity, and is a perpendicular or hybrid band. The narrower spectrum of $C_2H_4 \cdot HF$ exhibits inhomogeneity due to dispersion of rotational transitions, while the $C_2H_4 \cdot HCl$ spectrum is essentially homogeneous. Other sources of inhomogeneity, including Fermi resonance, are discussed in terms of their effects on band shapes and intensities.

INTRODUCTION

In recent years spectroscopists studying dynamics of molecules, and in particular those studying the infrared photodissociation of van der Waals molecules, have observed broad, featureless absorption bands.[1-5] Strictly, the widths of such bands can only provide an upper limit for the rate of an unspecified decay process involved in the transition. The profile of the observed band and its intensity, in instances in which the fraction of molecules dissociating is measured, are used to assert that such bands are essentially homogeneous.[1,2,4] Broadening due to a distribution of initial states (and, indeed, absorbing species) and to the inevitable distribution of final states is asserted to be negligible compared to the natural width of the transition. Thus, by taking into account laser power

and fluence effects, the decay rate of the initial state can be deduced from the spectral width.

Of course, the procedure described above hinges on the assertion of complete homogeneity within a band. In several laboratories, two-laser experiments have been performed to confirm the assumption of initial-state homogeneity in the photodissociation of van der Waals molecules.[2a,2b,5b] However, such experiments do not demonstrate the absence of final state inhomogeneity. There are notable instances for which such arguments are tenuous. For example, rotational constants[6] of $C_2H_4 \cdot HF$ and $C_2H_4 \cdot HCl$ are of the order of one-tenth of the observed photodissociation widths.[1b] Given that all photodissociation experiments are performed at finite temperature, the question of homogeneity in these cases requires closer examination.

Using a classical diatomic model, Reuss and co-workers[5b] have shown convincingly that another type of inhomogeneity--orientational inhomogeneity--is important and have used this model to reconcile disparate measurements on $(C_2H_4)_2$. However, for experiments performed at low temperatures, a full quantum mechanical description is necessary to describe quantitatively the effects of orientational inhomogeneity.

In this paper we present a phenomenological model for photodissociation of multilevel systems, which includes the types of inhomogeneity described above. It is a generalization of a two-level-with-decay model described earlier

for interpretation of van der Waals molecule photodissociation spectra.[7] In Section II the model is presented with equations of motion for the density matrix. Approximations are described which lead to an analytical formula for the photodissociation spectrum. The result, which is applicable to experiments in which the decay rate is greater than the Rabi frequencies, shows the relationship between lineshapes, intensities and inhomogeneity.

In Section III observed photodissociation spectra of $(C_2H_4)_2$, $C_2H_4 \cdot HF$ and $C_2H_4 \cdot HCl$ are interpreted with the inhomogeneous lineshape model. In each case, the photodissociation profiles are essentially single Lorentzians. $(C_2H_4)_2$ has been studied by several groups[1a,2a,5b,8] and while there is qualitative agreement, there has been some question about differences observed. In the discussion below, which was motivated by the work of Geraedts et al.,[5b] disparity in the measured widths is reconciled using the full inhomogeneous model. $C_2H_4 \cdot HF$ and $C_2H_4 \cdot HCl$ exhibit narrower photodissociation spectra so that at moderate fluences the dispersion of initial and final rotational states is the most important source of inhomogeneity. Limits on the inhomogeneity, decay rates and temperature for these clusters consistent with observations are deduced from the multilevel model. Section III also includes a brief discussion of the infrared transition moments of ethylene clusters and other sources of inhomogeneity.

2. PHOTODISSOCIATION MODEL

Figure 1 depicts a simple model which includes essential features of an inhomogeneous photodissociation experiment. The model is an ensemble of non-interacting molecular systems, each with a manifold of lower and upper states designated by the indices l and u. Only transitions between the two manifolds are allowed and these occur only by interaction with radiation. Transitions within the manifolds are forbidden. Interaction matrix elements are given by

$$V_{nm} = -\frac{\hbar}{2}\,\Omega_{nm}\,(e^{i\nu t} + e^{-i\nu t}) \tag{1}$$

with

$$\Omega_{nm} = \frac{\underset{\sim}{\mu}_{nm}\cdot\underset{\sim}{E}}{\hbar} \tag{2}$$

where ν is the frequency of the applied field and Ω_{nm} is the Rabi frequency of the $n \rightarrow m$ transition. The Rabi frequency includes the transition moment $\underset{\sim}{\mu}_{nm}$, the electric field intensity E, and orientational effects. In addition to population being pumped between the manifolds, population in the upper sublevels can decay, ultimately into a dissociative continuum at rates given by the γ_u, which are not necessarily equal. The energy of any sublevel is given by ω_i while the separation of the lowest levels of the two manifolds is ω_o. The splitting of sublevels is small

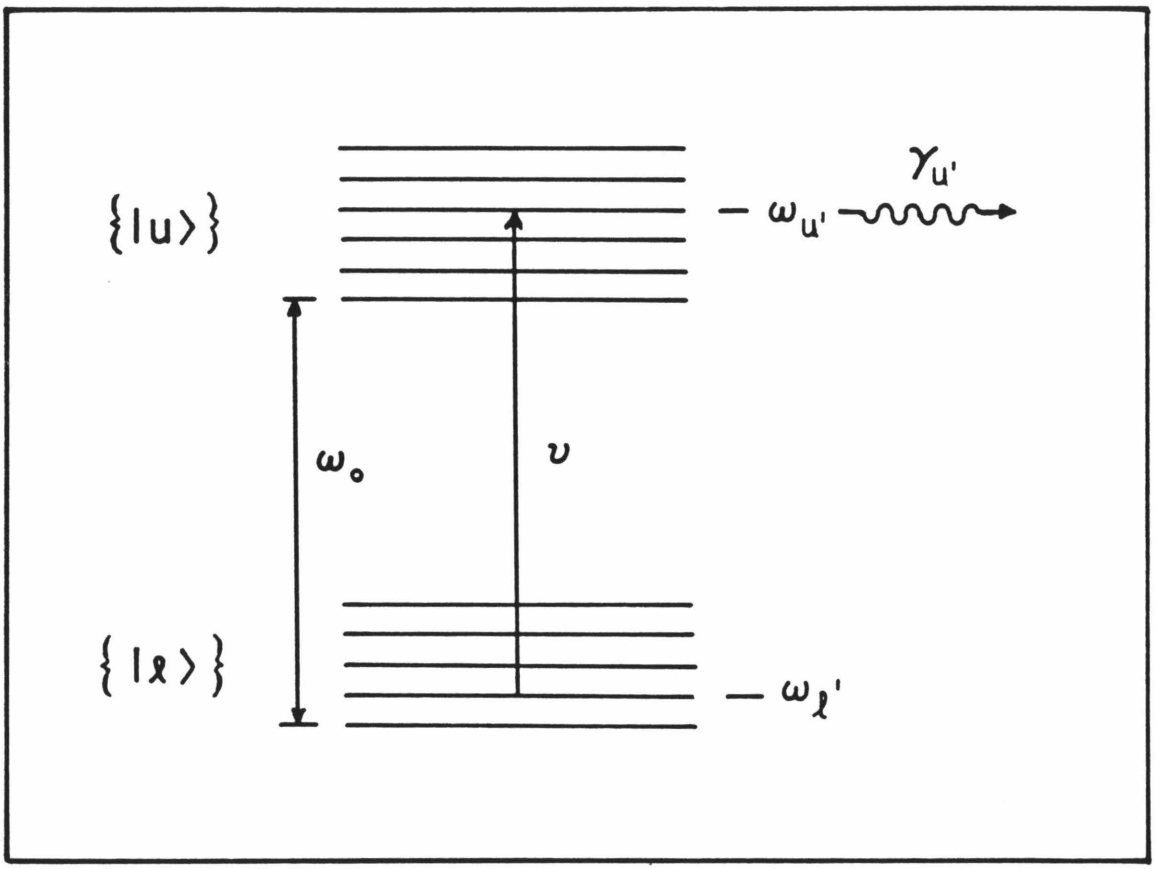

FIGURE 1. Multilevel photodissociation model.

compared by ω_o, while the frequency of the applied radiation is comparable to ω_o.

A. Density Matrix

The general form of the equations of motion for the density matrix elements in the Schrödinger representation is[9]

$$\dot{\rho}_{nm} = -(i\omega_{nm} + \gamma_{nm})\rho_{nm} - \frac{i}{\hbar}\sum_k (V_{nk}\rho_{km} - \rho_{nk}V_{km}) \tag{3}$$

where $\omega_{nm} = \omega_n - \omega_m$ and $\gamma_{nm} = \frac{1}{2}(\gamma_n + \gamma_m)$. This definition of γ_{nm}, for which population relaxation is the only dephasing mechanism, is appropriate for ensembles of simple non-interacting systems. This is because in such a case an n,m basis can be selected for which the interaction Hamiltonian is traceless.[10] Rapid oscillation, which is a consequence of the inherent time dependence of stationary states, can be reduced with the substitition:

$$\bar{\rho}_{ul} = \rho_{ul}\, e^{ivt} \tag{4}$$

With eqs. (1), (4), and the rotating wave approximation[9] the rate equations become

$$\dot{\rho}_{uu'} = -i\omega_{uu'}\rho_{uu'} - \gamma_{uu'}\rho_{uu'} + \frac{i}{2}\sum_l (\Omega_{ul}\bar{\rho}_{lu'} - \bar{\rho}_{ul}\Omega_{lu'}) \tag{5a}$$

$$\dot{\bar{\rho}}_{ul} = (i\Delta_{ul} - \gamma_{ul})\bar{\rho}_{ul} + \frac{i}{2}(\sum_{l'} \Omega_{ul'}\rho_{l'l} - \sum_{u'} \rho_{uu'}\Omega_{u'l}) \tag{5b}$$

$$\dot{\rho}_{ll'} = -i\omega_{ll'}\rho_{ll'} + \frac{i}{2}\sum_{u} (\Omega_{lu}\bar{\rho}_{ul'} - \bar{\rho}_{lu}\Omega_{ul'}) \tag{5c}$$

where $\Delta_{ul} = v - \omega_{ul}$.

In photodissociation experiments the signal which is measured is proportional to the fraction of molecules which dissociate or remain undissociated after irradiation for time t. The fraction of molecules remaining undissociated at any time is given by the trace of the density matrix. Initially the phases of the constituent systems of the ensemble are randomly distributed and population is distributed according to the Boltzmann distribution. Thus appropriate initial conditions for the integration of eqs. (5) are

$$\rho_{nm}(0) = \frac{e^{-\omega_n/kT}}{\sum_i e^{-\omega_i/kT}} \qquad n=m$$
$$= 0 \qquad n\neq m \tag{6}$$

B. Lineshape Formula

Consideration of typical experimental conditions leads to a useful formula for the inhomogeneous photodissociation lineshape. When fit to a two level model, the results of the

ethylene cluster experiments described below yield decay rates of the order of $\gamma_u \simeq 10^{12}$ sec^{-1} while Rabi frequencies are of the order of $\Omega_{ul} \simeq 10^7$ sec^{-1}, i.e., $\gamma_u >> \Omega_{ul}$. Since $\omega_o >>$ kT and γ_u is large, only states in the lower manifold are populated. Under such conditions numerical solution of eqs. (5) shows that the lower state populations, ρ_{ll}, vary slowly with a decay rate of the order of Ω_{ul}^2/γ_u. Upper state populations achieve small steady state values of the order of $\rho_{uu} \approx (\Omega_{ul}/\gamma_u)^2$. Off-diagonals of the type $\rho_{ll'}$ and $\rho_{uu'}$ oscillate at frequencies $\omega_{ll'}$ or $\omega_{uu'}$ but remain small with amplitudes of the order $(\Omega_{ul}/\gamma_u)^2$.

With these considerations eq. (5b) can be approximated by

$$\dot{\bar{\rho}}_{ul} = (i\Delta_{ul} - \gamma_{ul})\bar{\rho}_{ul} + \frac{i}{2}\Omega_{ul}\rho_{ll} \tag{7}$$

Noting that ρ_{ll} changes negligibly in time $1/\gamma_u$, eq. (7) can be integrated to give

$$\bar{\rho}_{ul} = -\Omega_{ul}\rho_{ll}\,(2\Delta_{ul} + i\gamma_u)^{-1} \tag{8}$$

Substituting this result into eq. (5c) and integrating gives for the diagonal elements

$$\rho_{ll}(t) = \rho_{ll}(0)\,\exp\left[-\sum_u \frac{\Omega_{ul}^2\,\gamma_u t}{4\Delta_{ul}^2 + \gamma_u^2}\right] \tag{9}$$

where $\rho_{ll}(0)$ is given by eq. (6). The fraction of molecules remaining after irradiation time t is then

$$F(t) = \sum_{l} \rho_{ll}(0) \exp\left[-\sum_{u} \Omega_{ul}^{2} \gamma_{u} t (4\Delta_{ul}^{2} + \gamma_{u}^{2})^{-1}\right] \quad (10)$$

This lineshape formula is an intuitive generalization of that derived for a two-level system,[7] in which the sums collapse to single terms. The sum over l, which accounts for initial state inhomogeneity, is a superposition of the spectra for each lower level weighted by their initial populations. This leads to a non-exponential dependence of F(t) on laser power, in contrast to the two-level case. The sum over u in eq. (10), which accounts for final state inhomogeneity, is the sum of the rates at which population of level l is lost to each upper level. In addition to decay rates, it includes detailed transition moments for each sublevel.

The lineshape, eq. (10), differs from a two-level formula in two ways. Firstly, if the spread of transitions is comparable to γ_u the lineshape is not a simple exponential of a Lorentzian, as might be inferred from the limited experimental data. Secondly, even with negligible dispersion in frequency, overlapping transitions have different transition moments. An example is the M^2 dependence of the intensities of degenerate transitions comprising a single rotational line. The variation in transition moments causes sublevels to be depleted at

different rates; this may be thought of as orientational hole burning in the case of M levels. With large fractions dissociated, results resemble the behavior of a two level system; however, parameters obtained with such an analysis differ from those determined using eq. (10). The classical orientational hole burning model of Geraedts et al.[5b,5c] includes only the second effect and is restricted to linear molecules (or K = 0 states in non-linear molecules).

Figure 2 shows power dependence curves exhibiting the orientational inhomogeneity induced by linearly polarized light. The slope of the line from the two level model gives the vibrational transition moment. The two solid curves are obtained from eq. (10) for perpendicular and parallel transitions of a molecule at $4^{\circ}K$ with $(C_2H_4)_2$ rotational constants (see below). In order to show only orientational effects the transition frequencies were adjusted to coincide with ω_o in these plots. The dashed curves are the power dependences for a classical linear molecule. The four inhomogeneous plots show positive curvature from the two-level model with the parallel bands showing the most dramatic deviation. Since this is a saturation effect, it is only apparent at moderate-to-high fluences ($>10 mJ/cm^2$) and occurs with concomitant linebroadening. The classical and quantum mechanical curves differ significantly for the parallel bands but much less so for the perpendicular bands.

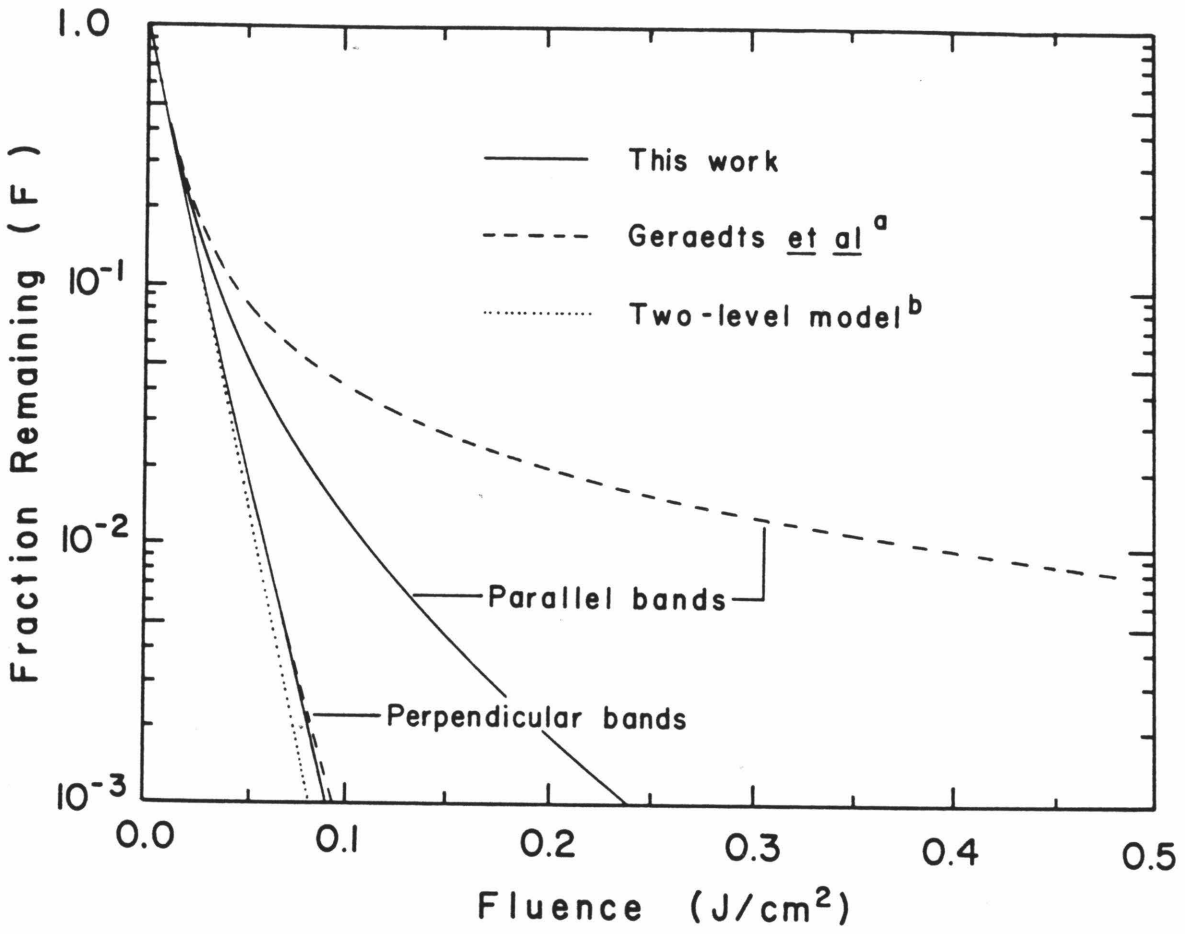

FIGURE 2. Power dependences on resonance showing orientational inhomogeneity. To facilitate comparison, the parameters used were the same as used in Figure 1 of reference 5b. These were $\langle\mu\rangle^2 = 0.071\ D^2$ and $\gamma = 11.0\ cm^{-1}$. The solid curves used, in addition, the rotational constants of $(C_2H_4)_2$ (see text) and T = 4°K.

(a) References 5b and 5c.

(b) Reference 7.

The quantum mechanical results are a function of temperature, while the classical plots are not.

Power dependences will reflect, in general, a superposition of effects described, and will show positive curvature in all cases. A transition moment derived assuming the two-level model would yield a value lower than the actual transition moment. Transition moments determined from integrated intensities will be less than the true transition moment since, from eq. (10)

$$\int_{-\infty}^{\infty} (-\ln F)\,d\nu \leq \pi \frac{t}{2} \sum_{l,u} \rho_{ll}(0)\,\Omega_{ul}^{2} \qquad (11)$$

The equality, which is rigorously true for a two-level system, is satisfied if the fraction dissociated is small.

3. APPLICATION

Here we interpret photodissociation spectra of $(C_2H_4)_2$, $C_2H_4 \cdot HF$ and $C_2H_4 \cdot HCl$ using the multilevel model. Photodissociation has been measured in these clusters by exciting the ν_7 out-of-plane bending mode of ethylene. In each case a single broad symmetric profile in the region of the ν_7 frequency of free ethylene has been observed and analyzed using two-level models.

Each spectrum was calculated using eq. (11) with sums over all rotational transitions in a single vibrational band. We also allowed that signals measured were not due purely to bi-molecules by including an undissociating mole fraction in the calculations. Finally, all predissociating levels were assumed to decay at the same rate.

A. $(C_2H_4)_2$

Ethylene dimer generated considerable interest when its remarkably broad, intense, photodissociation spectrum was first observed by Gentry and coworkers.[2d] Results of recent experiments are listed in Table I. Geraedts et al[5b] have reconciled the differences in these results, using the classical model for orientational averaging. Their analysis of the disparity in widths suggests that the transition is a parallel band with both transition moments nearly parallel to the dimer axis. Below we interpret the various measurements using the full inhomogeneous lineshape model.

Establishing the structure of ethylene dimer is the first step in calculating the inhomogeneous spectrum. The geometry has not been determined experimentally, but several ab initio calculations have been performed.[11] These indicate that the structure resembles the packing of C_2H_4 in crystals with the partners in a skewed-parallel configuration. For this discussion we will assume that the ethylene molecules are locked with planes parallel and

TABLE I. Results for $(C_2H_4)_2$.

$\gamma(cm^{-1})$	$\langle\mu\rangle^2(10^{-3}D^2)$	$\omega_o(cm^{-1})$	Fluence (mJ/cm^2)	Reference
Previously reported results:				
17.5±1.4	87.6±10.9	952.8±0.2	40.0	2a
12.2±1.2	96 ±18[a]	952.3±0.5	3.8	1a
10.9±0.8	53 ±10	952.4±0.2	0.50	5b
This work:			θ[b](degrees)	T°K
12.0	87.0	952.55	25.0	16.0
12.0	87.0	952.55	90.0	22.0

[a]This value is 3 times the value reported in ref. 1a.

[b]θ is the angle between the transition moment and the dimer axis.

separated by 4.1 Å. This structure is at best an approximate picture of $(C_2H_4)_2$ but since the spectrum is very broad it is relatively insensitive to the rotational constants. The important quantity is the skew angle, θ, which we define as the angle between the transition moments (normal to the ethylene planes) and the dimer axis. As θ is adjusted from 0° to 90° the ν_7 spectrum will evolve from a parallel band to a perpendicular band.

Figure 3 shows wavelength and power dependence data for $(C_2H_4)_2$ photodissociation observed by Hoffbauer et al.[2a] These data were obtained in a molecular beam with a translational temperature of 16 K and a laser fluence of 0.04 J/cm^2. The dotted curve through the spectrum is the best fit Lorentzian, valid for a completely homogeneous transition, with parameters listed in the first line of Table I. The observed power dependence is reasonably well reproduced by the same parameters assuming a mole fraction of about 10^{-3} is nondissociating. Note that at the peak of the spectrum approximately 95% of the molecules are dissociated so that orientational effects should be significant.

The thick solid and dashed curves reproduce the high fluence data using the inhomogeneous model, with parameters obtained at low fluence. The two calculated curves were contrived to bracket the high fluence data by adjusting the temperature, the angle θ and, within their quoted uncertainties, the low fluence parameters. The numbers used are

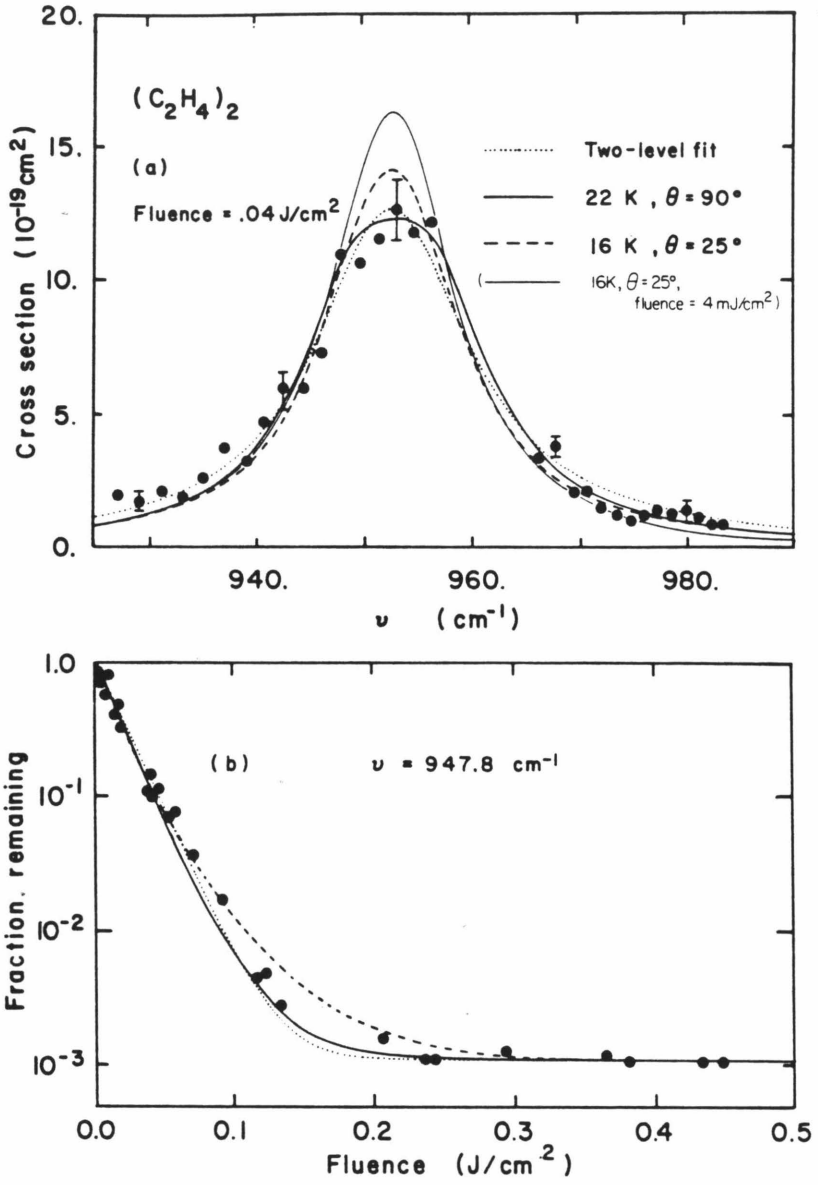

FIGURE 3. Comparison of the inhomogeneous model and results for $(C_2H_4)_2$ at 16°K. (a) Spectrum with a fluence of 0.04 J/cm^2. (b) Power dependence at 947.8 cm^{-1}. Experimental data are reproduced from reference 2a. The dotted curve was generated using a two-level model with parameters listed on the first line of Table I, assuming a nondissociating mole fraction of 0.001. The thick solid and dashed curves were calculated using eq. (10) with parameters listed in Table I and a non-dissociating mole fraction of 0.001. The thin solid curve in Figure 3a was calculated with a fluence of 4 mJ/cm^2 and θ = 25°.

shown in Table I. The dashed curve corresponds to $\theta = 25^{\circ}$. Since the power dependence would show more pronounced positive curvature as the parallel band limit is approached, 25° is the lower limit of θ. The thick solid curve corresponds to the upper limit, $\theta = 90^{\circ}$. The temperatures determined in the calculations are close to the translational temperature of the beam, which is expected; however, we caution that the spectra are sensitive to the rotational state distribution, which is known to be non-Boltzmann in molecular beams.[12] Ref. 2a also states that the observed lineshape is no different at 4K or as the fluence is changed. The thin solid curve shown in Figure 3a was calculated at 0.004 J/cm^2 and 16K with $\theta = 25^{\circ}$; the calculated curve at 4K shows a similar, but smaller discrepancy. The experiment is such that these were measured with poorer signal to noise so that differences may not have been evident.

Figure 3 shows that the high and low fluence data can be reconciled quantitatively. Our conclusion is that the skew angle θ is between 25° and 90° which brackets the angles predicted by theoretical calculations. The $(C_2H_4)_2$ ν_7 spectrum is certainly not a parallel band and has a strong perpendicular component. The essential conclusions of earlier work remain intact.

B. $C_2H_4 \cdot HF$ and $C_2H_4 \cdot HCl$

Results of recent measurements on $C_2H_4 \cdot HF$ and $C_2H_4 \cdot HCl$ in supersonic molecular beams are listed in Table II. Equilibrium structures determined from rotational constants are t-shaped with the diatomic axis perpendicular to the ethylene plane and the hydrogen of the diatom pointed towards the C=C bond.[6] The ν_7 photodissociation spectra of these clusters [1b] are significantly narrower and more blue shifted than $(C_2H_4)_2$ as indicated by the two-level parameters listed in Table II.

The geometry and rotational constants determined in microwave experiments[6] indicate that inhomogeneous broadening due to disperson of rotational transitions may be significant. Even if the temperature were very low, initial rotational state inhomogeneity persists since the C_2H_4 nuclear spins do not equilibrate. The structures of the complexes, if rigid, require that the ν_7 transition occurs as a parallel band.

The solid lines in Figure 4 and 5 are least squares fits of the inhomogeneous lineshape model to $C_2H_4 \cdot HCl$ and $C_2H_4 \cdot HF$ photodissociation data. The parameters and their upper and lower limits are listed in Table II. These limits are true 95% confidence limits taking into account non-linearities and parameter correlation in the model. They reflect the high degree of correlation among the parameters (with the exception of ω_o). For this reason more

TABLE II. Results for $C_2H_4 \cdot HF$ and $C_2H_4 \cdot HCl$.

	$\gamma(cm^{-1})$	$\langle\mu\rangle^2(10^{-3}D^2)$	$\omega_o(cm^{-1})$	X[a]	T°K
$C_2H_4 \cdot HF$					
Two level parameters:[b]	3.38±0.37	44.2±2.8	974.8±0.1		
Multilevel parameters:					
best values	1.59	76.8	974.4	0.59	1.5
upper limits	2.40	102.		0.73	0.7
lower limits	0.95	55.2		0.51	1.9
$C_2H_4 \cdot HCl$					
Two level parameters:[b]	1.62±0.24	51.9±3.3	964.3±0.1	0.69±0.03	
Multilevel parameters:					
best values	1.57	49.7	964.1	0.73	0.4
upper limits	1.80	67.6		1.00	2.6
lower limits	0.90	36.1		0.65	0.0

[a] X is the mole fraction of the dissociating van der Waals molecule.

[b] Reference 1b.

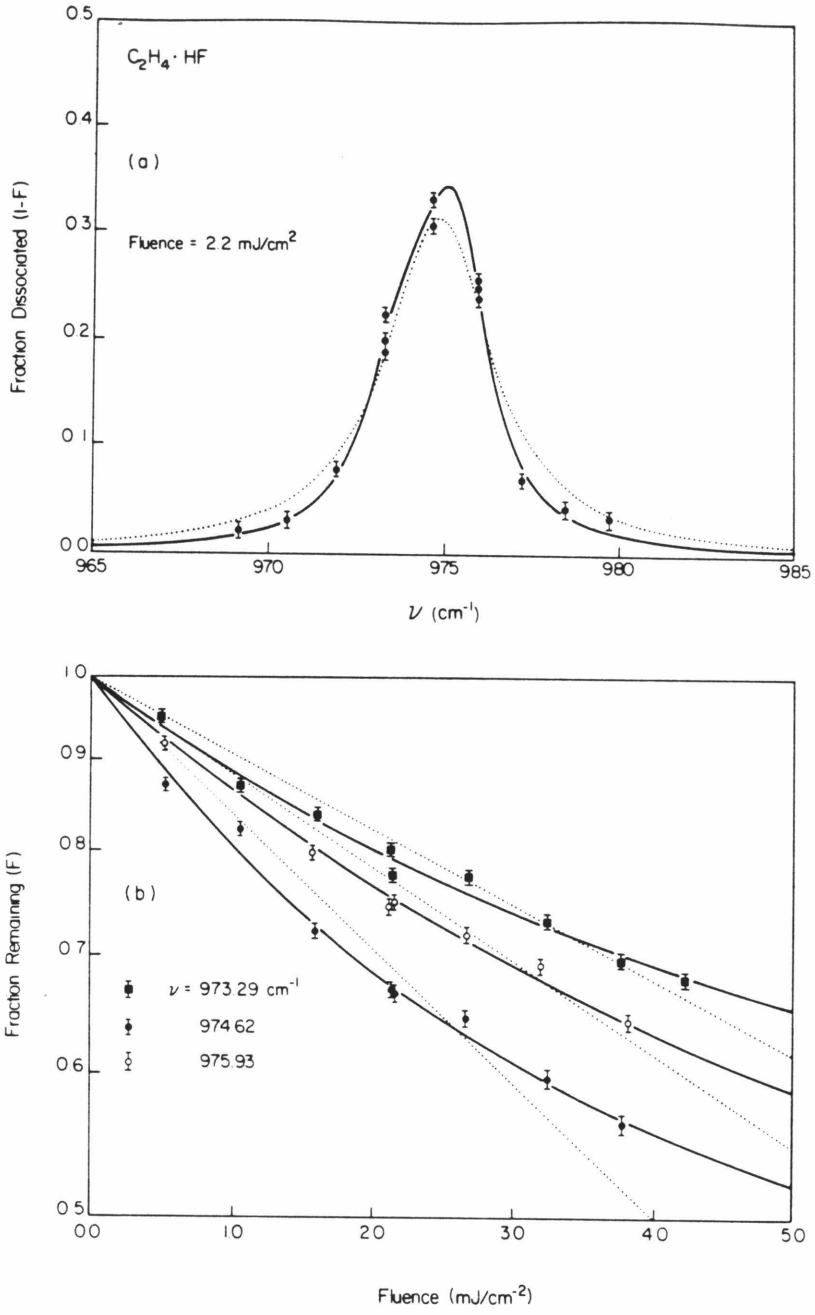

FIGURE 4. Comparison of multilevel and two-level fits to experimental results for $C_2H_4 \cdot HF$. (a) Spectrum at 2.2 mJ/cm^2. (b) Power dependences at three wavelengths. The dotted line is the best two-level fit. The solid line is the best multilevel fit. See Table II for parameters. Error bars are one standard deviation.

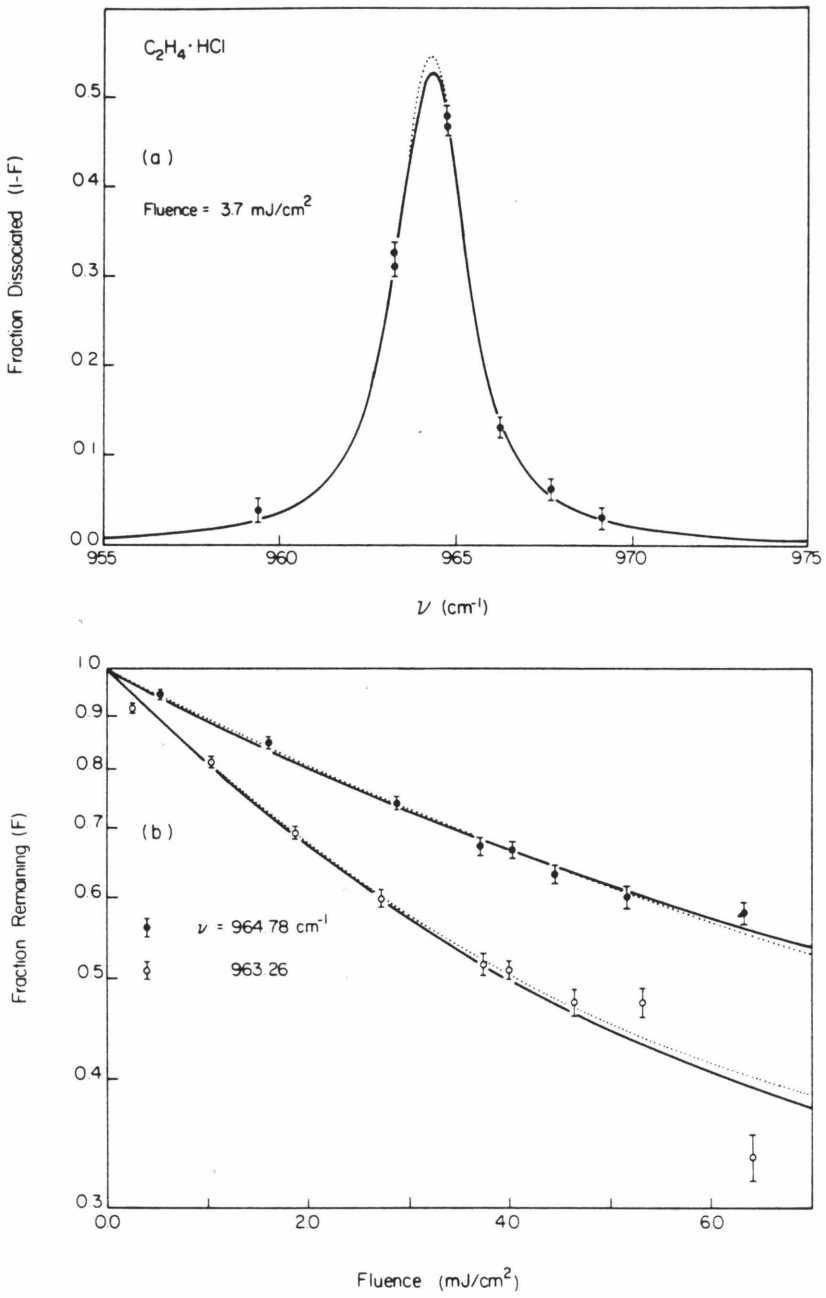

FIGURE 5. Comparison of multilevel and two-level fits to experimental results for $C_2H_4 \cdot HCl$. (a) Spectrum at 3.7 mJ/cm^2. (b) Power dependences at two wavelengths. The solid line is the best multilevel fit. See Table II for parameters. Error bars are one standard deviation.

significance should be attached to the range of acceptable values rather than the best fit values. It is not likely that rotational temperatures were lower than 1 K but the fact that the least-squares fits permit lower temperatures indicates that the spectra are nearly homogeneous.

There are differences in the parameters obtained with the inhomogeneous model and those originally obtained using a two-level homogeneous model. These original parameters are listed in Table II and were used to generate the dotted curves in Figure 4 and 5. The $C_2H_4 \cdot HF$ data were originally fit assuming that the molecules detected were purely $C_2H_4 \cdot HF$. The multilevel fit strongly indicates an impure sample. Therefore, the transition moment obtained in the multilevel fit is higher. Since $C_2H_4 \cdot HF$ has larger rotational constants than $C_2H_4 \cdot HCl$, it is more likely to exhibit inhomogeneous effects. This explains why the width obtained in the multilevel fit is a factor of two lower than that obtained in the two-level fits. Indeed, the best multilevel fit in Figure 4 shows asymmetry associated with rotational inhomogeneity.

The differences in the fits to the $C_2H_4 \cdot HCl$ data are smaller for two reasons. First, the data were originally fit to a two-level model with an undissociating mole fraction. This was justified since there appeared to be other species present with different spectra (e.g., $(C_2H_4)_2 \cdot HCl$). Second, since $C_2H_4 \cdot HCl$ has smaller rotational

constants inhomogeneous effects are expected to be less pronounced than in $C_2H_4 \cdot HF$.

In summary, we see that the essential results of previous analysis have changed slightly. The widths of $C_2H_4 \cdot HF$ and $C_2H_4 \cdot HCl$ are comparable and significantly narrower than that of $(C_2H_4)_2$. The transition moment of $C_2H_4 \cdot HF$ is larger than thought previously and may be greater than that of $C_2H_4 \cdot HCl$. Both transition moments are enhanced compared to C_2H_4.

C. Vibrational Transition Moment

We have observed that ethylene clusters have greater ν_7 vibrational transition moments than would be expected based on the 0.188 D transition moment of free ethylene.[13] We propose an electrostatic model to explain the observed enhancement of the ν_7 vibrational transition moments in $C_2H_4 \cdot HF$ and $C_2H_4 \cdot HCl$, and, by extension, that in $(C_2H_4)_2$. In the model, which has qualitatively predicted the blue shifts,[1b] the van der Waals partners are viewed as interacting collections of point charges. If the polarizability of the passive partner, e.g., HF or HCl, is included it is clear that ν_7 will cause oscillation of the induced dipole and thereby enhance the ν_7 transition moment. Because of the geometry, the magnitude of the induced dipole depends on the component of polarizability parallel to the diatomic axis. Using formal charges based on isolated molecule proper-

ties,[1b] experimental cluster geometries,[6] and polarizabilities[14,15] $\alpha_{//}(HF) = 0.99$ Å^3 and $\alpha_{//}(HCl) = 2.79$ Å^3 the calculated ν_7 transition moments are 0.21D and 0.24D for $C_2H_4 \cdot HF$ and $C_2H_4 \cdot HCl$, respectively. The agreement between the calculated and observed values is only qualitative but it shows that the polarizability effect should be significant. Since blue shifts predicted by this model are only about one-third of those measured, it is likely that the interaction leading to enhanced transition moments is underestimated in this model. Allowing charge density in ethylene to redistribute upon hydrogen bonding would certainly enhance the polarizability effect. It is likely that the same mechanism accounts for the observed enhancement of ethylene transition moments in $(C_2H_4)_2$ which, assuming the squared transition moments sum, are 0.21D.

Fermi resonance, amplified by the perturbative presence of partners in ethylene clusters has been proposed as the mechanism underlying the blue shifts.[16] The infrared inactive ν_8 mode of ethylene occurs at 940 cm^{-1}.[17] In the cases of $C_2H_4 \cdot HF$ and $C_2H_4 \cdot HCl$ this explanation is implausible given the large observed shifts, indicative of a very strong interaction, and the fact that no new bands have been measured. A decrease in intensity in the infrared active mode, which is certainly not occurring, would be expected if there were Fermi resonance with an inactive mode.[18] In addition to showing intensity enhancement, the

interaction in $(C_2H_4)_2$ appears to be weaker than in $C_2H_4 \cdot HF$ and $C_2H_4 \cdot HCl$. Thus, a weak-bonding-induced Fermi resonance in the ethylene constituents is less likely.

D. Sources of Inhomogeneity

In the analysis of the photodissociation spectra above, we have considered only rotational and orientational inhomogeneity as is appropriate for a distribution of transitions in a single vibrational band. There are other sources of inhomogeneity which should be discussed. Fermi resonance of the type described above involving perturbed C_2H_4 vibrational modes could introduce final state inhomogeneity but, for reasons outlined above, is not operative in $(C_2H_4)_2$, $C_2H_4 \cdot HF$ or $C_2H_4 \cdot HCl$. Another sort of final state inhomogeneity, which may be viewed as a type of Fermi resonance, would arise if it were possible to excite combinations of ν_7 with the low frequency stretching and librational van der Waals modes. Hindered internal rotation has been observed in the loosely bound $Ar \cdot C_2H_4$ and $Ne \cdot C_2H_4$ molecules.[19] In the latter example a 12.5 cm^{-1} barrier causes splittings in the ν_7 band of the order of 10 cm^{-1} with relative intensities approximately given by rotational transition moments. Corresponding excitation of the tightly bound clusters described here would involve larger splittings, with intensities better described by vibrational selection rules. Such transitions have not been observed

and are expected to be only weakly allowed. A conceivable source of initial state inhomogeneity, in addition to rotational populations, is initial population in van der Waals modes which would give rise to hot bands. We expect that the populations of such low frequency modes reflect the rotational temperature in supersonic expansions and are thus not significantly populated.

4. SUMMARY

A general inhomogeneous lineshape model for describing predissociation spectra has been presented. The model is restricted to cases where the molecules of the ensemble under study are non-interacting and where the predissociation rate is greater than the Rabi frequency.

Application of the model to $(C_2H_4)_2$ photodissociation shows that orientational inhomogeneity is an important effect at moderate fluences. Reconcilation of high and low fluence data has shown that the ν_7 ethylene mode in the dimer occurs as a perpendicular or hybrid band.

Application of the model to $C_2H_4 \cdot HF$ and $C_2H_4 \cdot HCl$ photodissociation has shown that these species bridge the regime in which inhomogeneity becomes important. Although the $C_2H_4 \cdot HF$ spectrum is empirically homogeneous, the natural width is a factor of two smaller than the inhomogeneous width. In contrast, rotational inhomogeneity has an insignificant effect on the appearance of the $C_2H_4 \cdot HCl$ spectrum.

ACKNOWLEDGEMENTS

The authors thank W. R. Gentry and J. Reuss for helpful communications and for providing results before publication. This work was supported by the Division of Chemical Sciences, Office of Basic Energy Sciences, U. S. Department of Energy.

REFERENCES

1. (a) M. P. Casassa, D. S. Bomse and K. C. Janda, J. Chem. Phys. 74, 5044 (1981). (b) M. P. Casassa, C. M. Western, F. G. Celii, D. E. Brinza and K. C. Janda, J. Chem. Phys. 79, 3227 (1983).

2. (a) M. A. Hoffbauer, K. Liu, C. F. Giese and W. R. Gentry, J. Chem. Phys. 78, 5567 (1983). (b) M. A. Hoffbauer, K. Liu, C. F. Giese, and W. R. Gentry, J. Phys. Chem. 87, 2096 (1983). (c) M. A. Hoffbauer, C. F. Giese and W. R. Gentry, J. Chem. Phys. 79, 192 (1983). (d) M. A. Hoffbauer, W. R. Gentry and C. F. Giese, in Laser Induced Processes in Molecules, edited by K. Kompa and S. D. Smith, Springer Series in Chemical Physics (Springer, Berlin, 1978), Vol. 6.

3. M. F. Vernon, J. M. Lisy, H. S. Kwok, D. J. Krajnovich, A. Tramer, Y. R. Shen and Y. T. Lee, J. Phys. Chem. 85, 3327 (1981).

4. G. Fischer, R. E. Miller and R. O. Watts, Chem. Phys., 80, 147 (1983).

5. (a) J. Geraedts, S. Stolte and J. Reuss, Z. Phys. A-Atoms and Nuclei 304, 167 (1982). (b) J. Geraedts, M. Snels, S. Stolte, and J. Reuss, Chem. Phys., in press. (c) J. Geraedts, M. Waayer, S. Stolte, and J. Reuss, Faraday Discuss. Chem. Soc. 73, 375 (1982).

6. (a) J. A. Shae and W. H. Flygare, J. Chem. Phys. 76, 4857 (1982). (b) P. D. Aldrich, A. C. Legon, and W. H. Flygare, J. Chem. Phys. 75, 2126 (1981).

7. M. P. Casassa, F. G. Celii and K. C. Janda, J. Chem. Phys. 76, 5295 (1982).

8. D. S. Bomse, J. B. Cross and J. J. Valentini, J. Chem. Phys. 78, 7175 (1983).

9. M. Sargent, III, M. O. Scully and W. E. Lamb, Jr., Laser Physics (Addison-Wesley, Reading, Mass., 1974).

10. S. Mukamel, Chem. Phys. 31, 327 (1978).

11. (a) A. van der Avoird, P. Wormer, F. Mulder and R. Berns, Topics in Current Chemistry 93, 1 (1980). (b) G. J. H. van Hes and A. Vos, Acta. Cryst. B33, 1653 (1977).

12. T. E. Gough and R. E. Miller, J. Chem. Phys. 78, 4486 (1983).

13. T. Nakanaga, S. Kondo and S. Saëki, J. Chem. Phys. 70, 2471 (1979).

14. (a) J. S. Muenter, J. Chem. Phys. 56, 5409 (1972). (b) A. J. Perkins, J. Phys. Chem. 68, 654 (1964).

15. (a) E. W. Kaiser, J. Chem. Phys. 53, 1686 (1970). (b) N. J. Bridge and A. D. Buckingham, Proc. Roy. Soc. London A295, 334 (1966).

16. J. Geraedts, S. Stolte and J. Reuss, Chem. Phys. Lett. 97, 152 (1983).

17. J. L. Duncan, D. C. McKean and P. D. Mallinson, J. Mol. Spectrosc. 45, 221 (1973).

18. J. Overend, in Infrared Spectroscopy and Molecular Structure, edited by M. Davies (Elsevier, New York, 1963).

19. C. M. Western, M. P. Casassa and K. C. Janda, submitted to J. Chem. Phys. for publication.

Chapter 7

Infrared Photodissociation of the Hindered Internal Rotors $Ne \cdot C_2H_4$ and $Ar \cdot C_2H_4$

INFRARED PHOTODISSOCIATION OF THE HINDERED INTERNAL ROTORS $Ne \cdot C_2H_4$ AND $Ar \cdot C_2H_4$

Colin M. Western, Michael P. Casassa[a] and Kenneth C. Janda[b]

Arthur Amos Noyes Laboratory of Chemical Physics,[c]
California Institute of Technology
Pasadena, California 91125

ABSTRACT

Infrared photodissociation spectra of the van der Waals molecules $Ne \cdot C_2H_4$ and $Ar \cdot C_2H_4$ are reported. Spectra obtained near the ν_7 frequency of free ethylene exhibit the sharpest and most complex structure yet observed for an ethylene-containing van der Waals molecule. Calculated

---

[a]Atlantic Richfield Foundation Fellow and Proctor & Gamble Fellow.

[b]Alfred P. Sloan Fellow.

[c]Contribution No._____

spectra based on a hindered-internal rotor model are in satisfacory agreement with those observed. The barrier heights for hindered rotation of C_2H_4 about the C=C axis are 12.5 cm^{-1} and 30 cm^{-1} for $Ne \cdot C_2H_4$ and $Ar \cdot C_2H_4$, respectively. The natural linewidths, 0.5 cm^{-1} for $Ne \cdot C_2H_4$ and 3.0 cm^{-1} for $Ar \cdot C_2H_4$, are compared to those of other ethylene-containing clusters and it is concluded that the widths reflect vibrational predissociation, constrained by conservation of angular momentum.

INTRODUCTION

During recent years, infrared photodissociation spectra of a series of ethylene-containing van der Waals molecules have been reported. These include ethylene bound to C_2H_4,[1-4] C_2D_4,[2] SF_6,[3] HF, HCl, NO,[5] Ne, Ar, Kr[1] and Xe.[3] With the exception of the Ne, Ar and Kr clusters, excitation of these weakly bound molecules at frequencies near the 950 cm^{-1} ν_7 mode of ethylene leads to dissociation in a single, symmetrical band of frequencies. The widths of such spectra, convoluted with orientational and saturation effects, are a measure of the decay of the initially excited state - i.e., transfer of energy from the ν_7 vibration to other modes of the molecule. The observed position, intensity and band-type give information about the van der Waals interaction.

The appearance of the bands, for the most well-characterized clusters, indicates that these molecules have rigid structures. For example, the ν_7 motion - an out-of-plane hydrogen bending - occurs as a simple parallel band in $C_2H_4 \cdot HF$ and $C_2H_4 \cdot HCl$,[5] and as a hybrid band in $(C_2H_4)_2$.[6] These observations are consistent with known and calculated geometries. If the structures were hindered internal rotors, the spectra would be expected to have several distinct subbands, resembling the ν_7 perpendicular band of free ethylene.

Here we report photodissociation spectra of $Ne \cdot C_2H_4$ and $Ar \cdot C_2H_4$ which exhibit the complex band-type expected for hindered internal rotors. A hindered internal rotation model is presented which satisfactorily reproduces experimentally measured line positions and intensities. Parameters determined with this model include the barrier to internal rotation by ethylene about its C=C axis and the decay rate. The decay time for $Ne \cdot C_2H_4$ is the longest yet observed for ethylene clusters.

We note that structure in both these spectra has been observed before,[1] although partially obscured by larger clusters in the previous $Ar \cdot C_2H_4$ experiments. The broad symmetrical absorption observed in our previous experiments was mistakenly attributed to $Ar \cdot C_2H_4$. We presume this to be the case for $Kr \cdot C_2H_4$ which also exhibited underlying structure. Higher sensitivity and resolution in the present experiments has made these new assignments possible.

EXPERIMENTAL

The experimental procedure has been described previously.[1,5] Van der Waals molecules were formed in supersonic molecular beams and detected with a mass spectrometer. Throughout the 0.5 msec flight time from the source to the detector, the beam was irradiated by a low power ($\sim$10 W/cm^2) cw infrared laser. The laser induced attenuation of the cluster signal was measured as a function of laser power, wavelength, and source conditions. Sensitivity and precision were improved over our earliest experiments by more sophisticated signal averaging techniques and by monitoring the laser power in the interaction volume with each data point. Expansion gases were dilute mixtures of C_2H_4 in Ne, Ar and He, all available from commercial sources.

Spectra reported here were obtained monitoring the parent ion mass spectrometer signals $C_2H_4Ne^+$ and $C_2H_4Ar^+$ although, to help in assignment, spectra at other masses were also surveyed. In both cases the expansion conditions were made increasingly dilute in C_2H_4 and milder (lower stagnation pressures) in order to ensure correct assignment of observed signals to the simplest complexes $Ne \cdot C_2H_4$ and $Ar \cdot C_2H_4$. A CO_2 laser was used in measurements on both molecules. In the case of $Ne \cdot C_2H_4$, the same laser was operated as an N_2O laser by using a different gas mixture. The N_2O laser fills in some of the gaps in the tuning curve

of the CO_2 laser and helped to resolve some of the extraordinarily sharp structure in the $Ne \cdot C_2H_4$ spectrum.

RESULTS

Figure 1 shows the photodissociation spectrum of $Ne \cdot C_2H_4$ obtained measuring the $NeC_2H_4^+$ signal (m/e 48) in a beam formed by expansion of C_2H_4 in Ne and He. This spectrum shows no significant dependence on source conditions over the range possible with our apparatus. Using the nozzle and mixture shown in Figure 1, it was possible to vary the pressure from 50 to 300 psig. Over this range, the spectrum remains constant while the $NeC_2H_4^+$ signal varies over an order of magnitude, and passes through a maximum. The intensities of other clusters, e.g., $(C_2H_4)_2$, also grow steadily. By using a larger nozzle ($\sim$100 μm diameter), we have extended the pressure range over which the $NeC_2H_4^+$ spectrum remains constant down to 800 torr. Note also that this spectrum is identical to the $Ne \cdot C_2H_4$ spectrum reported previously[1], except that the N_2O laser has afforded higher resolution. Molecules contributing to dissociation at m/e 48 are evidently the same under all of these conditions. Since the spectrum persists even with the weakest expansions, we conclude that these spectra are in fact due to $Ne \cdot C_2H_4$.

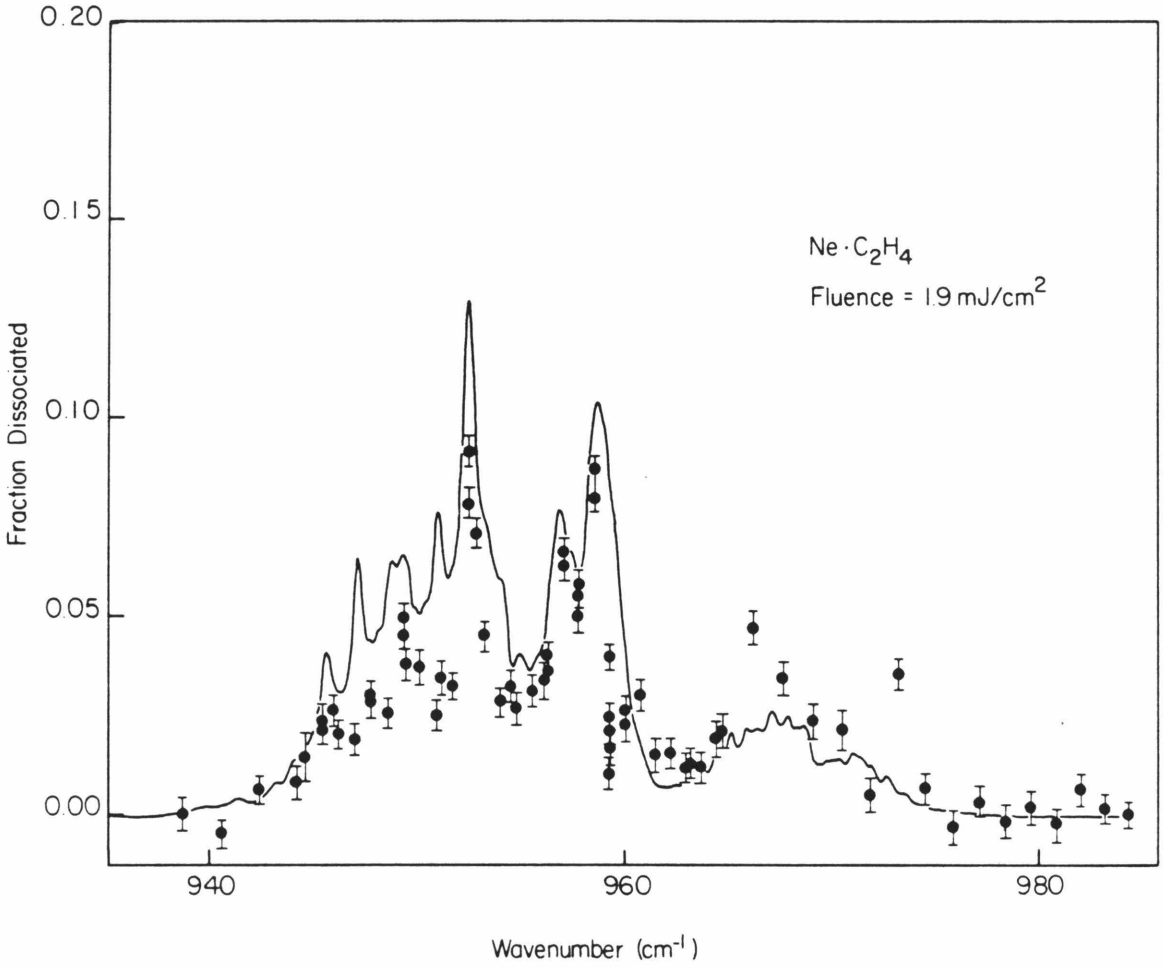

FIGURE 1. Photodissociation spectrum of $Ne \cdot C_2H_4$ with a laser fluence of 1.9 mJ/cm^2. The gas mixture was 0.5% C_2H_4, 10.0% He and 89.5% Ne, and was expanded through a 35 μm pinhole at 95 psig. The solid curve was calculated using the parameters listed in Table I.

Figure 2 shows the spectrum of $Ar \cdot C_2H_4$ obtained by monitoring the $C_2H_4Ar^+$ signal (m/e 68) produced by expansion of C_2H_4 in Ar and He. The spectrum shown in Figure 2 is the low pressure limiting spectrum for $Ar \cdot C_2H_4$. The intensities of the strongest features are, within experimental certainty, constant in the range 400 torr to 1000 torr. As further evidence that this spectrum is due to $Ar \cdot C_2H_4$, the same spectrum has been obtained at high pressures in an extremely dilute expansion (0.01% C_2H_4, 20% Ar, 72% Ne, 8% He at 200 psig).

Unlike the $Ne \cdot C_2H_4$ spectrum, the $Ar \cdot C_2H_4$ measurements are significantly influenced by changes in source conditions.[7,8] If the pressure is increased, or if the ethylene concentration is reduced relative to Ar, the broad feature at 956 cm^{-1} shifts to 950 cm^{-1} and grows in intensity. By noting the absence of pure ethylene clusters in such expansions, this broad feature which grows in can be attributed to clusters of the type $C_2H_4Ar_n$ where $n \geq 2$. Dissociation of these clusters, which partially obscured the structure shown in Figure 2, was wrongly assigned to $Ar \cdot C_2H_4$ in our previous work.[1] The limiting spectrum reported here occurs near the limits of experimental sensitivity. It is conceivable that apparent breadth of the feature near 956 cm^{-1} in Figure 2 is due to small residual concentrations of $C_2H_4Ar_n$.

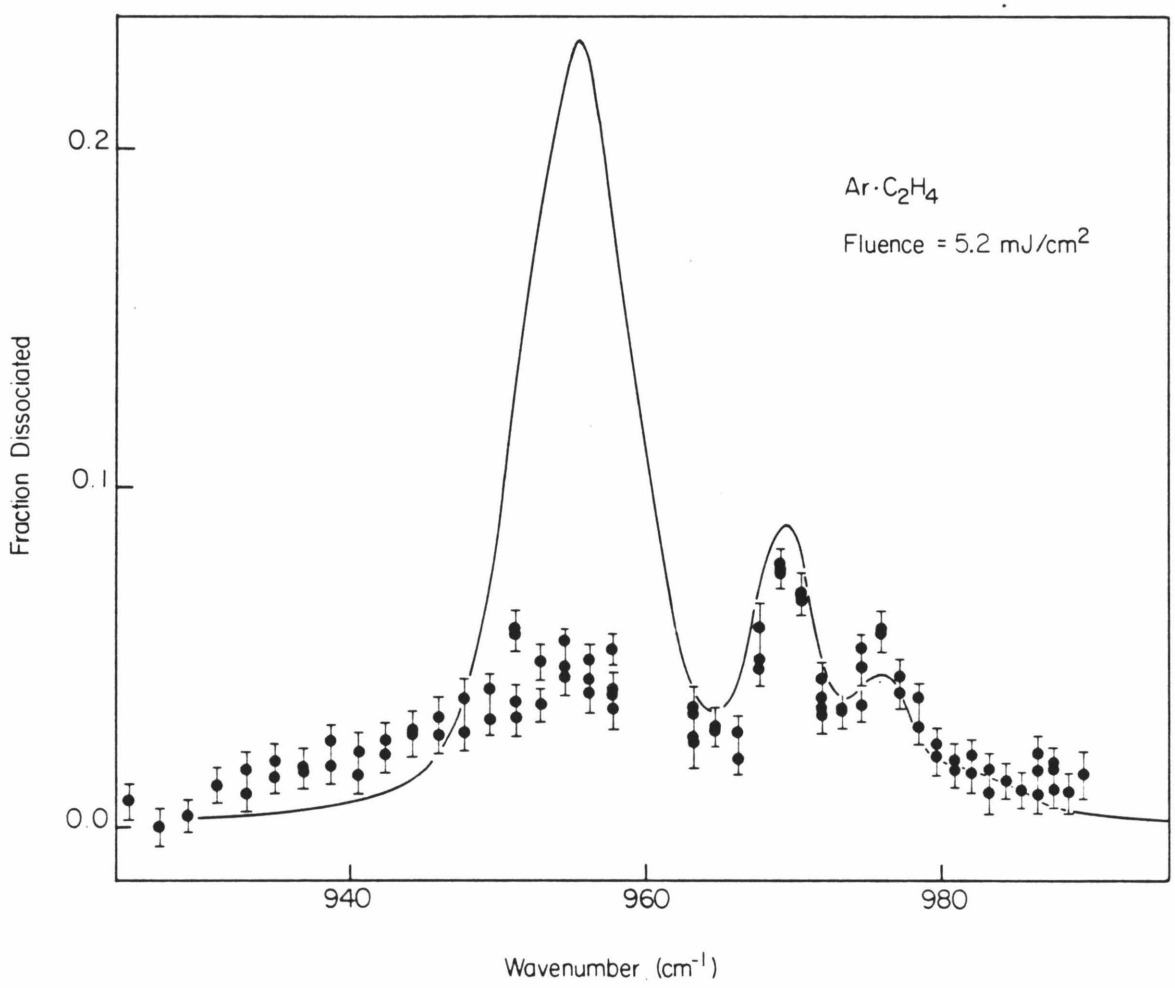

FIGURE 2. Photodissociation spectrum of $Ar \cdot C_2H_4$ with a laser fluence of 5.2 mJ/cm^2. The gas mixture was 1% C_2H_4, 20% Ar and 79% He and was expanded through a 100 μm pinhole at 5 psig.

Hindered Rotor Model

The observed spectra of $Ne \cdot C_2H_4$ and $Ar \cdot C_2H_4$ do not resemble any of our previous ethylene cluster spectra. In particular, the spectra are too complex to assign a rigid molecular structure, as we did for $C_2H_4 \cdot HCl$. The splittings of 5-10 cm^{-1} are too small to be considered as conventional vibrational combination bands so it becomes necessary to use a hindered internal rotation model.

In the model described below, we treat only the rotation about the C=C axis as internal rotation, ignoring the other two van der Waals modes. Normal mode calculations using estimated atom-atom potentials for $Ne \cdot C_2H_4$, with Ne symmetrically positioned about the C_2H_4 plane, indicate that this simplification is reasonable. With Ne-Ne and Ne-He Lennard-Jones potentials used to approximate the Ne-C and Ne-H interactions, the rotation about the C=C axis has a vibrational frequency of 5 cm^{-1} and the other two van der Waals modes - C_2H_4 end-over-end rotation and $Ne \cdot C_2H_4$ stretching - are 28 and 46 cm^{-1}, respectively. These latter two modes would be best treated as simple vibrations. We note that this distinction is less clear in $Ar \cdot C_2H_4$ where the corresponding normal model frequencies are 31 cm^{-1}, 35 cm^{-1} and 45 cm^{-1}. (The normal mode calculations involve infinitesmal changes in atomic positions about the equilibrium geometry, and as such may not reflect the actual internal rotation barrier heights.)

The approach we use follows that of Bauder et al.[9] The coordinate system is shown in Figure 3. We divide the atoms into two sets: top atoms, and frame atoms. In our picture of $Ne \cdot C_2H_4$, Ne is the frame atom and the atoms of C_2H_4 are the top atoms. There are two corresponding axis systems with origins fixed in the molecule: the frame axes - x_f, y_f, z_f - which correspond to the usual body fixed axis system, and the top axis system - x_t, y_t, z_t - which has its origin at the center of mass of the top and is fixed with respect to the top atoms. We choose these axes such that the z-axes are parallel to each other and to the C=C bond, The frame y-axis, is along the $Ne \cdot C_2H_4$ bond and the top y-axis is perpendicular to the C_2H_4 plane. γ is the angle between the two y-axes. Thus, $\gamma=0$ corresponds to Ne lying above the C_2H_4 plane.

The theory for this type of hindered rotor has been given by Bauder et al.[9] Unfortunately, their paper appears to contain several errors in the equations, so it was necessary to rederive them. The classical kinetic energy is given by

$$2T = (\omega_x, \omega_y, \omega_z, \dot{\gamma}) \begin{bmatrix} I_{xx}+I\sin^2\gamma & -I\cos\gamma\sin\gamma & 0 & 0 \\ -I\cos\gamma\sin\gamma & I_{yy}-I\sin^2\gamma & 0 & 0 \\ 0 & 0 & I_{zz} & I \\ 0 & 0 & I & I \end{bmatrix} \begin{bmatrix} \omega_x \\ \omega_y \\ \omega_z \\ \dot{\gamma} \end{bmatrix} \qquad (1)$$

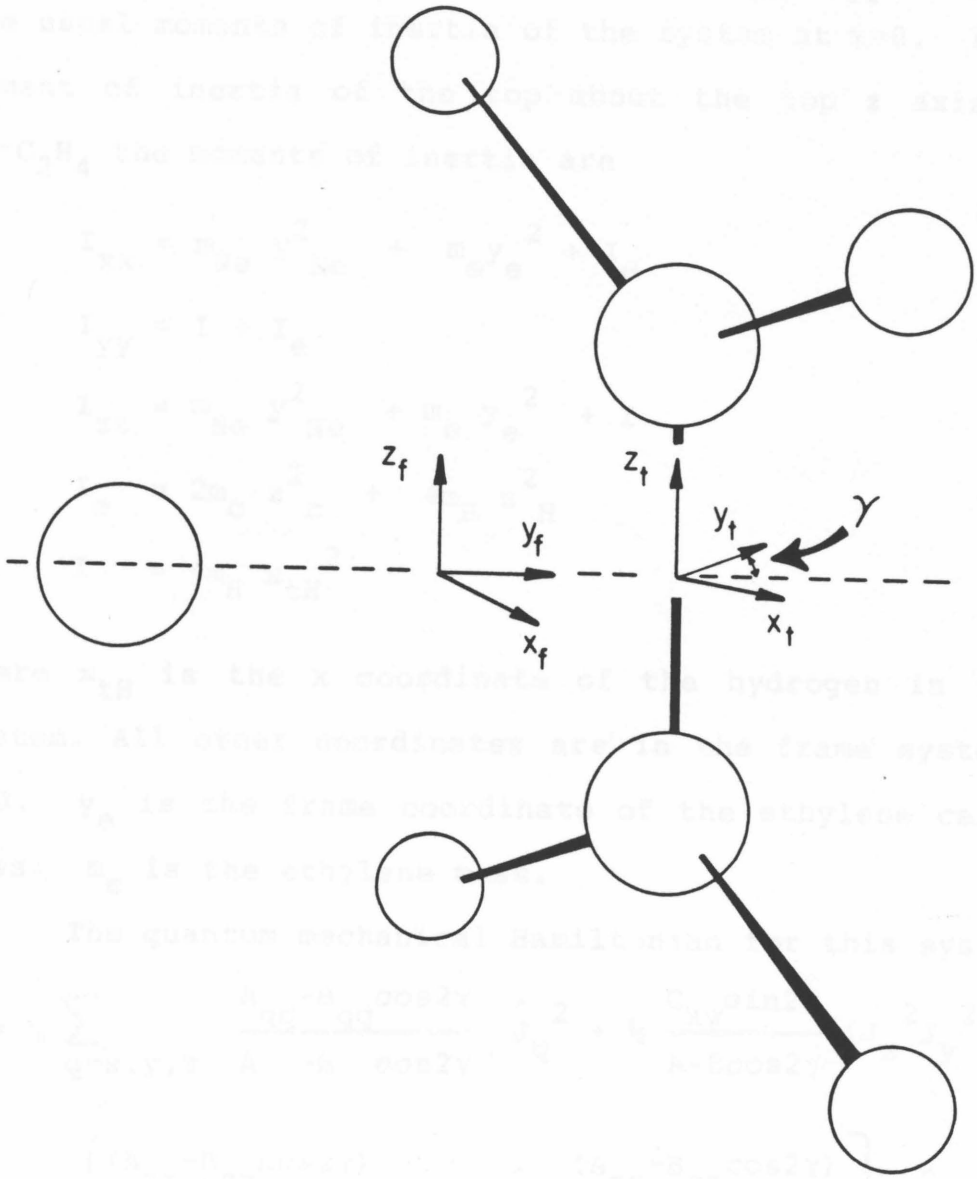

FIGURE 3. Coordinate system for the hindered internal rotor model.

where ω_x, ω_y and ω_z are the projections onto the frame axes of the angular velocity of the frame. I_{xx}, I_{yy} and I_{zz} are the usual moments of inertia of the system at $\gamma=0$. I is the moment of inertia of the top about the top z axis. For $Ne\cdot C_2H_4$ the moments of inertia are

$$\begin{aligned} I_{xx} &= m_{Ne}\, y^2_{Ne} + m_e y_e^2 + I_e \\ I_{yy} &= I + I_e \\ I_{zz} &= m_{Ne}\, y^2_{Ne} + m_e\, y_e^2 + I \\ I_e &= 2m_c\, z^2_c + 4m_H\, z^2_H \\ I &= 4m_H\, x_{tH}^2 \end{aligned} \tag{2}$$

where x_{tH} is the x coordinate of the hydrogen in the top system. All other coordinates are in the frame system with $\gamma=0$. y_e is the frame coordinate of the ethylene center of mass. m_e is the ethylene mass.

The quantum mechanical Hamiltonian for this system is

$$\begin{aligned} H = \tfrac{1}{2} \sum_{q=x,y,z} & \frac{A_{qq}-B_{qq}\cos 2\gamma}{A-B\cos 2\gamma}\, \hat{J}_q^2 + \tfrac{1}{2}\frac{C_{xy}\sin 2\gamma}{A-B\cos 2\gamma}\,(J_x^2 J_y^2 + J_y^2 J_x^2) \\ & -\tfrac{1}{2}\left[\frac{(A_{zz}-B_{zz}\cos 2\gamma)}{A-B\cos 2\gamma}\,\hat{J}_\gamma + \hat{J}_\gamma\,\frac{(A_{zz}-B_{zz}\cos 2\gamma)}{A-B\cos 2\gamma}\right]\hat{J}_z \\ & +\tfrac{1}{2}\left[\hat{J}_\gamma + \tfrac{1}{4}(\hat{J}_\gamma \ln(A-B\cos 2\gamma))\right]\frac{(A_{\gamma\gamma}-B_{\gamma\gamma}\cos 2\gamma)}{A-B\cos 2\gamma} \\ & X\left[\hat{J}_\gamma - \tfrac{1}{4}(\hat{J}_\gamma \ln(A-B\cos 2\gamma))\right] + V(\gamma) \end{aligned} \tag{3}$$

where $\hat{J}_\gamma = -i\hbar\partial/\partial\gamma$.

The symbols containing A and B are algebraic functions of the moments of inertia, eq. (2), which arise from inverting the coefficient matrix in eq. (1). J_x, J_y and J_z are the usual body fixed projections of the overall angular momentum. The hindering potential, $V(\gamma)$, is expanded as a series in $\cos 2j\gamma$ for ease of calculation of matrix elements:

$$V(\gamma) = \sum_j \tfrac{1}{2} V_{2j}(1 - \cos 2j\gamma) \qquad (4)$$

The symmetry of the expected equilibrium structure is C_{2v}. However, the fact that ethylene can rotate within the complex must be taken into account and using the methods of Longuet-Higgins[10] the symmetry group of the molecule is isomorphic to D_{2h}, the point group of ethylene itself. Furthermore, the molecule has four distinct nuclear spin states with statistical weights 7, 3, 3, and 3, as has C_2H_4.

The basis functions chosen were products of internal rotor wavefunctions. The internal rotor basis was

$$1/\sqrt{2\pi}\ ,\ 1/\sqrt{\pi}\cos\gamma,\ 1/\sqrt{\pi}\cos 2\gamma \ \ldots\ 1/\sqrt{\pi}\cos 2n\gamma$$

$$1/\sqrt{\pi}\sin\gamma,\ 1/\sqrt{\pi}\sin 2\gamma \ \ldots\ 1/\sqrt{\pi}\sin(2n+1)\gamma$$

The overall rotation wavefunctions were Wang symmetrized top wavefunctions with L=0 or 1:

$$|JKLM> = \sqrt{\frac{-(-1)^{J+L}}{2}} \left((-1)^{K} |J-KM> - (-1)^{J+L} |JKM> \right),$$

and, for K=0,

$$|J0LM> = |J0M> \text{ with } J+L \text{ odd only.}$$

The matrix elements of the Hamiltonian can be evaluated analytically using these basis functions.

For a given total angular momentum, J, and irreducible representation of D_{2h}, we made up a matrix using all combinations of the above that transformed as the above. The matrix was truncated at some value of the internal rotor quantum number, n, and diagonalized to give the energy levels. This maximum value of n was chosen by checking for convergance in the eigenvalues of the matrix. A value ~ 5 was sufficient for barriers of 10 cm^{-1}. A check on the computer program consists of making certain that the energy levels are reasonable in two limiting cases of $V(\gamma)$. For the limit of zero barrier for rotation, the J=0 states have the energy levels of a diatomic molecule with a moment of inertia of $I(I_{zz} - I)/I_{zz}$. As the barrier becomes large ($\sim$1000 cm^{-1} for $Ne \cdot C_2H_4$) the energy levels become those of an asymmetric rotor with slightly anharmonic vibrations.

Calculation of Photodissociation Spectra

The transitions observed are due to absorption by the ν_7 mode of ethylene. The orientation of the transition dipole for ν_7 is perpendicular to the ethylene plane. The

frame-fixed components of the dipole moment are thus $(-\mu\sin\gamma,\ \mu\cos\gamma,\ 0)$ and the interaction with an electric field polarized along the z-axis is

$$\underline{\mu}\cdot\underline{E} = \frac{|E||\mu|}{\sqrt{2}}\left[(-D^{1*}_{0-1}(\omega) + D^{1*}_{01}(\omega))\sin\gamma - i(D^{1*}_{0-1}(\omega) + D^{1*}_{01}(\omega))\cos\gamma\right] \quad (5)$$

where the $D^{J*}_{KM}(\omega)$ are the rotation matrices defined by Brink and Satchler.[11] The matrix of the dipole operator, eq. (5), in our basis can be evaluated by standard means, and the transition dipole moments of the system are found by transforming the matrix using the eigenvector from diagonalization of the Hamiltonian.

These transition dipole moments are then convoluted into a photodissociation spectrum using[6]

$$F = \sum_i \rho_i \exp\left[-\sum_f \Omega^2_{if}\,\gamma_f t\,(4\Delta^2_{if} + \gamma_f^2)^{-1}\right] \quad (6)$$

Equation (6) is a general lineshape formula for an inhomogeneous vibrational predissociation spectra. F is the fraction of molecules remaining after irradiation for time t. The sums are over all rotational sublevels, including the M sublevels, of the vibrational ground state (i) and final state (f). The ρ_i are the Boltzmann factors for the ground state levels and include weighting factors for

non-equilibrated nuclear spins. The Ω_{if} are the Rabi frequencies, defined as $(\underline{\mu}_{if} \cdot \underline{E})/\hbar$, for the system transition moments described above. The γ_f are the decay rates for the upper vibrational levels and are assumed to be equal in the calculations below. Finally, Δ_{if} is the difference between the laser frequency ω, and the resonant frequency ω_{if} of the i-f transition.

Spectra were calculated for $Ar \cdot C_2H_4$ and $Ne \cdot C_2H_4$ for a range of values of the double well potential parameter V_2, the decay rate γ, the separation of the partners, R, and the temperature. Calculated spectra which best agree with observed spectra, as ascertained by visual inspection, are shown in Figures 1 and 2. The corresponding parameters are given in Table I. The agreement in the case of $Ne \cdot C_2H_4$ is quite good, with a one-to-one correspondence between position of most observed and calculated maxima, as well as comparable intensities. Peaks in the calculated $Ar \cdot C_2H_4$ spectrum also coincide with those observed, but the distributions of intensity disagree.

The calculated spectra are most sensitive to the absolute value of the double well potential parameter, V_2, which determines the separation of the most intense subbands. For both $Ne \cdot C_2H_4$ and $Ar \cdot C_2H_4$ the best agreement with experiment was obtained with a negative V_2, which corresponds to a planar equilibrium structure with $\gamma = 90°$. For both molecules, intensity is less uniformly distributed throughout the band with positive V_2 than with negative

TABLE I. Parameters used in calculated photodissociation spectra.

Cluster	V_2 (cm^{-1})	γ (cm^{-1})	ω_o (cm^{-1})	$\langle\mu\rangle^2$ ($10^{-3}D^2$)	R (Å)	T (K)
$Ne \cdot C_2H_4$	-12.5	0.5	949.1	35.3	2.92	3.0
$Ar \cdot C_2H_4$	-30.0	3.0	953.9	35.3	3.30	5.0
C_2H_4[a]	--	--	949.0	35.3	--	--

[a] Reference 13.

V_2. While this indicates that the structure is planar, the simplicity of the model and the sparse experimental data preclude definite determination of the geometry. However, the existence of a two-fold barrier to internal rotation of ethylene about is C=C bond is well established.

The calculated spectra were less sensitive to the values of the other parameters. The equilibrium separation of the rare-gas atom from C_2H_4 was taken to be that determined using pair-wise Lennard-Jones potentials with the rare-gas symmetrically disposed above the C_2H_4 plane. Spectra calculated with bond lengths 10% shorter or longer than this were subtly different in appearance with the longer bond lengths tending to concentrate end-over-end rotational substructure within the principle subbands. This narrowing effect could be compensated in part by adjusting the temperature or natural width. In the calculations, rotational temperatures were assumed to be in the range of those determined for other clusters in similar expansions[2,5,12] and natural widths were taken to be the approximate widths of the narrowest observed spectral peaks. As such, these are upper limits for the homogeneous widths. The vibrational transition moment was assumed to be that of free ethylene.[13] Because of the limited experimental data, these parameters could not be more precisely determined. Similarly, consideration of potential terms of higher order than V_2 was not warranted.

DISCUSSION

A. The van der Waals interaction

Unlike ethylene clusters previously observed, $Ne \cdot C_2H_4$ and $Ar \cdot C_2H_4$ must be considered as hindered internal rotors. The corresponding internal motion in $C_2H_4 \cdot HF$, $C_2H_4 \cdot HCl$, $(C_2H_4)_2$ or $C_2H_4 \cdot C_2F_4$ may be better described as a vibration since no internal rotor subbands have been observed for these molecules. Excitation of this motion along with ν_7 would then be described as a vibrational combination band, with corresponding low intensity, and would be well shifted from the ν_7 origin. In the cases of $(C_2H_4)_2$ and $C_2H_4 \cdot C_2F_4$, the internal motion may be restricted by steric effects. The bonding interactions in $C_2H_4 \cdot HF$ and $C_2H_4 \cdot HCl$, which are quite strong, evidently pose a substantial barrier to internal rotation by C_2H_4. The slight blue shift of the band origin in the rare gas clusters from that of free ethylene (ν_7 = 949 cm^{-1})[13] may be attributable to repulsive interaction of the rare-gas and the wagging hydrogen atoms. The extent of this interaction will, of course, depend on the actual equilibrium geometry and the hindered rotor level.

The observed spectra are in qualitative agreement with those calculated with a double-well hindered internal rotor model. As noted above, the agreement is much better for $Ne \cdot C_2H_4$ than $Ar \cdot C_2H_4$. While the explanation for this must await more experimental data and a more detailed model, we

can point out factors which have not been considered in this work.

The model includes only internal rotation about the C=C axis in complexes where this bond is perpendicular to the line joining the rare gas and the ethylene center of mass. This structure is analogous to that of $Ar \cdot C_2H_2$, and by analogy with $C_2H_4 \cdot HF$ and $C_2H_4 \cdot HCl$, the noble-gas is expected to be above the C_2H_4 plane. It is therefore surprising that the calculations predict a planar structure. Since this prediction depends on the sign of V_2, while the gross appearance of the spectra depend only on $|V_2|$, we hesitate to dismiss the non-planar structure.

As noted above, only the interaction term V_2 was considered because this led to good agreement between the calculated and observed subband positions. While this indicates that the internal rotor potential is well approximated by $\frac{1}{2}V_2(1-\cos 2\gamma)$, it is likely that higher order terms would be necessary for quantitative agreement. We did not explore this open-ended question because of the limited data and because of uncertainties introduced by the approximations described below.

The consideration of a single dimension of internal rotation is justified in the case of $Ne \cdot C_2H_4$ because, based on Lennard-Jones pair-wise potentials, the librational motion of C_2H_4 about the C=C axis is considerably freer than end-over-end motion of C_2H_4 or the van der Waals stretching. (The normal mode frequencies are 5 cm^{-1}, 28 cm^{-1} and 46 cm^{-1}

respectively.) As such one could expect the low frequency mode to dominate the spectrum. In contrast, the corresponding $Ar \cdot C_2H_4$ modes are comparable. (The normal mode frequencies are 31 cm^{-1}, 35 cm^{-1} and 45 cm^{-1}.) Thus, in the case $Ar \cdot C_2H_4$, the other internal modes might also have to be considered.

Two factors which could influence peak intensities have been ignored. First is the influence of the Ne or Ar polarizability on the ν_7 transition moment. The oscillating dipole induced on the rare gas by ethylene ν_7 motion can enhance the vibrational transition moment. This effect, which has been observed for other ethylene clusters, should be a function of internal rotor level and should be more pronounced in $Ar \cdot C_2H_4$ than in $Ne \cdot C_2H_4$. The second effect, a type which has been observed in $(C_2H_2)_2$ spectra,[14] is a rotational-level dependent decay rate.

B. Photodissociation dynamics

The homogeneous linewidths of van der Waals molecule photodissociation spectra reflect the lifetime of the initially excited state. Since these lifetimes are a measure of the rate for intramolecular vibrational energy flow, the mechanism for the decay is of considerable interest. There has been some question about whether the decay mechanism is best described as a direct dissociative

process or as energy transfer to other modes which is fast compared to subsequent dissociative steps.

The upper limits for the homogeneous linewidths of $Ne \cdot C_2H_4$ make this the longest lived ethylene complex yet observed. Previous studies have produced linewidths in a surprisingly narrow range. For example, the ν_7 modes of $C_2H_4 \cdot HF$ and $C_2H_4 \cdot HCl$ exhibit widths of approximately 1.6 cm^{-1}.[6] The widths observed for $(C_2H_4)_2$ and $C_2H_4 \cdot C_2F_4$ are 12.0 cm^{-1} and 6.0 cm^{-1}, respectively.[1] Thus, the range of linewidths observed for C_2H_4 clusters now encompasses perhaps two orders of magnitude. As discussed below, trends in these data are consistent with predissociation constrained by angular momentum conservation. This indicates that widths are indeed determined by energy transfer to the weakly bound modes. Such transfer would lead to rapid dissociation of the complex. This conclusion is consistent with many observations of vibrational predissociation from electronically excited states.[15] In general, while excited clusters are not observed, their fragments are observed.

Energy conservation requires that the fragments of $(C_2H_4)_2$, $C_2H_4 \cdot HF$ and $C_2H_4 \cdot HCl$ predissociation, induced by pumping ν_7, cannot be vibrationally excited. It has been predicted,[16] and measured,[2,17] that translation is a relatively inefficient channel for dissipation of energy in excess of the dissociation energy. Rotation is then the principal channel for product energy release.

Ewing has presented a model for energy transfer into rotation which is analogous to his momentum gap model for V→T relaxation.[16] Some conclusions are 1) a perturbation to couple the excited vibration to rotation is necessary; 2) the rate is enhanced if ΔJ, the rotational quantum number change, is small; 3) the energy gap, $E_{\nu_7} - D_o - E_J$ (where E_{ν_7}, D_o and E_J are the energies of the initially excited mode, the van der Waals bond and product rotation, respectively), should be small to minimize translational energy release. Also, since initial states of the complex have little angular momentum, the final angular moment of the products must cancel.

Ethylene dimer excited in the ν_7 mode meets the above criteria for rapid V-T,R dissociation. The coupling between the wide amplitude motion of ν_7 and fragment rotation ought to be quite efficient, since the dimer is thought to have a staggered planes-parallel structure.[6] By exciting rotation about the carbon-carbon axis of each ethylene the entire $E_{\nu_7} - D_o$ can be released as rotational energy while conserving angular momentum. The final rotational quantum numbers need not be greater than 10.

$C_2H_4 \cdot HCl$ is less able to satisfy the above criteria for two reasons. The structure of $C_2H_4 \cdot HCl$ has the HCl molecule pointing between the carbon atoms[18] thereby reducing any impulsive coupling from ν_7. Instead the coupling may be electrostatic since the bond dipoles involved are large. Second, $E_{\nu_7} - D_o$ for $C_2H_4 \cdot HCl$ is esti-

mated to be 400 cm^{-1}.[5] To divide the final angular momentum evenly between C_2H_4 and HCl would require HCl to accept most of the excess energy with J = 4 or 5. The energy gap between n = 4 and 5, however, is over 100 cm^{-1} with the result that translation must provide a substantial energy sink unless a fortuitous resonance is involved. The same statements apply to $C_2H_4 \cdot HF$, except that in this case energy release, $E_{\nu_7} - D_o$, is expected to be smaller.

In $Ne \cdot C_2H_4$ and $Ar \cdot C_2H_4$ only orbital angular momentum can offset any ethylene rotational excitation. Thus decay channels available to $Ne \cdot C_2H_4$ and $Ar \cdot C_2H_4$ are least efficient. Because of its lower mass, Ne can carry more kinetic energy with less orbital angular momentum than Ar. Thus, if all else were equal, we would expect the $Ne \cdot C_2H_4$ width to be greater than the $Ar \cdot C_2H_4$ width. Unfortunately, our model has permitted determination only of upper limits of the widths.

The above arguments are consistent with the inverse linewidths for the series $(C_2H_4)_2$, $C_2H_4 \cdot HF$ and $Ne \cdot C_2H_4$ which are 0.44, 3.4 and $\geq$10 psec, respectively. The above model affords a physical interpretation of the data and leads to qualitative predictions which can be tested. For instance, product velocity distributions for $Ne \cdot C_2H_4$ may show substantial translational energy release. In the case of $C_2H_4 \cdot HCl$ or $C_2H_4 \cdot HF$ perhaps a structured time of flight "spectrum" of the fragments would be observed due to widely spaced rotational energy levels.

Two other broadening mechanisms which are dismissed in the following discussion are pure dephasing and resonant

energy transfer to other strongly bound modes of the molecule. Both mechanisms would mimic the density of states of internal modes which are not involved in the initial spectroscopic excitation (the "bath" modes).

The pure dephasing mechanism depends on the partitioning of degrees of freedom into system and bath modes.[19] For the clusters whose spectra exhibit single symmetric bands - $(C_2H_4)_2$, $C_2H_4 \cdot C_2F_4$, $C_2H_4 \cdot HCl$ and $C_2H_4 \cdot HF$ - the bath modes would include all degrees of freedom other than ν_7. For the rare gas clusters which exhibit separate bands for internal rotation, the internal rotor levels may be excluded from the bath. In this picture, dynamics within the bath modes cause broadening, i.e., pure dephasing, of transitions among the observed degrees of freedom.[19] However, pure dephasing depends on population numbers in such a way[20] that this mechanism may be ruled out as the origin of the line broadening in these clusters at low temperatures.

The non-dissociative resonant energy transfer mechanism is likely to be inoperative because it has been shown that increased densities of strongly bound bath modes have no effect on the widths. For example, widths of $(C_2H_4)_3$ and $C_2H_4 \cdot C_2F_4$ are narrower than that of $(C_2H_4)_2$.[1] Also, a recent study of OCS-alkane clusters has shown no correlation of the widths and the alkane vibrational state density.[21] Finally, the fact that $(C_6H_6)_3$ excited in C-H stretching modes fragments into $(C_6H_6)_2 + C_6H_6$ instead of $3(C_6H_6)$[22]

argues against uniform redistribution of energy before dissociation.

Summary

Highly structured infrared photodissociation spectra of the van der Waals molecules $Ne \cdot C_2H_4$ and $Ar \cdot C_2H_4$ have been reported. A hindered rotor model for internal rotation by cluster-bound C_2H_4 about its C=C axis has been presented. Absorption frequencies calculated from this model are in excellent agreement with observations, while absolute intensities are in qualitative agreement. Barrier heights for hindered rotation of C_2H_4 are 12.5 cm^{-1} and 30 cm^{-1} for $Ne \cdot C_2H_4$ and $Ar \cdot C_2H_4$, respectively. The upper limits for the natural linewidths are 0.5 cm^{-1} for $Ne \cdot C_2H_4$ and 3.0 cm^{-1} for $Ar \cdot C_2H_4$. These correspond to lifetimes of ≥ 10 psec for $Ne \cdot C_2H_4$ and ≥ 1.7 psec for $Ar \cdot C_2H_4$. Comparison to widths of other ethylene containing clusters leads to the conclusion that the widths reflect vibrational predissociation constrained by conservation of angular momentum.

ACKNOWLEDGEMENT

The authors thank J. L. Beauchamp for the CO_2 laser, and the Division of Chemical Sciences, Office of the Basic Energy Sciences, U. S. Department of Energy for on-going support. Finally, we would like to thank Professor George Ewing for numerous helpful suggestions.

REFERENCES

1. M. P. Casassa, D. S. Bomse and K. C. Janda, J. Chem. Phys. 74, 5044 (1981).

2. M. A. Hoffbauer, K. Liu, C. F. Giese and W. R. Gentry, J. Chem. Phys. 78, 5567 (1983).

3. J. Geraedts, M. Snels, S. Stolte and J. Reuss, Chem. Phys., in press.

4. G. Fischer, R. E. Miller and R. O. Watts, Chem. Phys., 80, 147 (1983).

5. M. P. Casassa, C. M. Western, F. G. Celii, D. E. Brinza and K. C. Janda, J. Chem. Phys. 79, 3227 (1983).

6. M. P. Casassa, C. M. Western and K. C. Janda, J. Chem. Phys., submitted for publication.

7. Note that even as the spectrum is a function of expansion pressure, log-log plots of cluster intensity vs. pressure would imply the cluster signal is reasonably pure. Because of fragmentation we have found that mass spectroscopy is of limited utility in assigning spectra. See reference 8 for demonstrations of this point.

8. A. van Deursen, and J. Reuss, Int. J. Mass. Spectrom. Ion Phys. 23, 109 (1977).

9. A. Bauder, E. Mathier, R. Meyer, M. Ribeaud and Hs. H. Günthard, Molecular Physics 15, 597 (1968).

10. H. C. Longuet-Higgins, Molecular Physics 6, 445 (1963).

11. D. M. Brink and G. R. Satchler, Angular Momentum (Clarendon Press, Oxford, 1975).

12. (a) D. E. Brinza, Ph.D. Thesis, California Institute of Technology, Pasadena, California (1983). (b) B. A. Schwartz, Ph.D. Thesis, California Institute of Technology, Pasadena, California (1983).

13. T. Nakanaga, S. Kondo and S. Saëki, J. Chem. Phys. 70, 2471 (1979).

14. R. D. Pendley and G. E. Ewing, J. Chem. Phys. 78, 3531 (1983).

15. K. C. Janda, Acc. Chem. Phys., in press.

16. G. E. Ewing, Faraday Discuss. Chem. Soc. 73, 325 (1982).

17. D. S. Bomse, J. B. Cross and J. J. Valentini, J. Chem. Phys. 78, 7175 (1983).

18. (a) P. D. Aldrich, A. C. Legon and W. H. Flygare, J. Chem. Phys. 75, 2126 (1981). (b) J. A. Shea and W. H. Flygare, J. Chem. Phys. 76, 4857 (1982).

19. S. Mukamel, Chem. Phys. 31, 327 (1978).

20. A. H. Zewail, Acc. Chem. Res. 13, 360 (1980).

21. M. A. Hoffbauer, C. F. Giese and W. R. Gentry, J. Chem. Phys. 79, 192 (1983).

22. M. F. Vernon, J. M. Lisy, H. S. Kwok, D. J. Krajnovich, A. Tramer, Y. R. Shen and Y. T. Lee, J. Phys. Chem. 85, 3327 (1981).

Chapter 8

Decay-Mechanisms in Vibrationally Excited van der Waals Molecules

I. Introduction

In the previous chapters, van der Waals molecule photodissociation spectra were interpreted using as a model pairs of discrete levels, coupled in the presence of light. For chemical dynamics the most interesting parameters determined are the phenomenological decay constants. Though this type of model provides a reasonable physical picture of the photodissociation process, as evidenced by generation of a consistent set of parameters for a wide variety of experiments, there is little intrinsic dependence on the nature of the decay mechanism. In this chapter, conceivable decay processes are defined in a very schematic way and their importance in van der Waals molecule photodissociation is discussed. We shall see that the description of decay processes depends largely on the physical picture one chooses. We conclude that the observed linewidths of ethylene containing van der Waals molecules can be interpreted unambiguously as the result of population relaxation processes.

Before proceeding, a vocabulary must be agreed upon. The phenomenological rates mentioned are determined from homogeneous linewidth measurements (having considered contributions due to saturation and inhomogeneity) and as such, give the rates of decay of the off-diagonal density matrix elements for two optically coupled states. Since these are a measure of the phase coherence of the

excitation of the ensemble, these rates are called dephasing rates. There are two types of dephasing processes (DP) which contribute to the dephasing rate. These are population relaxation (PR), which also appears as decay of the diagonal elements of the density matrix, and pure dephasing processes (PDP) by which phase coherence is lost without concomitant population loss.

In Section II, the simplest lineshape model is presented with a discussion of its stipulations (in our application) for decay processes. Included is a discussion of the population relaxation mechanism. Sections II and III draw heavily from a profound article by Mukamel[1] on the nature of dephasing in isolated molecules. Section II addresses the nature of DP in a global description of the van der Waals molecule system. This is the picture adopted by many theoreticians calculating PR rates for van der Waals molecules. In Section III, reduced descriptions of the van der Waals molecules are proposed and, with the help of the work of Zewail et al,[2] the implications of these pictures for DP in van der Waals molecules are discussed.

II. The Lineshape Model

The lineshape model derives from a highly idealized system described by a Hamiltonian of the form

$$H = H_o + H' + V \qquad (1)$$

The zero order Hamiltonian has two discrete eigenfunctions, $|a\rangle$ and $|b\rangle$, and continuum eigenfunctions $|E,\beta\rangle$. E denotes the <u>total</u> energy of the continuum level and β denotes a set of other parameters which uniquely specify the state. The time-independent interaction Hamiltonian, H', weakly couples the upper level $|a\rangle$, and states of the continuum. V represents the interaction of an oscillating electric field which couples $|a\rangle$ and $|b\rangle$.

The most general state function of the system is

$$|\psi(t)\rangle = \sum_n c_n(t)|n\rangle = \sum_n b_n(t)e^{-i\omega_n t}|n\rangle \qquad (2)$$

where the sum is over all eigenfunctions of H_o (an integral for the continuum states). We can avoid explicitly treating the continuum states in the density matrix by noting that the rate of decay of the discrete state $|a\rangle$ resonantly coupled to the continuum, ignoring V for the moment, is given by

$$\dot{b}_a(t) = -\left[\frac{\gamma_{PR}}{2} + i\frac{\delta E}{\hbar}\right] b_a(t) \qquad (3)$$

Equation (3) follows from (2) and approximate solution of the Schrodinger equation.[3,4] The first-order decay constant is given by

$$\frac{\gamma_{PR}}{2} = \frac{\pi}{\hbar}\int d\beta \; |\langle \beta, E=E_a | H' | a \rangle|^2 \; \rho(\beta, E=E_a) \qquad (4)$$

which resembles decay formulas used by several theoreticians - primarily Beswick[5] and Ewing.[6] The matrix element in (4) leads to the familiar momentum and energy gap propensity rules for state-to-state rates. The density of states and integration over internal degrees of freedom cause the rate to depend on the availability of final states. The quantity δE is simply the shift of the discrete state energy due to coupling with the continuum and henceforth will be ignored.

Using (2), (3) and the definition of the density matrix element, $\rho_{nm} = c_n^* c_m$, the density matrix rate equations are

$$\begin{aligned}
\dot{\rho}_{aa} &= -\gamma_{PR}\rho_{aa} - \frac{i}{\hbar}(V_{ab}\rho_{ba} - c.c.) \\
\dot{\rho}_{bb} &= \qquad\qquad + \frac{i}{\hbar}(V_{ab}\rho_{ba} - c.c.) \qquad (5) \\
\dot{\rho}_{ab} &= -(i\omega_o + \gamma_{DP})\rho_{ab} + \frac{i}{\hbar}V_{ab}(\rho_{aa} - \rho_{bb})
\end{aligned}$$

where $\omega_o = (E_a - E_b)/\hbar$ and $\gamma_{DP} = \gamma_{PR}/2 + \gamma_{PDP}$. We have added γ_{PDP} for generality, although there has been no

explicit mechanism introduced which could be responsible for PDP. The fraction of molecules remaining undissociated under our experimental conditions is

$$Tr(\rho) = \exp\left[-\omega_R^2\, \gamma_{DP} t/(2\Delta\omega^2 + \gamma_{DP}^2)\right] \qquad (6)$$

where ω_R is the Rabi frequency, t is the irradiation time and $\Delta\omega$ is the difference between the laser frequency and ω_o.

With regard to the decay mechanisms, the stipulations of the model in the approximation of (6) are:

(i) The width (FWHM) of ln $Tr(\rho)$ which is measured in our experiments is $2\gamma_{DP}$.

(ii) The PR rate is much greater than the Rabi frequency. In our experiments, ω_R is typically 10^7 sec^{-1}.

(iii) The PR is irreversible, but need not be directly to the "dissociated" state. It is conceivable that there are states of the continuum for which the fragments have little relative kinetic energy. However, whatever the initial decay, it must inevitably lead to dissociation.

Stipulations (i) and (ii) indicate that the upper limit for γ_{PR} is $2\gamma_{DP}$, while the lower limit is ω_R. Stipulation (iii) indicates that the upper limit for the dissociation rate,[7] as determined by our experimental geometry,

is of the order of 10^{-4} sec^{-1}. In our analyses we have argued that both the widths, $2\gamma_{DP}$, and the dissociation rate are given by γ_{PR}.

The physical picture of van der Waals molecule photodissociation described above is appealing in its simplicity and has been applied successfully in many cases. (It has been used as an essentially phenomenological model with parameters adjusted to fit experimental results.) The discussion of γ_{PR} has firmly rooted the first order decay constant in theory. The following sections are aimed at understanding the physics underlying γ_{PDP}.

III. Dephasing in a Complete Description of the System.

Theoretical work on line broadening in van der Waals molecules[5,6] has for the most part employed global Hamiltonians of (usually idealized) complexes with all degrees of freedom treated on equal footing. The time independent part of the Hamiltonian is that of eq. (1), but now H_o may have many bound levels and adjacent continua. In calculations on model van der Waals molecules, eigenfunctions of H_o have involved the internal degrees of freedom (vibration and rotation) of the constituents and degrees of freedom of the van der Waals bond. The interaction Hamiltonian only includes residual terms involving no new degrees of freedom.

In the basis of eigenfunctions of H_o the Hamiltonian is[1]

$$H_o = \Sigma |m> E_m <m|$$
$$H' = \sum_{m \neq n} |m> V_{mn} <n| \qquad (7)$$

In the view of the calculations mentioned, off-diagonal terms in H' induce transitions (PR) in the $\{|m>\}$ basis. Diagonal terms merely cause energy shifts in the $|m>$ levels and could in principle be included in H_o. In any case, there is no PDP in this complete picture. The only DP corresponds to PR.

The complete description, with the Hamiltonian partitioned as in (7), reduces to the lineshape model (or, more precisely, the density matrix for multilevel system in Chapter 5) if the optical Hamiltonian only connects discrete levels of H_o. That is, the prepared state is a superposition of discrete states (not generally an eigenfunction itself). There is some experimental evidence, though not conclusive, that the optically prepared state in van der Waals molecule experiments does not include an appreciable continuum component. In the spectra of $HF \cdot C_2H_4$ and $HCl \cdot C_2H_4$, for example, only vibrational fundamentals

are observed, the transition moments are comparable to that of free ethylene and the lines are symmetrical. If the prepared superposition states did have substantial continuum character, one might expect to observe instead Fano lineshapes.[8]

This description preserves the distinction between PR and actual dissociation outlined in Section II. Experimental attempts to determine if the dissociation mechanism is in fact the line-broadening PR have been inconclusive.[9] Trends in widths measured in van der Waals molecular spectra are consistent with propensity rules for dissociation calculated with full descriptions. For example, widths increase in the series $Ne \cdot C_2H_4$ < $HF \cdot C_2H_4$ < $(C_2H_4)_2$ reflecting dissociation constrained by angular momentum conservation.

In practice, adoption of the picture described is most useful (i.e., allows us to draw physical insight from experiments) if it is possible in the excitation step to keep track of all degrees of freedom of the complex. In the case of the simple van der Waals molecules studies, this is arguably the case. Structure in the spectra of $Ar \cdot C_2H_4$ and $Ne \cdot C_2H_4$, for example, is due to combinations of vibration and hindered rotation of C_2H_4, giving a measure of the spacings and populations of these levels. As described in the next section, including unobserved degrees of freedom in the model can lead to pure dephasing.

As an aside, we note that the Hamiltonian (7) need not be partitioned and, in principle, the basis of eigenfunctions of the full Hamiltonian could be determined. In this new basis the time evolution of the optically prepared superposition state could only be described as dephasing without PR. This alternative picture, though completely equivalent to the one described above, would be preferable (i.e., would lend more physical insight) if the initially prepared superposition state was appreciably mixed with the continuum levels of H_o.

IV. Dephasing in a Reduced Description of the System

In a reduced description, the Hamiltonian is partitioned into terms which operate in two distinct spaces[1]:

$$H = H_S(Q_S) + H_B(Q_B) + H_{SB}(Q_S,Q_B) \qquad (8)$$

where Q_S represents the degrees of freedom which are of interest (the "system") while Q_B represents the other degrees of freedom (the "bath"). Modes may be relegated to the bath if they are only weakly coupled to system variables - this is especially helpful if the bath is enormous or can be treated in some approximate way. From the experimental standpoint the bath may be thought of as an unobserved part of the system.

Focussing attention on the system variables alone, the system properties are determined by the reduced density matrix

$$\rho^S = Tr_B(\rho) \tag{9}$$

where the right hand side is the partial trace of the density matrix of the global system, over the space of the bath system.[10] By performing the partial trace, the properties of the bath, if correlated to activity in Q_S, are implicitly included in ρ^S. In particular, dynamics occurring in the bath appear as PDP terms in $\dot{\rho}^S$.[1,2,11] PDP arises as a result of adopting a reduced description and therefore could, in principle, be removed by expanding Q_S.[1]

Zewail and colleagues[2] have provided an insightful description of PDP which is qualitatively applicable here. Let s and b label the eigenfunctions of H_S and H_B. The PDP decay rate of the off-diagonal element $\rho^S_{ss'}$, is[2]

$$\gamma_{PDP} = \frac{\pi}{\hbar} \sum_{b,b'} W_b |\langle sb|H_{SB}|sb'\rangle - \langle s'b|H_{SB}|s'b'\rangle|^2 \delta(E_b - E_{b'}) \tag{10}$$

The form of (10) indicates that PDP in ρ^S is due to population flow amongst the bath levels. Aside from the matrix elements in (10) important features are the delta function, by which a large density of states near E_b would enhance

γ_{PDP}, and the Boltzmann factor, W_b, which permits only populated bath levels to contribute to PDP.

The question of how to partition the Hamiltonian in a reduced description of van der Waals molecules is an interesting one. We propose that the partitioning should reduce ρ^S to an extent consistent with the observations of experiments. Below, the implications of this type of partitioning and eq. (10) for ethylene cluster experiments are discussed. It should be emphasized that the discussion is qualitative and that approximations by which (10) is derived[2] do not strictly apply here.

Spectra of $Ar \cdot C_2H_4$ and $Ne \cdot C_2H_4$ show combinations of ethylene ν_7 vibration and hindered rotation. Therefore, the ν_7 coordinate and rotational degrees of freedom of ethylene constitute Q_S. Remaining degrees of freedom relegated to Q_B are all other ethylene vibrational modes, the end-over-end rotation of the complex, and the radial coordinate for separation of the partners.[12] Under our experimental conditions, $kT \simeq 3\ cm^{-1}$ so that the only bath modes populated would be rotation of the complex.[13] Together these do not contain enough energy to excite the other bath modes, and in any case angular momentum constraints forbid such population flow. We conclude that in <u>this</u> reduced description of $C_2H_4 \cdot Ar$ and $C_2H_4 \cdot Ne$ that γ_{PDP} does not appreciably affect the measured linewidth.

In the spectra of $C_2H_4 \cdot HF$ and $C_2H_4 \cdot HCl$ only the vibrational transition is observed so that Q_S is reduced to

the ν_7 coordinate. Q_B absorbs the remaining internal degrees of freedom of both partners. Based on our experience, we expect that librational frequencies of C_2H_4 in these molecules are greater than kT (i.e., greater than those of $C_2H_4 \cdot Ar$ and $C_2H_4 \cdot Ne$). Furthermore, the librational frequency of HF in $C_2H_4 \cdot HF$ is thought to be of the order of 400 cm^{-1}.[14] Again, we conclude, based on equation (10) in this reduced description, that PDP does not contribute to the observed linewidths.

The reduced descriptions of $(C_2H_4)_2$ and $C_2H_4 \cdot C_2F_4$ also include only ν_7 in Q_S. Little is known about the potentials in these cases, but it is expected that the density of states in the bath modes is higher than that in the previous examples, and that all the bath mode frequencies are lower. Although (10) shows that γ_{PDP} is larger in these cases, experimental results imply that γ_{PDP} does not significantly influence measured widths. For example, the homogeneous width of $(C_2H_4)_2$ is the same at 4 K and 16 K,[15] despite the influence of the Boltzmann factor in (10). The spectrum of $C_2H_4 \cdot C_2F_4$ is narrower than that of C_2H_4, even though the former has lower bath frequencies. Finally, the width for $(C_2H_4)_3$ is less than that for $(C_2H_4)_2$ despite increased density of resonant bath modes.

V. Summary

Dephasing processes in several descriptions of van der Waals complexes have been outlined, along with expressions for heretofore phenomenological rate constants. Consideration of these expressions and experimental measurements has led to the conclusion that observed linewidths are best interpreted as population decay and not pure dephasing. As this conclusion is based on a qualitative discussion, there is need for a good experiment or theory to further elucidate the problem of dephasing in van der Waals molecules. A direct measurement of population evolution would be of great significance. From a theoretical standpoint, it would be interesting to study the matrix elements in equation 10.

REFERENCES

1. S. Mukamel, Chem. Phys. 31, 327 (1978).
2. a) K. E. Jones and A. H. Zewail, in Springer Series in Chemical Physics, Vol. 3: Advances in Laser Chemistry, edited by A. H. Zewail (Springer, Berlin, Heidelberg, New York, 1978), p. 196. b) K. E. Jones, A. H. Zewail and D. J. Diestler, ibid, p. 258. c) D. J. Diestler and A. H. Zewail, J. Chem. Phys. 71, 3103 (1979).
3. C. Cohen-Tannoudji, B. Diu and F. Laloe, Quantum Mechanics (Wiley-Interscience, Paris, 1977), Vol. 2, p. 1350.
4. Equation (4) gives a first-order decay rate valid for all time $t >> 1/\Delta$ where $\hbar\Delta$ is the width of the right hand side of (4) as a function of E (replace $E=E_a$ with E in (4)). As such (4) is more general than Fermi's golden rule which predicts linear decay valid for $t << \gamma_{PR}^{-1}$. See ref. 3.
5. J. A. Beswick and J. Jortner, Adv. Chem. Phys. 47, 363 (1980).
6. G. E. Ewing, Faraday Discuss. Chem. Soc. 73, 325 (1982).
7. We define dissociation rate as the effective first-order decay constant one would observe if directly measuring dissociation. This could in fact be due to a rate-limiting intermediate step.

8. U. Fano, Phys. Rev. 124, 1866 (1961).

9. D. S. Bomse, J. B. Cross and J. J. Valentini, J. Chem. Phys. 78, 7175 (1983).

10. Reference 3, Vol. 1, p. 305.

11. U. Fano, Rev. Mod. Phys. 29, 74 (1957).

12. Since dissociation is observed, one might suggest that the dissociation coordinate should be included in the system space. However, dynamics affecting the spectrum occur in time $t \simeq \gamma_{DP}^{-1}$ while practical restrictions prevent detection of dissociation until $t \simeq 10^{-4}$ sec.

13. Manifestations of end-over-end rotational inhomogeneity have been observed (Chapter 6), but individual sublevels have not been resolved.

14. L. Andrews, G. L. Johnson and B. J. Kelsall, J. Chem. Phys. 76, 4857 (1982).

15. M. A. Hoffbauer, K. Lin, C. F. Giese and W. R. Gentry, J. Chem. Phys. 78, 5567 (1983).

Chapter 9

Summary

The important parameters determined by lineshape fits to vibrational predissociation spectra of ethylene-containing clusters are listed in Table I. All of these data were obtained from bands observed near the frequency of the ν_7 in-phase out-of-plane bending mode of ethylene. The parameters are the band origin, ω_o, the homogeneous width, γ, and corresponding lifetime, τ, the squared transition moment for infrared absorption, $<\mu>^2$, and the barrier to internal rotation, V_2. Observations that have been made can be divided into three categories pertaining to the spectroscopic transition, the van der Waals interaction and the dynamics of dissociation.

A. Spectroscopy

There are dramatic differences in the appearance of some of the ethylene cluster spectra, all excited in the C_2H_4 ν_7 mode, as illustrated in Figure 1. However, all of the observed spectra can be interpreted using as a model two groups of levels with the upper group experiencing irreversible decay. In many cases, it is possible to reduce the model to a homogeneous two-level system. The most detailed model incorporated rotational and spatial inhomogeneity to reconcile ethylene dimer results over a wide range of laser powers and temperature.

The position, intensities and appearance of the bands are consistent with the idea that the spectroscopically

TABLE I. Parameters determined for ethylene cluster photodissociation.

Cluster	ω_o (cm^{-1})	γ (cm^{-1})	τ psec	$\langle\mu\rangle^2$ ($10^{-3}D^2$)	V_2 (cm^{-1})
$Ne \cdot C_2H_4$	949.1	≤ 0.5	≥ 10.0	--	-12.5
$Ar \cdot C_2H_4$	953.9	≤ 3.0	≥ 1.7	--	-30.0
$C_2H_4 \cdot HF$	974.4(1)	1.59(81)	3.3 (22)	77. (25)	--
$C_2H_4 \cdot HCl$	964.1(1)	1.57(67)	3.4 (25)	52. (16)	--
$C_2H_4 \cdot NO$	951.5(5)	7.4 (12)	0.72(10)	50.9(48)	--
$C_2H_4 \cdot C_2F_4$	954.7(2)	6.0 (8)	0.89(10)	46.2(63)	--
$(C_2H_4)_2$	952.3(5)	12.0 (2)	0.44(5)	96.0(18)	--
$(C_2H_4)_3$	952.3(5)	11.0 (2)	0.50(7)	141.0(33)	--
C_2H_4[a]	949.0	--	--	35.5(14)	--

[a]Reference 14.

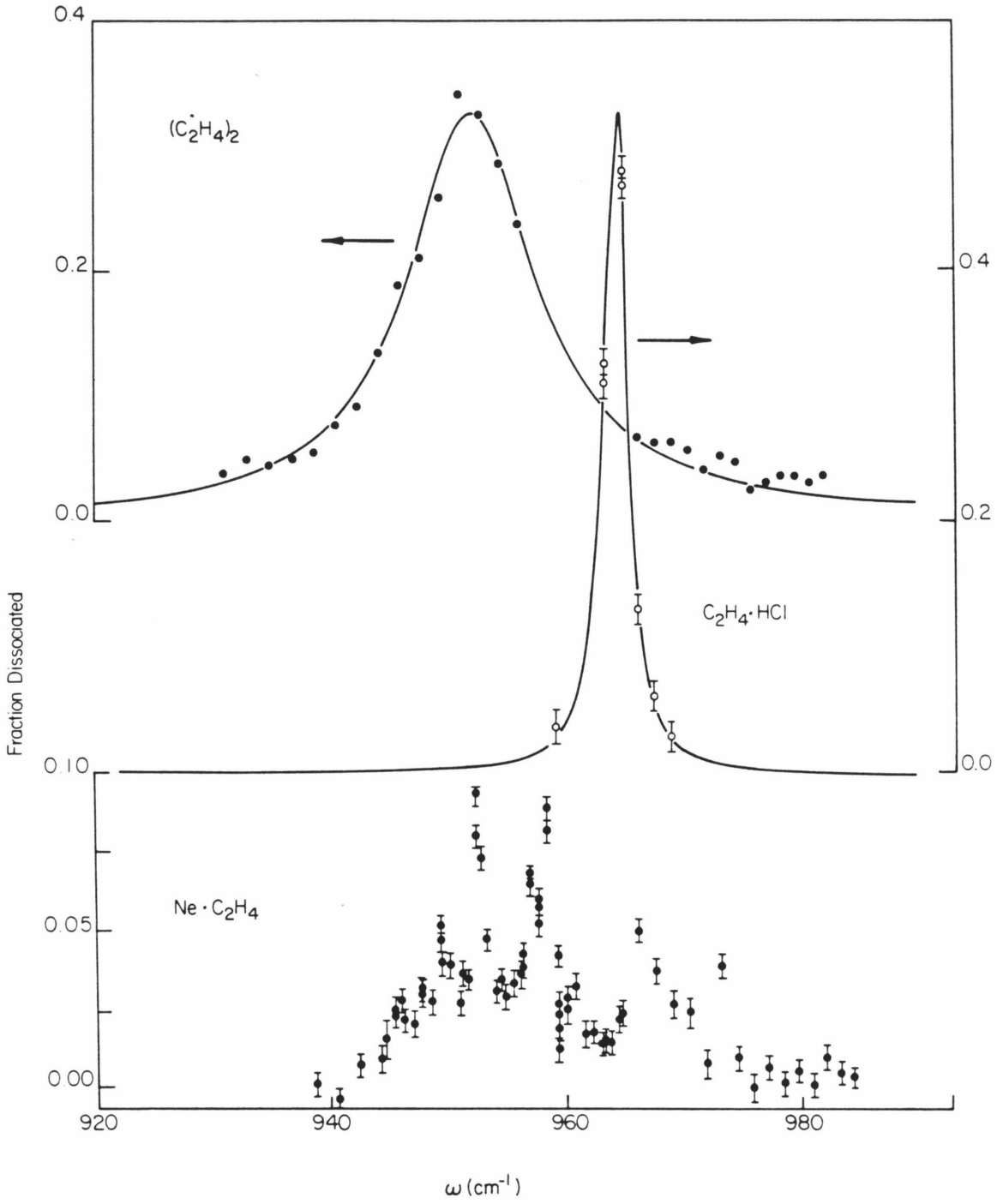

FIGURE 1. Comparison of $(C_2H_4)_2$, $C_2H_4 \cdot HCl$ and $C_2H_4 \cdot Ne$ infrared photodissociation spectra. Note the different intensity scales and fluences: 3.8 mJ/cm^2, 3.7 mJ/cm^2 and 1.9 mJ/cm^2, respectively.

excited motion closely resembles the ν_7 mode of free ethylene. As indicated by the spectral profile and known structures, this motion occurs as a parallel band in clusters with HF and HCl, and as a hybrid band in $(C_2H_4)_2$. These clusters exhibit single symmetric bands, unlike $Ne \cdot C_2H_4$ and $Ar \cdot C_2H_4$ whose spectra are more richly structured. The structure results from excitation of combinations of ν_7 motion and hindered internal rotation by ethylene.

All of the spectra exhibit a blue shift relative to the ν_7 fundamental of free ethylene, with the hydrogen bonded clusters having the most pronounced shift. Similarly, the non-rare gas clusters show enhanced intensity relative to the monomer.

B. The bonding interaction

The observation of parallel bands for $C_2H_4 \cdot HF$ and $C_2H_4 \cdot HCl$ is expected since the measured structures of these clusters have the diatomic above the ethylene plane.[1] In order to reconcile measurements of $(C_2H_4)_2$ widths at different laser powers and temperatures,[2-4] the band type must be hybrid or perpendicular. It is certainly not a parallel band. A hybrid band would be expected based on the crystal structure[5] and ab initio calculations.[6]

$Ne \cdot C_2H_4$ and $Ar \cdot C_2H_4$ are evidently quite loose complexes compared to the other clusters in Table I. They

are the only clusters wherein it is possible to excite internal rotations. The others may be rigid because of strong, directional hydrogen bonds, or because the internal motion is sterically hindered.

In the case of the hydrogen-bonded clusters, the blue shifts are attributable to an electrostatic interaction rather than stiffening of the C-H bonds induced by charge redistribution upon hydrogen bonding. This is supported by the fact that only the out-of-plane modes of C_2H_4 exhibit a shift in the infrared spectra of the matrix isolated clusters.[7] The slight blue shifts in the non-hydrogen bonded clusters may be due to a repulsive valence interaction which compensates for red-shifting induction and dispersion interactions. The slight blue shift observed for ethylene dimer could be due to resonant dipole coupling.[8] The small shift suggests that the resonant dipole interactions nearly cancel, which would occur if the ethylene planes were parallel but skewed 55°. This is consistent with the conclusion above that ν_7 occurs as a hybrid band.

The observed intensity enhancements are largely attributable to interaction of the C_2H_4 ν_7 oscillation and the polarizable, but otherwise passive, van der Waals partner. The oscillating induced dipole provides the enhanced intensity. Note that the transition moments listed in Table I are quite uniform, with the exception of $C_2H_2 \cdot HF$, with an average squared transition moment per ethylene subunit equal to 48.3×10^{-3} D^2. The large enhancement for $C_2H_4 \cdot HF$ may

reflect a change in the charge distribution in the C-H bonds upon hydrogen bonding, although not so large as to effect the observations mentioned in the previous paragraph.

C. Photodissociation dynamics

The range of the observed lifetimes of ethylene clusters is relatively narrow compared to range expected on the basis of early theories.[9,10] However, trends observed are consistent with dissociation constrained angular momentum conservation.[11] This is also consistent with the observation[4,12] that fragment rotation is an important degree of freedom absorbing the excess energy. It is also encouraging to note that Ewing has calculated an ethylene dimer dissociation rate, using a curve crossing model for V→R,T energy transfer,[13] which is comparable to the observed rate.

It has been inferred from the observed widths that the broadening mechanism is in fact vibrational predissociation. Two other decay mechanisms cannot be categorically dismissed until the population evolution is observed directly. These are relaxation to other states not immediately leading to dissociation and pure dephasing processes. Nondissociative relaxation has been ruled out in ethylene clusters since it would involve transfer of substantial vibrational energy to weakly bound modes and multiple quantum transitions. Conservation of energy and angular momentum alone would

severely restrict such a process. The pure dephasing mechanism has been ruled out because pure dephasing depends on occupation numbers in such a way that it is precluded in these molecules at low temperatures. In either case, trends expected have not been observed.

D. The future

Clearly, there is a great deal yet to be learned. This work at the very least provides a strong methodological foundation for obtaining and interpreting the photodissociation spectra of van der Waals molecules. The ethylene cluster measurements also provide a substantial body of data on which to build. More spectra of different types of clusters and vibrations are needed to discern trends. Direct measurements of the time evolution of the initially excited state would be of tremendous significance. The same can be said for measurements of product state distributions. Previously reported measurements of the translational energy content of $(C_2H_4)_2$ photodissociation fragments should be reexamined in view of orientational saturation effects and the hybrid nature of the dimer ν_7 transition described in this thesis. Higher resolution spectra of $Ne \cdot C_2H_4$ and $Ar \cdot C_2H_4$ are needed.

The molecules studied here are probably too complicated for detailed theoretical study. However, data are now available for $(HF)_2$[15] and are likely soon to be available for

a molecule like Ar·HF. These should give impetus to theoretical work in this field. Finally, our absolute intensity measurements reflect the charge distributions in the van der Waals clusters. Such measurements could serve as a check for calculated charge distributions.

REFERENCES

1. (a) P. D. Aldrich, A. C. Legon and W. H. Flygare, J. Chem. Phys. 75, 2126 (1981). (b) J. A. Shea and W. H. Flygare, J. Chem. Phys. 76, 4857 (1982).
2. M. A. Hoffbauer, W. R. Gentry and C. F. Giese, in Laser-Induced Processes in Molecules, edited by K. L. Kompa and S. D. Smith (Springer-Verlag, Berlin, Heidelberg, New York, 1979).
3. M. P. Casassa, D. S. Bomse and K. C. Janda, J. Chem. Phys. 74, 5044 (1981).
4. M. A. Hoffbauer, K. Lin, C. F. Giese and W. R. Gentry, J. Chem. Phys. 78, 5567 (1981).
5. G. J. H. van Hes and A. Vos, Acts. Cryst. B33, 1653 (1977).
6. A. van der Avoird, P. E. S. Wormer, F. Mulder and R. M. Berns, Topics in Current Chemistry 93, 1 (1980).
7. L. Andrews, G. L. Johnson and B. J. Kelsall, J. Chem. Phys. 76, 5767 (1982).
8. J. Geraedts, S. Stolte and J. Reuss, Z. Phys. A304, 167 (1982).
9. G. Ewing, Chem. Phys. 29, 253 (1978).
10. J. A. Beswick and J. Jortner, J. Chem. Phys. 68, 2277 (1978).
11. G. E. Ewing, Faraday Discuss. Chem. Soc. 73, 325 (1982).
12. D. S. Bomse, J. B. Cross and J. J. Valentini, J. Chem. Phys. 78, 7175 (1983).

13. G. E. Ewing, Chem. Phys. 63, 411 (1981).

14. T. Nakanaga, S. Kondo and S. Saeki, J. Chem. Phys. 70, 2471 (1979).

15. A. S. Pine and W. J. Lafferty, J. Chem. Phys. 78, 2154 (1983).